# Functional characterization of the MICOS subcomplex Mic60-Mic19 in mitochondrial crista junction formation

Inaugural-Dissertation

to obtain the academic degree

Doctor rerum naturalium (Dr. rer. nat.)

submitted to the Department of Biology, Chemistry and Pharmacy of Freie Universität Berlin

by

Manuel Hessenberger

from Gmunden/Austria

2017

Die vorliegende Arbeit wurde im Zeitraum August 2013 bis Juli 2017 in der Abteilung – Strukturelle Biologie – am Max-Delbrück-Center (MDC) Berlin unter der Anleitung von Prof. Dr. Oliver Daumke angefertigt.

| | |
|---|---|
| 1. Gutachter | Prof. Dr. Oliver Daumke |
| 2. Gutachter | Prof. Dr. Udo Heinemann |

Disputation am 18.01.2018

# Danksagung

Ich möchte mich sehr herzlich bei Professor Oliver Daumke für die Möglichkeit zur Mitarbeit in seiner Arbeitsgruppe, die spannenden Projekte, die Betreuung und Unterstützung in den letzten vier Jahren bedanken. Danke, dass ich spontan von der Brown University (Rhode Island, USA) an das Max-Delbrück-Centrum für Molekulare Medizin in Berlin-Buch in seine Forschergruppe wechseln durfte.

Des Weiteren möchte ich mich bei Professor Udo Heinemann für die vielen hilfreichen Diskussionen während unserer gemeinsamen Gruppentreffen bedanken. Seine hervorragende Strukturbiologievorlesung über drei Jahre hat mein theoretisches Wissen über dieses Thema außerdem sehr erweitert.

Ein großer Dank gilt auch unserem Kollaborationspartner Prof. Dr. Martin van der Laan für den wissenschaftlichen Austausch, die Korrekturen und Bearbeitungen unseres gemeinsamen Manuskripts. Auch für die privaten Gespräche während meiner Zeit in Berlin bin ich sehr dankbar.

Bei Dr. Bettina Purfürst und Dr. Severine Kunz bedanke ich mich für die Mitarbeit an unserer Publikation und für die perfekte Instandhaltung und Betreuung der Elektronenmikroskope.

Herzlichen Dank an Arthur Melo, Stephan Grunwald und Dr. Stephen Marino für die Diskussionen und Anregungen zu meinem Projekt, aber auch für die tiefe Freundschaft, die während dieser Zeit entstanden ist.

Ich möchte mich auch bei allen Kollegen und Kolleginnen der Arbeitsgruppe Prof. Daumke für die bereits etablierten Protokolle, Diskussionen und Unterstützungen bedanken. Einen besonderen Dank an Stephan Grunwald, Marie Witt und meine Schwiegermutter Heidrun Eibl-Göschl für das Korrekturlesen dieser Arbeit.

Einen herzlichen Dank an Dr. Ralf Zerbes, Dr. Heike Rampelt, Audrey Xavier und Dr. Hauke Lilie für die Diskussionen und Mitarbeit an unserer gemeinsamen Publikation.

Ebenso möchte ich mich bei unseren technischen Angestellten Sabine Werner, Jeanette Schlegel und besonders bei Carola Bernert für das Instandhalten des Labors bedanken, welche während dieser Zeit eine gute Freundin geworden ist.

Bei Birgit Cloos möchte ich mich für die administrative Organisation und die persönlichen Gespräche bedanken.

Danke auch an Dr. Yvette Roske für ihre Unterstützung und die gemeinsamen Stunden und Unterstützung am Elektronenspeicherring BESSY II, Adlershof Berlin.

Herzlichen Dank auch an das gesamte Team des MDC Berlin, von der Administration bis zum Wareneinkauf.

Ein großes Dankeschön an die österreichische Akademie der Wissenschaften für die Bewilligung des DOC-Stipendiums zur Finanzierung meiner Doktoratsarbeit.

Ich möchte mich auch bei meinen früheren Arbeitsgruppenleitern wie Prof. Dr. Robert Schwarzenbacher und Prof. Dr. Hans Brandstetter von der Universität Salzburg bedanken. Diese Forscher haben die Begeisterung für die Wissenschaft in mir geweckt und mich während der Ausbildung immer unterstützt.

Ein besonderes Dankeschön gilt meiner großen Familie, insbesondere meinen beiden Brüdern für die langjährige emotionale Unterstützung und meinen Eltern für die finanziellen Hilfen. Ganz besonders möchte ich mich bei meiner Mutter für ihren unermüdlichen Glauben an mich bedanken!

Das größte Dankeschön gilt meiner Frau Clarissa, nicht nur für das Korrektur lesen dieser Arbeit, sondern auch für die vielen aufmunternden privaten und beruflichen Gespräche. Sie ist für mich der Fels in der Brandung auf den ich mich immer verlassen kann. Ebenso möchte ich meiner Tochter Catharina Danke sagen, dass ihr süßes Lächeln mich immer an das Wichtige im Leben erinnert.

# Index

# 1 Abstract

The investigation of mitochondrial structure and function has developed into an active area of research. A lot of progress was made on understanding the role of mitochondria in energy production and apoptosis, but there is still a profound lack of knowledge how mitochondria obtain their specific shape required for proper function. In particular, the formation of invaginations of the inner mitochondrial membrane termed cristae involves a plethora of different proteins, but it has remained unclear how they contribute to the remodeling of cristae membranes.

The newly identified mitochondrial contact site and cristae organizing system (MICOS) is crucial for the formation of crista junctions and mitochondrial inner membrane architecture. MICOS contains two core components. Mic10 shows membrane-bending activity, whereas Mic60 (mitofilin) forms contact sites between inner and outer membranes. In my PhD thesis, I show that Mic60 from the thermophile fungus *Chaetomium thermophilum* dimerizes via its coiled-coil region and deforms liposomes into thin membrane tubules, therefore displaying membrane-shaping activity. Furthermore, a membrane-binding site in the soluble intermembrane space-exposed part of Mic60 was identified. This membrane-binding site is formed by a predicted amphipathic helix between the conserved coiled-coil and mitofilin domains. The mitofilin domain negatively regulates the membrane-shaping activity of Mic60. It is also shown that the mitofilin domain of Mic60 strongly binds to the CHCH domain of Mic19. ITC experiments indicated that this high affinity interaction requires two conserved cysteines within the CHCH domain that form a predicted disulfide bridge. Binding of Mic19 to the mitofilin domain modulates the membrane remodeling activity. The Mic60-Mic19 subcomplex forms tetramers, which involves both the CHCH-mitofilin domain interactions, but also the coiled-coil domains of both proteins. Membrane binding and shaping by the conserved Mic60-Mic19 complex is crucial for crista junction formation, mitochondrial membrane architecture and efficient respiratory activity. Mic60 thus plays a dual role by shaping inner membrane crista junctions and forming contact sites with the outer membrane.

# 2 Introduction

## 2.1 The Mitochondrion

### 2.1.1 Mitochondrial origin

It is believed that mitochondria arise from an endosymbiotic event, e.g. by an uptake of a prokaryotic into a eukaryotic cell. During this process, also the genetic material from the bacteria was transferred to the eukaryote and can still be found within the mitochondrial DNA (mtDNA) (Ernster and Schatz, 1981). The mitochondrial genome is circular, around 16 kilobases in size and encodes 37 genes including subunits of the respiratory complexes (I, III and V), mitochondrial tRNA and rRNA (Chan, 2006).

A eukaryotic cell is composed of different organelles and compartments to fulfill specific functions in mobility, division and survival, like energy production. First mitochondrial-like structures were already reported in 1840s (Henle, 1841). The name "mitochondrion" arises from two Greek words, "mitos" (thread) and "chondros" (granule) (Ernster and Schatz, 1981). In 1964, a first high-resolution electron micrograph was taken from the Palade group, shedding light on the highly complex membrane structure (Figure 1) (Weibel and Palade, 1964).

Over the years, specific mitochondrial functions were discovered, like phospholipid transfer (Vance and Shiao, 1996), calcium signaling (Rizzuto et al., 2009), energy production via the electron-transport chain (Pratt, 2006) and many others. After discovering a role in apoptosis via the cytochrome *c* release (Wang and Youle, 2009), this field has obtained even increasing attention over the last years.

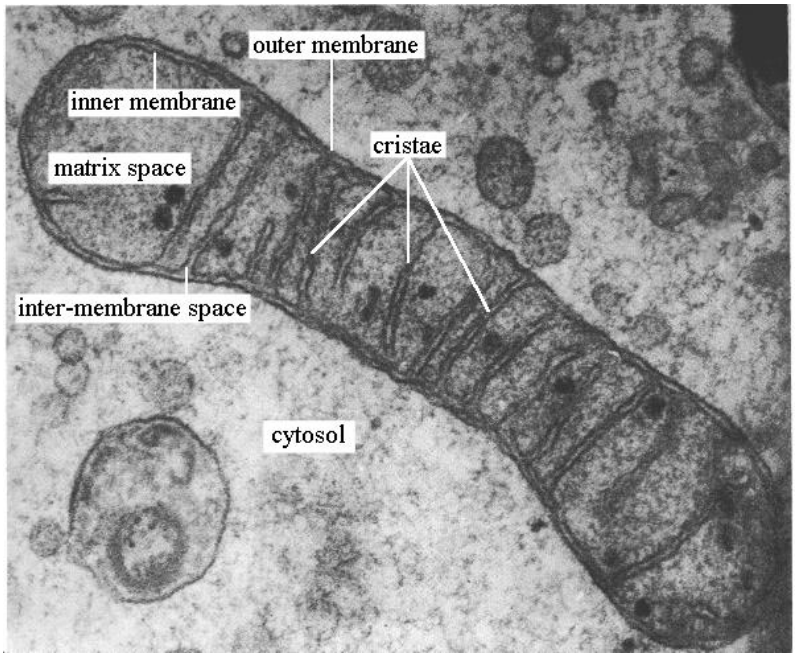


**Figure 1. Electron micrograph of a negatively stained mitochondrion revealed its complex architecture and their typical invaginations termed cristae. Picture taken from https://biomyershl.files.wordpress.com/**

### 2.1.2 Mitochondrial function

A main function of the mitochondria might be the energy production in the form of ATP; therefore, this organelle is also known as the powerhouse of the cell (Figure 2). The tricarboxylic acid (TCA) cycle or the Krebs cycle is located within the mitochondrial matrix and uses pyruvate, produced outside of the cell, to create enough NADH molecules to drive oxidative phosphorylation (Kornberg, 2000). In addition to energy production, this organelle is also involved in phospholipid transfer. This process provides a constant source of phospholipids for the mitochondrial membranes, which is, for example, important during mitochondrial fission and fusion events. The most important and specific lipid of mitochondria is cardiolipin (CL), which is directly synthesized from phosphatidic acid (PA) inside of the organelle (Houtkooper and Vaz, 2008). The lipid transfer itself mostly depends on mitochondria associated membranes (MAM), which links the ER to the mitochondrion. Next to lipid trafficking, MAM is the key element for $Ca^{2+}$ transfer between these organelles. Inner mitochondrial $Ca^{2+}$ levels are crucial for the metabolism but also for regulating apoptosis. Misregulation can lead to several neurodegenerative diseases but is also involved in cancer (Rizzuto et al., 2009).

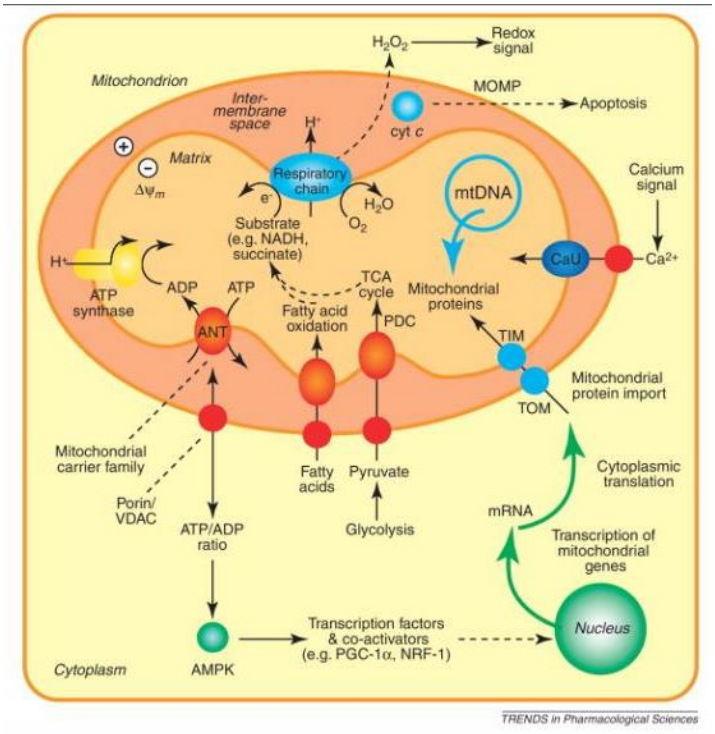


**Figure 2. A schematic representation of mitochondrial functions in healthy cells. Picture taken from (Smith et al., 2012)**

One mechanism during tumor cell development is the down-regulation of the apoptotic pathway. Two major pathways have been described. The extrinsic pathway is regulated by the tumor necrosis factor receptor (TNFR) located at the outer cell membrane and includes the TNF-induced and the Fas-Fas ligand-mediated model (Wajant, 2002). The intrinsic pathway represents the second pathway and is induced by the release of mitochondrial cytochrome *c* to the exterior. This activates the apoptotic protease activating factor – 1 (Apaf-1), finally leading to the formation of active caspase-3, which induces apoptosis (Kharbanda et al., 1997).

### 2.1.2.1 The electron transport chain

To provide energy for the cell, mitochondria can produce ATP via aerobic respiration, also known as oxidative phosphorylation (Figure 3). The starting product is glucose, which is converted to pyruvate during glycolysis outside of the mitochondria. Next, pyruvate is supplied to the citric acid cycle, located at the mitochondrial matrix to produce NADH and $FADH_2$ for the electron transport chain. Finally, generated $H^+$ ions, produced during the oxidative phosphorylation, drive the ATP-synthase.

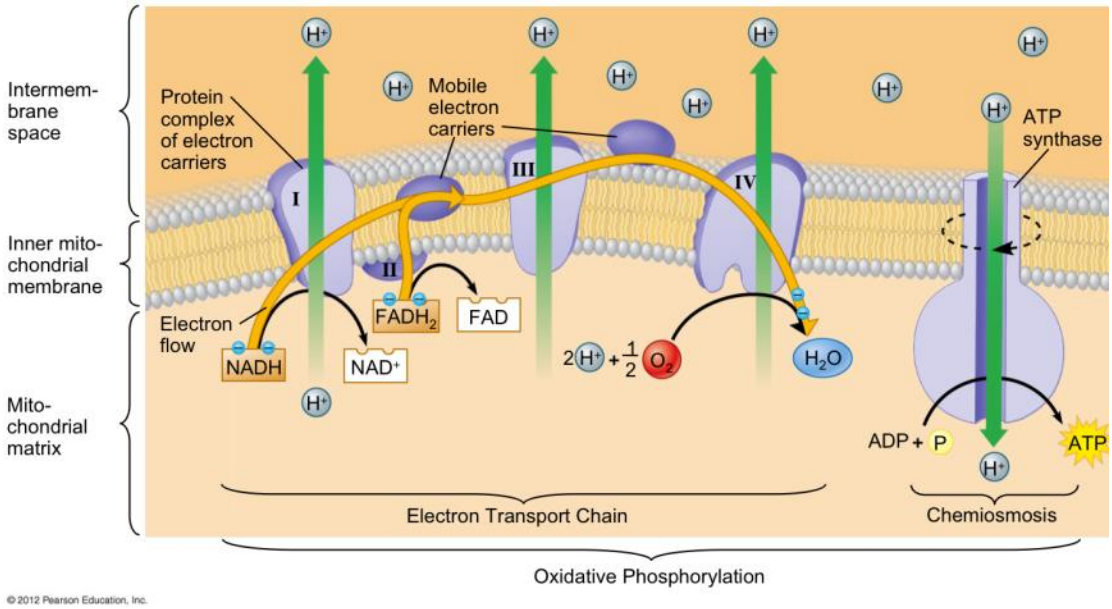


**Figure 3. The electron transport chain is located in the inner mitochondrial membrane and is essential for cellular energy supply. NADH and $FADH_2$ are used to produce $H^+$ ions, which drive the ATP-synthase to produce ATP as an energy source. For detailed description see text. Picture taken from https://www.unm.edu/**

The electron transport chain is located at the cristae membrane and includes four protein complexes, termed complex I-IV, where complex I, III and IV are the main compounds. Initially, two electrons of NADH are transferred to complex I, which contains the enzyme NADH dehydrogenase to produce four hydrogen ions to be pumped into the IMS. Complex II is not delivering any hydrogen ions but uses electrons from $FADH_2$ to be transported via ubiquinone (Q) to complex III. Ubiquinone moves inside the hydrophobic core of the lipid bilayer and connects complex I, II and III via their shared electron transporter molecule. Complex III is also known as cytochrome *c* reductase and is composed of cytochrome *b* and *c*. These proteins harbor a prosthetic heme group, which contains an iron ion that can be reduced and oxidized as it passes the electron. Electrons of cytochrome *c* are further transported to complex IV, which is also pumping protons through the membrane. Finally, complex IV, which contains two heme groups and three copper ions accept the electrons from cytochrome *c.* The bound oxygen molecule gets fully reduced and is further using two hydrogen ions to produce water. Complex IV pumps hydrogen ions across the membrane and all produced $H^+$ are used from the ATP synthase to create ATP (Alberts et al., 2002).

### 2.1.3 Mitochondrial structure

Mitochondria can vary in size, depending on the cell stage and condition. The overall morphology is characterized by the presence of discrete outer and inner membrane systems (Figure 4) (Endo and Yamano, 2009; Neupert and Herrmann, 2007; van der Laan et al., 2012; Zick et al., 2009).

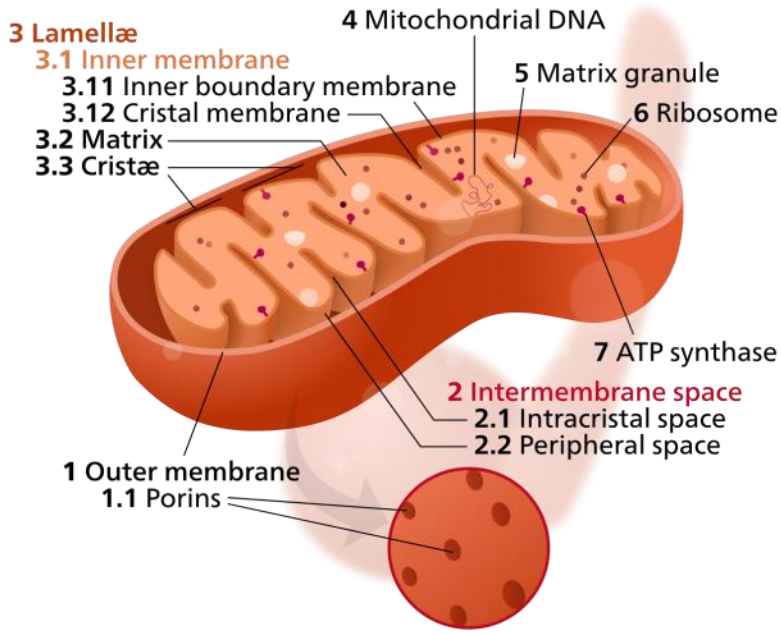


**Figure 4: A cartoon of the mitochondrion illustrates its typical double membrane shape and other specified areas. Picture taken from https://en.wikipedia.org/wiki/Mitochondrion**

The mitochondrial outer membrane (OM) is composed of phospholipids with a defined composition (Horvath and Daum, 2013). The OM is enriched with a large number of integral membrane proteins, also known as porins. These channels allow molecules of 5000 Da or less to pass the membrane. Around 99% of the ~1.000 different mitochondrial proteins are nuclear encoded and have to be imported into the mitochondria (Sickmann et al., 2003). Almost 60% of imported proteins are guided via an N-terminal pre-sequence to the translocase of the outer membrane (TOM) (Vogtle et al., 2009). Membrane proteins of the outer mitochondrial membrane are integrated, depending on their secondary structure contents. α-Helical proteins are mainly recognized and inserted by the mitochondrial import (MIM) complex and/or TOM. In contrast, β-barrel containing proteins are imported by TOM and integrated using the sorting and assembly machinery (SAM). Interestingly, mitochondria can also form an endoplasmic reticulum (ER)-mitochondria encounter structure (ERMES) to physically interact and communicate with the ER (Wiedemann and Pfanner, 2017).

The inner membrane space (IMS) is enclosed by the inner mitochondrial membrane (IM) and the OM and is characterized by a slightly reduced pH compared to the cytoplasm. This effect is the result of a constant influx of $H^+$-Ions into the IMS arising from the electron transport chain machinery. Proteins of the IMS often contain a cysteine motif, such as $Cx_3C$ and $Cx_9C$, and are forming intramolecular disulfide bonds. This reaction is catalyzed by an oxidoreductase termed mitochondrial intermembrane space import and assembly (MIA) machinery, which is able to perform oxidative protein folding (Chacinska et al., 2004).

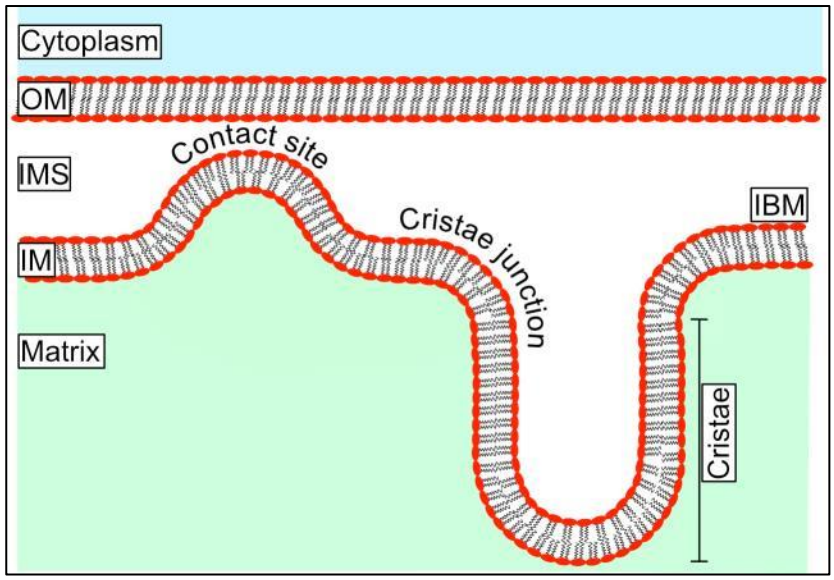


**Figure 5: Cartoon illustration of the mitochondrial membrane compartments. OM – outer membrane, IMS – inner membrane space, IM – inner membrane, IBM – inner bound membrane**

The mitochondrial IM is highly folded to increase the overall membrane surface and has a similar lipid composition compared to the OM but is highly enriched in CL, constituting up to 18% of the lipids (Horvath and Daum, 2013). Whereas the OM separates the mitochondria from the cytosol, the IM is comprised of the inner boundary membrane (IBM), which is closely opposed to the OM, and cristae membranes (Figure 5). Cristae are tubular or lamellar membranous invaginations of the IM, which can largely differ in size and shape, depending on the metabolic state and cell type (Mannella, 2006; Pernas and Scorrano, 2016; Zick et al., 2009). They exhibit a specific protein composition with a characteristic accumulation of respiratory chain (super-) complexes and $F_1F_o$-ATP synthase oligomers (Cogliati et al., 2013; Davies et al., 2011; Enriquez, 2016; Gilkerson et al., 2003; Vogel et al., 2006; Wurm and Jakobs, 2006). Cristae are linked to the IBM *via* tubular openings of

defined diameter termed crista junctions (CJs) (Mannella, 2006; Zick et al., 2009). It has been proposed that cristae formation and dynamics may be connected to the mitochondrial fusion and fission machineries (Barrera et al., 2016; Glytsou et al., 2016; Harner et al., 2016). Perturbations of these processes are observed in numerous pathologies including neurodegenerative diseases and cancer (Nunnari and Suomalainen, 2012; Pernas and Scorrano, 2016; Wai and Langer, 2016). Of note, remodeling of crista junctions to facilitate cytochrome *c* release from mitochondria is a key event in the induction of programmed cell death, called apoptosis (Frezza et al., 2006).

### 2.1.4 Mitochondrial fusion, fission and cristae formation

A variety of different proteins have been implicated in the remodeling and deformation of biological membranes. For example, Bin/Amphiphysin/Rvs (BAR) domain containing proteins scaffold membranes to induce membrane curvatures; in addition, some of them employ amphipathic helices which are inserted into the membranes for membrane remodeling events (Cui et al., 2013). Interestingly, it was shown that the amphipathic helices are the sensors for high membrane curvature and not the crescent-shaped BAR dimer (Bhatia et al., 2009). Remodeling of the inner mitochondrial membrane includes proteins like Optic Atrophy 1 (OPA1) (Figure 6) (Frezza et al., 2006; Olichon et al., 2003; Pernas and Scorrano, 2016), the ATP-synthase (Muhleip et al., 2016) and members of a newly identified mitochondrial complex (MICOS; see details in chapter 2.2) such as Mic60 and Mic10 (Barbot et al., 2015; Bohnert et al., 2015; Hessenberger et al., 2017; Tarasenko et al., 2017).

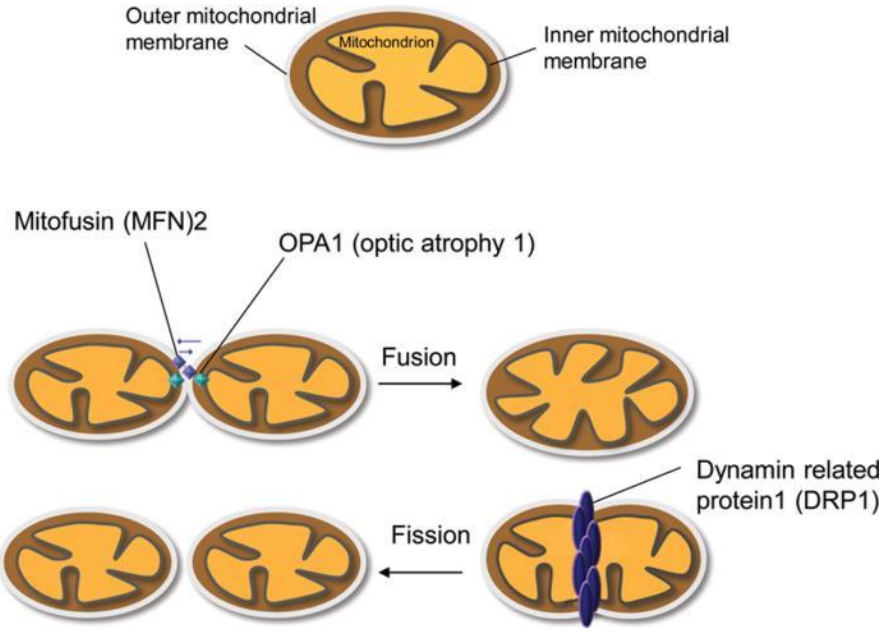


**Figure 6. Mitochondrial fusion and fission is essential in several cellular functions. Mitofusin (MFN) and Optic Atrophy 1 (OPA1) are well-characterized proteins involved in fusion. In contrast, the dynamin related protein1 (DRP1) has a crucial role in mitochondrial fission. Picture taken from (Milone and Benarroch, 2012).**

The name OPA1 is derived from autosomal dominant optic atrophy (ADOA), a genetic human disease caused by mutations in OPA1 (Alexander et al., 2000). OPA1 was identified in vertebrates as a dynamin-like GTPase that localizes to mitochondria and has a profound role in mitochondrial fusion and cristae formation (Olichon et al., 2003; Olichon et al., 2006). The functional homologue in yeast is called Mgm1 (Wong et al., 2000). In further studies, OPA1 was shown to be essential for mitochondrial fusion but dispensable for CJs formation (Barrera et al., 2016). Furthermore, mutations lead to abnormal mitochondrial morphology and mitochondrial dysfunction. Two forms of OPA1 are present in mitochondria: A long form (l-OPA1) is anchored to the inner mitochondrial membrane, and a short form (s-OPA1) represents the soluble variant after proteolytic cleavage of l-OPA1 (MacVicar and Langer, 2016). It was demonstrated that recombinant s-OPA1 associates with liposomes containing negatively charged phospholipids. Especially, cardiolipin was shown to increase the binding affinity to membranes (Ban et al., 2010). However, both OPA1-forms are essential for mediating fusion and require a functional GTPase domain (Griparic et al., 2007). Cells lacking OPA1 form cristae that appears as circular vesicles with reduced diameter (Olichon et al., 2003).

Recently, it was shown that OPA1 physically interacts with subunits of MICOS (Mic60 and Mic19) pointing to an interplay controlling cristae shape (Barrera et al.,

2016; Darshi et al., 2011; Glytsou et al., 2016). Co-immunoprecipitation experiments revealed efficient binding of OPA1 and Mic60. Interestingly, depletion of OPA1 leads to increased levels of Mic60 and decreased the efficiency of apoptosis. It was therefore suggested that OPA1 acts as an antiapoptotic factor (Barrera et al., 2016). Next to OPA1 and MICOS, also the ATP synthase is involved in the initiation of cristae formation by forming U- or V-shaped dimers (Muhleip et al., 2016). This became even more interesting after discovering a direct interaction between Mic10 and the $F_1F_o$-ATP synthase (Rampelt et al., 2017a).

The fusion of the outer mitochondrial membrane is induced, by tethering two opposing mitochondria. It has been proposed that this process is mediated by the dimerization of a dynamin-related GTPase termed Mitofusin (MFN) (Cao et al., 2017) and UGO1. In addition, the mitochondrial fusion and transport protein UGO1 was found to link the yeast mitofusin homolog fuzzy onion (Fzo) to Mgm1 (Mozdy and Shaw, 2003), therefore establishing a mitochondrial inner/outer membrane fusion complex. Furthermore, UGO1 was shown to directly interact with MICOS to promote mitochondrial fusion (Steffen et al., 2017). The fusion process depends on the interaction between Mfn1 and OPA1 during the formation of OM-IM contact sites (Cipolat et al., 2004).

Mitochondrial fission is triggered by the dynamin-like GTPase Dnm1l and may involve, in addition, the ER (Otera et al., 2010). Dnm1l is nuclear-encoded and guided to the OM where it assembles into a helical oligomer via a central stalk interface. GTP hydrolysis leads to a structural rearrangement of the oligomer, which further induces constriction of the membranes (Frohlich et al., 2013).

### 2.1.5 Mitochondrial protein import

Proteins encoded by the mitochondrial genome do not use the mitochondrial import pathway but are mostly subunits of the oxidative phosphorylation machinery (Schmidt et al., 2010). Mitochondria have evolved five main pathways for the import of nuclear-encoded proteins, which all employ the TOM complex (Figure 7) (Horvath et al., 2015). The classical pathway involves recognition of positively charged amphipathic α-helices at the N-terminus of substrates, representing the presequence (Habib et al., 2007). Such proteins are recognized by TOM receptors and are

translocated through an outer membrane channel formed by Tom40. After the import, they are detected by the translocase of the inner membrane (Tim23 complex) to be guided into the matrix (Endo and Yamano, 2009; Mokranjac and Neupert, 2010). A second pathway is used to import inner membrane proteins containing an internal targeting signal, which is not removed during import (de Marcos-Lousa et al., 2006). In contrast to other pathways, the next step does not involve Tim23; instead, the substrates are bound to small TIM chaperones to be further translocated to the carrier translocase Tim22 complex (Koehler, 2004). The formation of disulfide bonds at reducing conditions within the IMS is mediated by the MIA machinery, which represents the third pathway. Proteins are transported via TOM to MIA to introduce disulfide bonds (Chacinska et al., 2004; Hell, 2008). The fourth pathway is necessary to insert β-barrel containing membrane proteins into the OM and is using the SAM complex (Hohr et al., 2015). The final pathway is essential to integrate α-helical outer membrane proteins. This process is not yet fully understood but the MIM complex promotes the insertion of such signal-anchored proteins (Becker et al., 2008). This recognition does not necessarily involve the TOM complex (Wenz et al., 2014).

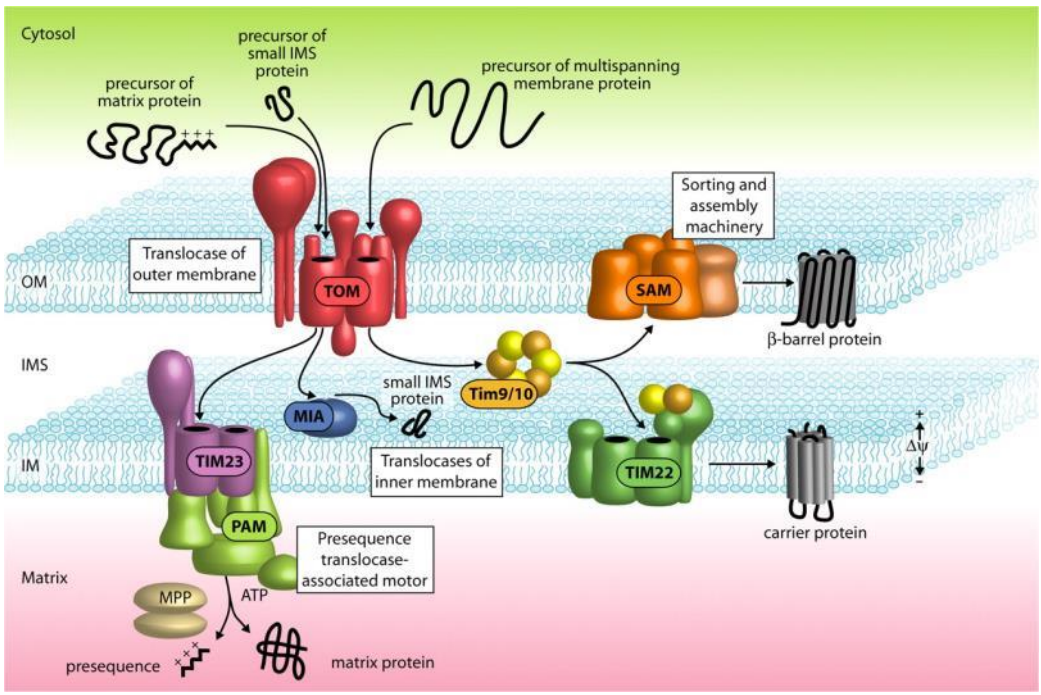


**Figure 7: Mitochondrial import of nuclear encoded proteins. Translocase of the outer membrane (TOM) regulates the import whereas the sorting and assembly machinery (SAM) integrates β-barrel proteins into the outer membrane. Translocases of the inner membrane (TIM) are gatekeepers between the inner membrane space (IMS) and the matrix. The mitochondrial intermembrane space import and assembly (MIA) machinery is necessary to introduce disulfide bonds in cysteine containing proteins. Picture taken from (Kutik et al., 2007). For the various import mechanisms, refer to the text.**

## 2.2 The MICOS complex

The identity and properties of the protein machineries controlling CJ formation are only slowly emerging. The mitochondrial contact site and cristae organizing system (MICOS) is an evolutionarily conserved multi-subunit protein assembly of the IM, which localizes to CJs and is crucial for their formation and maintenance. The MICOS complex is composed of at least six subunits in yeast that are nuclear-encoded and termed Mic10, Mic12, Mic19, Mic26, Mic27 and Mic60, where the number reflects the approximate molecular weight (Figure 9) (Harner et al., 2011; Hoppins et al., 2011; Munoz-Gomez et al., 2015a; Pfanner et al., 2014; von der Malsburg et al., 2011). In mammals two additional subunits, Mic25 and QIL1, can be found (Guarani et al., 2015).

### 2.2.1 The discovery of MICOS

The first described component of MICOS was Mic60 (Fcj1, mitofilin, IMMT or heart muscle protein (HMP)), published in 1996. It was shown, that Mic60 was exclusively found in mitochondria, containing an N-terminal mitochondrial target sequence and a coiled-coil region, exposed to the IMS (Odgren et al., 1996). One year later, evidence emerged that Mic60 is a transmembrane protein of the inner mitochondrial membrane (Gieffers et al., 1997). George B. John and colleagues observed that down-regulation of MICOS leads to increased apoptosis, abnormal IM structures and the disappearance of tubular or vesicular cristae. It was the first time suggested that Mic60 might be an organizer of the mitochondrial cristae morphology (John et al., 2005). Initially, it was thought that Mic60 is a single player in mitochondria, until it was found that it is part of a larger complex containing Sam50, metaxins 1 and 2, Mic19 and Mic25 (coiled-coil-helix coiled-coil-helix (CHCH) domain containing protein 3 and 6, respectively) (Xie et al., 2007). In 2011, the group of van der Laan identified Mic60 as part of MICOS, forming a complex with the remaining subunits, essential for mitochondrial membrane organization (von der Malsburg et al., 2011).

MICOS is an evolutionary conserved, ancient and widespread eukaryotic protein complex (Figure 8), which has an endosymbiotic origin from α-proteobacteria (Munoz-Gomez et al., 2015a; Munoz-Gomez et al., 2015b). Homologs for the majority of MICOS components were detected among animals and fungi.

Interestingly, only Mic60 and Mic10 were identified outside of these groups, which further gave evolutionary evidence that both might be core components of this complex. These results also indicate a basic cristae formation mechanism, which arose early in evolution and has remained relatively unchanged. Surprisingly, Munoz-Gomez et al identified a homolog of Mic60 present in α-proteobacteria with identical domain architecture compared to the eukaryotic variant (Munoz-Gomez et al., 2015a).

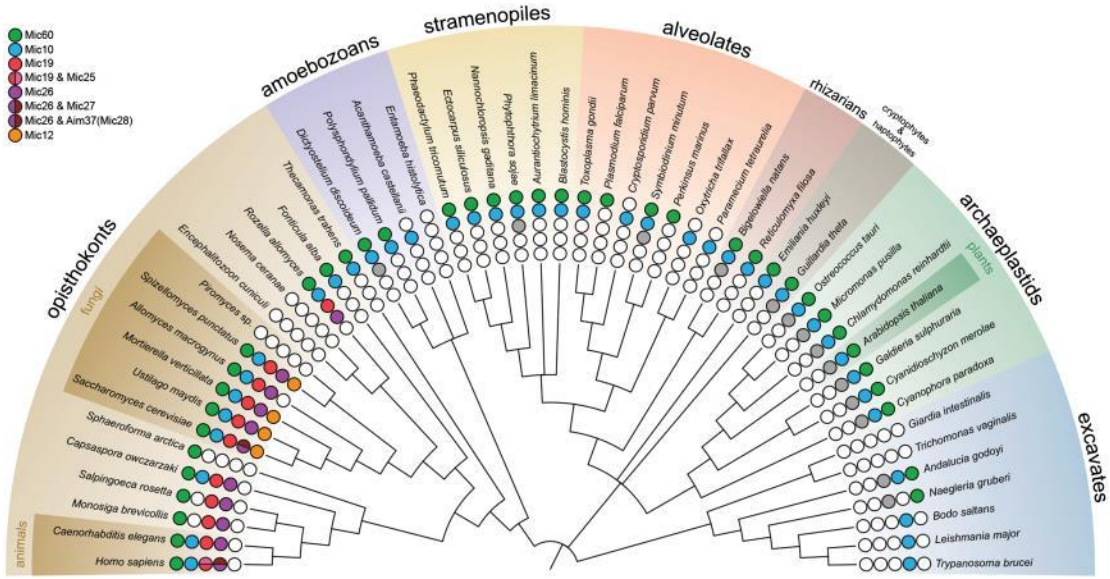


**Figure 8: Evolutionary distribution of MICOS. Homology searching methods like BLAST and HMM were used to identify MICOS subunits. Further information can be found in the original article (Munoz-Gomez et al., 2015a)**

### 2.2.2 MICOS organization and function

MICOS has a variety of functions in regulating mitochondrial IM architecture and organization. From 2011 to now, intense research efforts were directed to understand the molecular function and mechanism of MICOS, but how exactly this complex is assembled and how it maintains CJs remains unclear. So far, it is known that ablation of the MICOS core subunits Mic10 and Mic60 induces profound alterations of mitochondrial architecture: The loss of normal CJ structures leads to a detachment of cristae from the IBM and the accumulation of extended lamellar membrane stacks in the mitochondrial matrix (Alkhaja et al., 2012; Harner et al., 2011; Head et al., 2011; Hoppins et al., 2011; John et al., 2005; Mun et al., 2010; Rabl et al., 2009; von der Malsburg et al., 2011). Overexpression of Mic10 or Mic60 causes strong deformations of cristae membranes and/or crista junctions (Bohnert et al., 2015; Rabl et al., 2009).

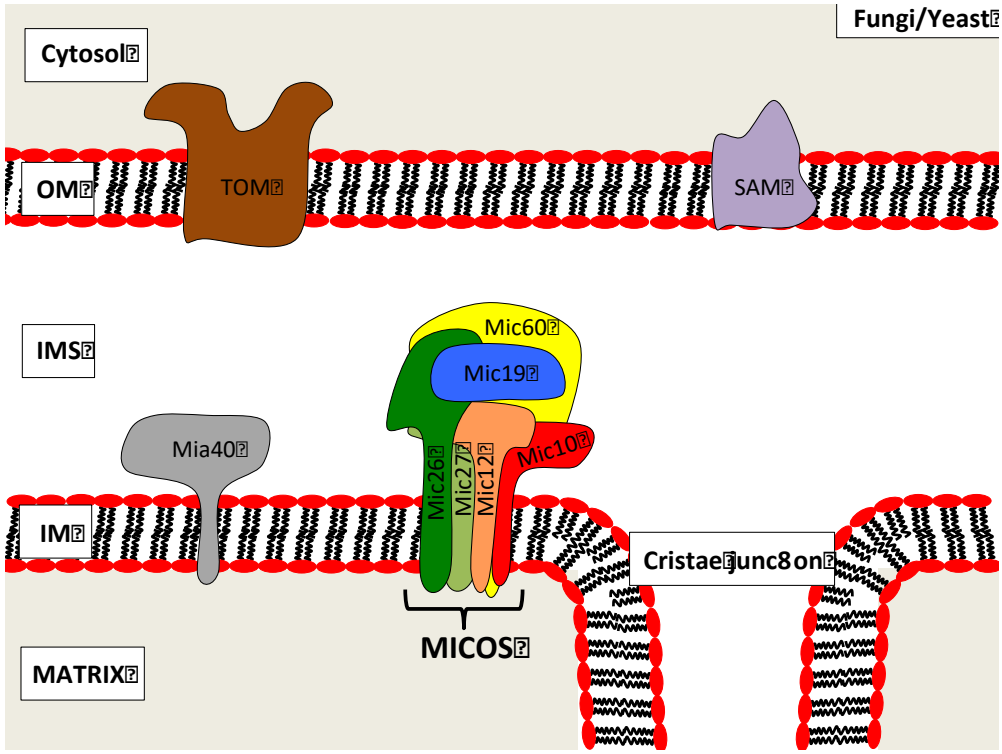


**Figure 9. In fungi/yeast the MICOS complex is composed of at least six, mainly membrane-bound proteins named Mic60 to Mic10. The MICOS complex is located in the inner mitochondrial membrane close to cristae junctions, facing the IMS. OM – outer membrane, IMS – inner membrane space, IM – inner membrane, TOM – translocase of the outer membrane, SAM – sorting and assembly machinery. Cartoon modified from (Zerbes et al., 2012b)**

Together with Mic10, Mic60 is one of the core components of MICOS and is inserted into the IM via an N-terminal transmembrane domain, yet the major part of the protein is soluble and exposed to the IMS. A central coiled-coil domain was suggested to act as a protein-protein interaction platform (Figure 10) (Darshi et al., 2011; John et al., 2005; Rabl et al., 2009; von der Malsburg et al., 2011). This domain is essential for MICOS function, as its deletion in yeast leads to growth defects and a reduced number of CJs. The conserved C-terminal mitofilin domain of Mic60 is crucial for the integrity of the MICOS complex, but its molecular function has remained unclear (Zerbes et al., 2012a). Mic60 constructs lacking the C-terminal domain are correctly localized and integrated into the membrane but induce similar growth defects and reduced number of CJs compared to ΔMic60 cells (Korner et al., 2012). Mic60 was shown to interact with partner protein complexes of the OM, like the general TOM complex and the SAM/TOB complex, mainly by its mitofilin domain. Mic60-dependent IM-OM contact sites have recently been implicated in mitochondrial lipid trafficking, a process critical for membrane remodeling (Aaltonen et al., 2016; Michaud et al., 2016). Mic60 forms a subcomplex with Mic19 (-Mic25),

which mediates the formation of direct physical contacts between both mitochondrial membrane systems and is thought to anchor CJs to the OM (Darshi et al., 2011; Ding et al., 2015; Guarani et al., 2015; Harner et al., 2011; Hoppins et al., 2011; Korner et al., 2012; Ott et al., 2015; van der Laan et al., 2016; Zerbes et al., 2012a). The molecular mechanism through which the Mic60-Mic19 subcomplex contributes to the formation of CJs is unknown.

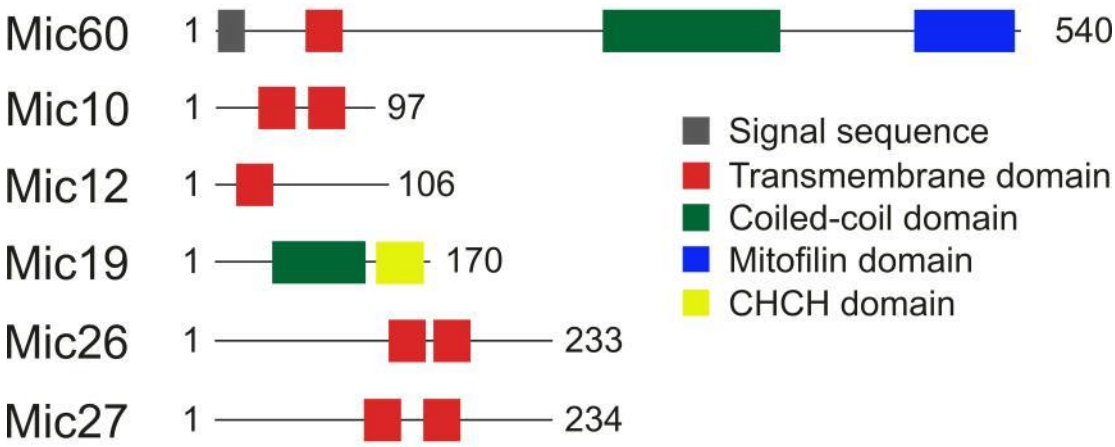


**Figure 10. The six MICOS components of yeast/fungi are illustrated. This cartoon was modified from (van der Laan et al., 2012) and Uniprot.org was used for domain identification.**

The Mic60 partner protein Mic19 is myristoylated at the N-terminus (Darshi et al., 2012): this co-translational modification can be important for protein-protein interactions and anchors proteins to the membranes (Resh, 1999). Further, Mic19 is comprised of a central coiled-coil domain and a C-terminal CHCH domain (Darshi et al., 2012). The latter contains two highly conserved cysteine residues that flank a loop region between two predicted α-helices and can form a disulfide bond *in vivo*. Mic19 of yeast and fungi are composed of a $Cx_{10}C$ motif instead of the typical $Cx_9C$ motif. Due to the reducing environment of the cytoplasm, this disulfide bond is only formed when it enters the IMS. Interestingly, the entire CHCH domain, but not the cysteine residues are essential for proper import into the mitochondria (Darshi et al., 2012). After entering the IMS, Mic19 gets oxidized by Mia40 and forms disulfide bonds, where only Mic19 containing an intramolecular disulfide bond can bind to Mic60 (Sakowska et al., 2015).

Mic10 is the second core component of MICOS and forms a second subcomplex with Mic12, Mic26 and Mic27. Mic10 is a small integral IM protein with two transmembrane domains that has recently been shown to oligomerize via conserved

glycine motifs, leading to the deformation of membranes *in vitro* and *in vivo* (Barbot et al., 2015; Bohnert et al., 2015). Accordingly, a function of Mic10 in bending the mitochondrial IM has been proposed. Not surprisingly, deletion of Mic10 leads to a similar strong mitochondrial phenotype, with less CJs and detached cristae membranes comparable to Mic60 knockout cells. Recently, it was shown that Mic10 binds the dimeric form of the $F_1F_0$-ATP synthase, which is essential for shaping the cristae rims. These results suggest a mechanism in which Mic10 supports the formation of ATP synthase oligomers and therefore plays a dual role in mitochondrial inner membrane architecture (Rampelt et al., 2017a).

Mic12 is composed of a single transmembrane helix where the main part is exposed to the IMS. It was discovered that this protein connects the Mic60 and Mic10 subcomplexes but its deletion in yeast shows a less pronounced morphological phenotype compared to Mic60 and Mic10. It is further assumed that yeast Mic12 is the human Mic12 ortholog QIL1 (Guarani et al., 2015; Zerbes et al., 2016).

Both Mic26 and Mic27 have two transmembrane helices. These proteins have a crucial role in binding lipids to form lipoproteins important for lipid transport (Alberts et al., 2002; Harner et al., 2014; Ott et al., 2015). How exactly Mic26 and Mic27 contributes to such processes remains unclear. However, the integral membrane protein Mic26 can be present in a glycosylated or non-glycosylated form and was shown to interact with Mic60, Mic10 and Mic27. Interestingly, depletion of Mic26 in yeast leads to an increased protein level of Mic27 but lower levels of Mic10. Down-regulation of Mic26 results in impaired mitochondrial respiration with only mild changes in mitochondrial morphology. In contrast, overexpression triggers swelling of the cristae and the formation of partly vesicular structures (Harner et al., 2014; Koob et al., 2015a, b). Mic27 is composed of two membrane helices with similar domain architecture as Mic26, where the main part of the protein faces the IMS. Knockdown of Mic27 only induces mild alterations to the inner membrane morphology but dramatically reduces the number of Mic10 oligomers. Mic27 is believed to be involved in the formation of stable Mic10 oligomers and therefore essential in MICOS complex organization (Ott et al., 2015; Zerbes et al., 2016).

### 2.2.3 MICOS interaction partners and related diseases

MICOS can be found in all eukaryotic cells and forms a network of interactions with other mitochondrial proteins like SAM, TOM, Mia40, TIM and many others (Figure 11) (van der Laan et al., 2016).

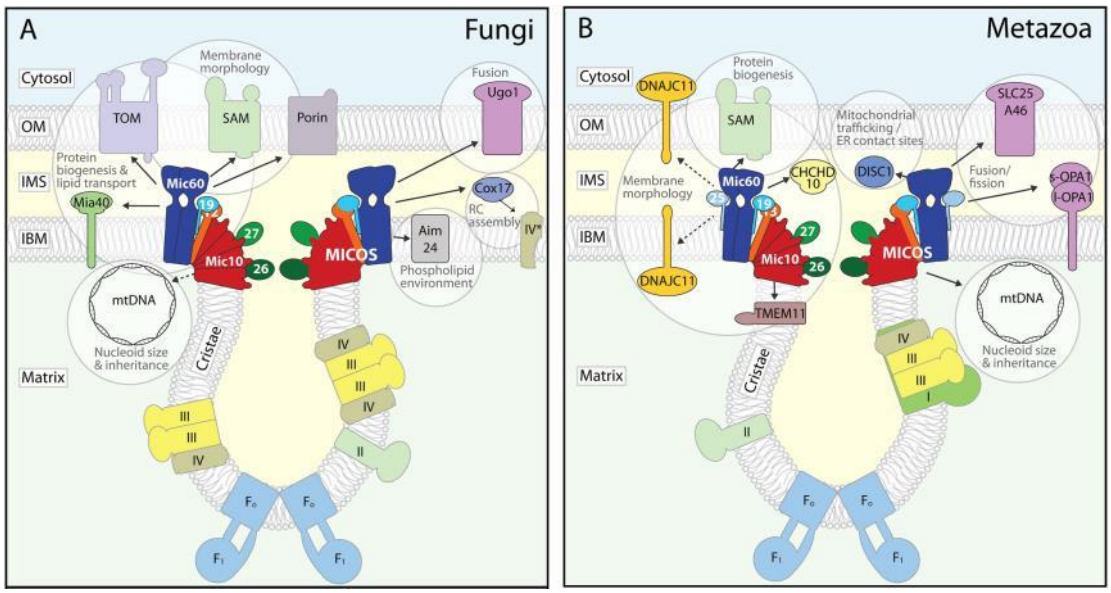


**Figure 11. The interaction network of MICOS in fungi (A) and metazoa (B) is illustrated. Interestingly, some MICOS interactions are shown to exist exclusively in metazoan or fungi. MICOS and its subcomplexes interact with proteins located in the outer mitochondrial membrane (OM), intermembrane space (IMS), inner bound membrane (IBM), cristae and also in the matrix (Rampelt et al., 2017b)**

As all MICOS components are nuclear-encoded, they must to be imported mainly by the TOM complex, which forms contact sites with Mic60 and interacts transiently with Mia40. The latter is not directly binding to TOM but promotes the import of cysteine-containing proteins. Mic60 is therefore the adapter between TOM and Mia40 and is responsible for positioning the oxidoreductase close to the exit of the TOM channel (Horvath et al., 2015). Once imported, reduced cysteines are recognized by Mia40, which introduces disulfide bonds to the target protein but is getting reduced during this process. To reactivate Mia40, electrons are taken up by the sulfhydryl oxidase Erv1 and further transported to oxidized cytochrome *c*. This reaction chain leads to the disulfide bond formation of Mia40, oxidation of Erv1 and to the reduction of cytochrome *c* (Chatzi et al., 2016).

Import of β-barrel proteins requires the sorting and assembly machinery SAM. The central component Sam50 interacts with Mic60 and Mic19 mainly via the POTRA domain (Darshi et al., 2011; Xie et al., 2007). The mitochondrial intermembrane

space bridging complex (MIB) contains MICOS and SAM and creates a second OM-IM contact site (Ott et al., 2015). TOM and SAM complexes also interact to form a supercomplex, which allows a more efficient import of β-barrel proteins (Qiu et al., 2013).

Human diseases, like neurodegenerative deafness and dystonia syndrome, are linked to a defect in the mitochondrial protein import pathway (Koehler et al., 1999). Furthermore, Mia40 and MICOS regulate the import of superoxide dismutase 1 (SOD1) mutants that causes amyotrophic lateral sclerosis (ALS) (Varabyova et al., 2013). It was further shown that human Mia40 is associated with the human branched-chain aminotransferase protein hBCATm, which acts as a redox chaperone controlling protein misfolding and aggregation. Such dysregulation is known to cause Alzheimer's disease (Chatzi et al., 2016).

Mitochondrial DNA is usually packed into DNA-protein complexes called nucleoids. As reported earlier, Mic60 is not only essential for MICOS assembly and stability but also involved in organization and inheritance of the mtDNA. Down-regulation of Mic60 leads to formation of giant mitochondria in mammals and also to nucleoids aggregates (Itoh et al., 2013; Li et al., 2016). This phenotype is known and often observed in aged or diseased mammalian cells, for example in mitochondrial cardiomyopathy (Yen and Klionsky, 2008). There is a long list of diseases (Figure 12), which are directly connected to decreased Mic60 levels like Epilepsy (Furukawa et al., 2011), Down syndrome (Myung et al., 2003), Parkinson's disease (Van Laar et al., 2009), Cancer (An et al., 2012) among others. In contrast, some diseases are caused by misregulation of proteins, which are physically interacting with MICOS. Disrupted-in-schizophrenia 1 (DISC1), for example, was shown to play an essential role in neurodevelopment including neuronal migration, neurogenesis and many others. DISC1 can be found inside of mitochondria and directly interacts with Mic60. As Mic60 is associated to the import machinery, it is speculated that the misregulation of DISC1 may be induced by a disrupted protein import (Park et al., 2010). Parkinson's disease (PD) is not only connected to reduced levels of Mic60 but also caused by a disturbed interaction of Mic60 with PTEN induced putative kinase 1 (Pink1). Pink1 contains a large serine/threonine kinase domain and is located inside and outside of the mitochondria. A proper function of Pink1 in developing dopaminergic neurons of the substantia nigra is required for normal mitochondrial

physiology but how inhibited binding to Mic60 can causes PD remains unclear (Weihofen et al., 2009).

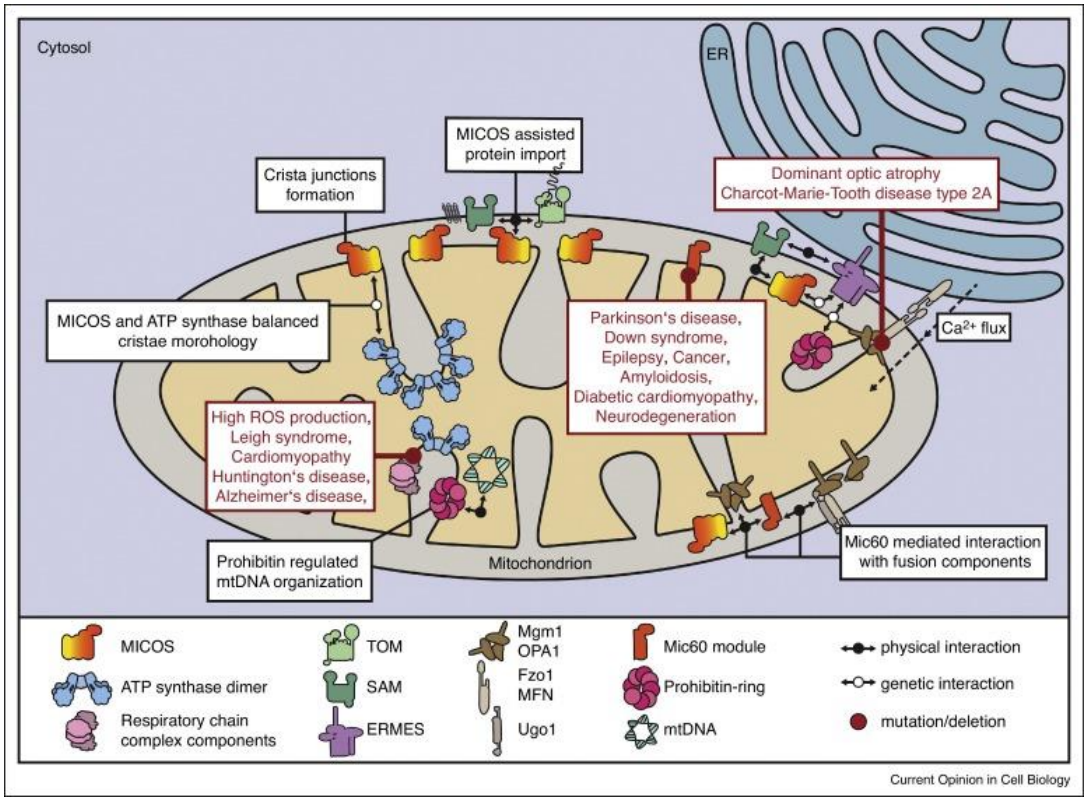


**Figure 12. The role of MICOS in health and disease. MICOS interacts physically but also genetically with a variety of proteins to fulfill crucial functions in mitochondrial fitness. Most mitochondrial diseases are linked to high or low levels of Mic60, one of the core component of MICOS (van der Laan et al., 2016).**

## 2.3 Objectives of this work

For many years, the morphology of mitochondria has been investigated in order to understand its influence on the function and maintenance of the organelle. Up to now, it is mostly unknown how cristae are formed and how their shape is controlled. It was shown that the MICOS complex has a critical role in regulating cristae shape and mitochondrial function. The aim of this thesis was to understand the molecular mechanisms of MICOS. In particular, I wanted to explore how the Mic60-Mic19 subcomplex assembles and contributes to cristae formation.

Homo- and hetero-oligomerization of MICOS components appear to mediate the assembly of the complex. Furthermore, Mic60 and Mic19 are known to form a subcomplex within MICOS. The first goal of this work was the biochemical characterization of the interaction domains in Mic60 and Mic19 and determination of quantitative binding numbers for this interaction. In this way, the exact regions crucial for MICOS assembly should be mapped as a prerequisite for the subsequent detailed functional analysis. Furthermore, I was aiming to characterize the membrane binding of Mic60 using liposome co-sedimentation assays and other biochemical methods in order to understand how the Mic60-Mic19 complex regulates mitochondrial invaginations and how it fulfills its function in mitochondria. Using a mutagenesis approach, the role of Mic60 membrane binding and complex formation with Mic19 on the morphology of cristae was explored.

As it is currently unknown how MICOS assembles and regulates cristae junctions, an understanding of this mechanism may lead to a more thorough understanding of MICOS-related diseases.

# 3 Material and Methods

## 3.1 Materials

This section contains information about the following reagents and compounds used for experiments done at the Max-Delbrück-Centrum Berlin.

### 3.1.1 Chemicals

Chemicals from the following companies were used: Roth (Karlsruhe, Germany), Sigma-Aldrich (Steinheim, Germany), Novagen (Darmstadt, Germany), Roche (Mannheim, Germany).

### 3.1.2 Enzymes

| | |
|---|---|
| DNase-I | Roche (Mannheim) |
| KOD Hot Start DNA polymerase | EMD Millipore (Darmstadt) |
| Taq DNA polymerase | New England Biolabs (Frankfurt am Main) |
| Restriction enzymes | New England Biolabs (Frankfurt am Main) |
| T4 DNA ligase | New England Biolabs (Frankfurt am Main) |

### 3.1.3 Kits

| | |
|---|---|
| innuPREP Plasmid Mini Kit | Analytikjena (Jena) |
| QIAquick gel extraction kit | QIAGEN |
| Pierce unstained protein MW marker | Thermo Fisher scientific (Hennigsdorf) |

### 3.1.4 Microorganisms

| | |
|---|---|
| *E. coli TG1* | *K12, supE,* hsdΔ5, *thi, Δ(lac-proAB), F'[traD36, proAB*$^{+}$*, lacl*$^{q}$*,* lacZΔM15] (Promega) |
| *E. coli BL21 (DE3)* | *B, F*$^{-}$*, hsdSB (rB*$^{-}$*, mB*$^{-}$*), gal, dcm. ompT, λ(DE3)* (Novagen) |

### 3.1.5 Vector

| | |
|---|---|
| pSKB_LNB | Modified pET28a plasmid (N-terminal Hexa Histag & a PreScission cleavage site, $Kan^R$) |

### 3.1.6 Protein Gels

| | |
|---|---|
| NuPAGE Bis-Tris precast gels 10 & 15 wells, 4-12% | Thermo Fisher scientific (Hennigsdorf) |
| NativePAGE Bis-Tris 10 wells, 4-16% | Thermo Fisher scientific (Hennigsdorf) |

### 3.1.7 Media and antibiotics

| | |
|---|---|
| Luria-Bertani (LB) | 10 g/l Bactotryptone, 10 g/l NaCl, 5 mM NaOH, 5 g/l yeast extract |
| Terrific Broth (TB) | 47.6 g powder + 4 ml 98% glycerol for 1 Liter medium |
| Kanamycinsulfate | 50 mg/ml, Carl Roth (Karlsruhe) |

### 3.1.8 Buffers

| | |
|---|---|
| TAE Buffer 10x | 3.72 g/l (0.01M), 12.01 g/l (0.2M), 48.46 g/l (0.4M), pH8.5 |
| Native PAGE Running Buffer (20x) | 1x used Thermo Fisher scientific (Hennigsdorf) |
| NuPAGE MES (MOPS) SDS Running Buffer (20x) | 1x used Thermo Fisher scientific (Hennigsdorf) |

## 3.2 Molecular biology methods

This section contains information about the molecular biological methods performed by me at the Max-Delbrück-Centrum Berlin.

### 3.2.1 Synthesis of cDNA

Codon-optimized cDNAs of Mic60 and Mic19 of *C. thermophilum* (UniProtID: G0SHY5 and G0S140, respectively) were commercially synthesized (Eurofins MWG).

### 3.2.2 Agarose gels

1% agarose gels were prepared and run at 100V and constant ampere for 50 minutes using 1x TAE buffer.

### 3.2.3 Isolation of plasmid DNA

DNA was isolated using innuPREP Plasmid Mini Kit (Analytikjena) according to the manufacturer's protocol.

### 3.2.4 Polymerase chain reaction (PCR)

Amplification of DNA fragments was done using KOD Hot Start DNA Polymerase (EMD Millipore) according to manufacturer's suggestions. PCR products were purified by running an agarose gel and extracted using QIAquick gel extraction kit (QIAGEN), according to the manufacturer's protocol.

### 3.2.5 DNA digestion

DNA was digested using enzymes from New England Biolabs (Frankfurt am Main) following the manufacturer's protocol. Digested products were purified using QIAquick gel extraction kit (QIAGEN), according to the manufacturer's protocol.

### 3.2.6 Ligation

DNA concentrations were determined by the UV/Vis method using a NanoDrop2000 (Thermo Scientific). Ligation was performed using 20 ng of Vector with a six fold molar excess of insert at room temperature for 2-4 hours using T4 DNA ligase (New England biolabs) according to the manufacturer's protocol.

### 3.2.7 Competent cells

Competent cells were prepared according to Seidman et al (http://www.openwetware.org/wiki/Gill:Calcium_chloride_competent_cells) with slight modifications. In brief, 100 ml LB medium was inoculated with 1 ml preculture and grown at 37 °C until an $OD_{600}$ of 0.6. The culture was incubated for 10 min on ice, pelleted at 1200 x g for 10 min at 4 °C, resuspended in 10 ml ice cold 0.1 M $CaCl_2$/10% glycerol, flash frozen in liquid nitrogen and stored at -80 °C.

### 3.2.8 Transformation

Transformation was performed using the heat shock method according to Sambrook et al (Sambrook et al., 1989).Ligated DNA was transformed in *E. coli TG1*, grown in LB-medium at 37 °C and isolated as already described. For protein expression, isolated DNA was transformed into *E. coli BL21 (DE3).*

### 3.2.9 Bacteria storage

1ml of the overnight culture was supplemented with 0.5 ml of 96% glycerol and stored at -80 °C.

### 3.2.10 Site directed mutagenesis

Site directed mutagenesis protocol and primer design was carried out using an already established protocol (Liu and Naismith, 2008) or overlap PCR.

### 3.2.11 DNA sequencing

DNA sequencing was done according to the company's protocol (Source Bioscience, Berlin) using their primers.

### 3.2.12 Constructs

**Table 1. List of used constructs. *H. sapiens* (h.s.), *S. cerevisiae* (s.c.), *C. thermophilum* (c.t.).**

| Protein | Species | Remark |
|---|---|---|
| Mic60_197-758 | h.s. | expressed partially soluble |
| Mic19_1-227 | h.s. | expressed insoluble |
| Mic60_74-538 | s.c. | expressed insoluble |
| Mic19_1-170 | s.c. | expressed soluble |
| Mic60_149-691 | c.t. | expressed soluble (high impurity) |
| Mic60_208-691 | c.t. | expressed soluble |
| Mic60_208-608 | c.t. | expressed soluble |
| Mic60_208-562 | c.t. | expressed soluble |
| Mic60_208-582 | c.t. | expressed soluble |
| Mic60_208-691ΔLBS1 | c.t. | expressed soluble |
| Mic60_208-691_R572D | c.t. | expressed soluble |
| Mic60_208-691_F573D | c.t. | expressed soluble |
| Mic60_208-691_RF572-573DD | c.t. | expressed soluble |
| Mic60_564-691 | c.t. | expressed insoluble |
| Mic60_623-692 | c.t. | expressed soluble but precipitated during concentration |
| Mic19_1-164 | c.t. | expressed soluble |
| Mic19_116-164 | c.t. | expressed soluble |
| Mic19_39-113 | c.t. | expressed soluble |
| Mic19_1-164_C132S | c.t. | expressed soluble |
| Mic19_1-164_C143S | c.t. | expressed soluble |
| Mic19_1-164_C132S,C143S | c.t. | expressed soluble |

## 3.3 Biochemical methods

### 3.3.1 Sequence alignment

Sequences were aligned using Clustal Omega (Sievers et al., 2011) and manually adjusted using Genedoc (Nicholas, 1997)

### 3.3.2 SDS- and Native-PAGE

Protein separation was performed using denaturing and non-denaturing, continuous SDS-polyacrylamide gel electrophoresis (SDS-PAGE). The protein weight and oligomeric states were estimated using Native PAGE. For reducing conditions, the loading-dye was supplemented with β-mercaptoethanol.

### 3.3.3 Expression and purification

All constructs were expressed in *Escherichia coli* BL21 DE3 cells. Bacteria were cultured in TB medium at 37 °C to an $OD_{600}$ of 0.6 followed by a temperature shift to 18 °C. Protein was expressed for 18 h by adding 200 µM isopropyl β-D-1-thiogalactopyranoside (IPTG). Cells were harvested by centrifugation, resuspended in lysis buffer containing 50 mM HEPES pH 7.5, 500 mM NaCl, 1 µM DNase (Roche) and 100 µM Pefabloc (Roth), and lysed by a microfluidizer (Microfluidics). Lysates were cleared by centrifugation at 40,000 x g for 45 min at 4°C. The supernatant was passed through 0.45 µm filters and applied to a 5 ml NiNTA column pre-equilibrated with 50 mM HEPES/NaOH pH 7.5, 500 mM NaCl, 20 mM imidazole. The column was extensively washed with this buffer. $His_6$-tagged protein was eluted with 50 mM HEPES/NaOH pH 7.5, 500 mM NaCl, 300 mM imidazole. The $His_6$-Tag was cleaved by adding His-tagged PreScission protease and dialyzed against 50 mM HEPES/NaOH pH 7.5, 500 mM NaCl overnight at 4 °C. The protein was re-applied onto the Ni-NTA column equilibrated to remove His-tagged protein. Unbound protein was concentrated and further purified by size-exclusion chromatography (SEC) using a Superdex-300 column for Mic60 and a Superdex-200 column (both from GE Healthcare) for Mic19 with 20 mM HEPES/NaOH pH 7.5, 150 mM NaCl as the running buffer. Protein fractions were pooled, concentrated and flash frozen in liquid nitrogen.

### 3.3.4 Analytical ultracentrifugation experiments

The following protocol was established and performed by Dr. Hauke Lilie (Martin Luther University Halle Wittenberg) using Mic60 from *Chaetomium thermophilum*, expressed and purified by me.

All measurements were performed in 20 mM HEPES/NaOH pH 7.3, 150 mM NaCl at 7 °C using an Optima XL-A centrifuge (Beckman, Palo Alto, CA) and an An50Ti rotor equipped with double sector cells. Depending on protein concentration, the distribution of the protein in the cell was monitored at 230 or 280 nm. Data were analyzed using the software SedFit(Schuck, 2000). Sedimentation velocity was run at 40,000 rpm for 3.5 h, sedimentation equilibrium was performed at 9,000 rpm.

### 3.3.5 Liposome co-sedimentation assay

Folch liposomes (total bovine brain lipids fraction I, Sigma) were dried under Argon stream and solubilized in 20 mM HEPES/NaOH pH 7.5, 150 mM NaCl. Liposomes at a final concentration of 1 mg/ml were incubated with 15 µM protein for 10 min at room temperature in a 40 µl reaction volume, followed by a 200,000 x *g* spin for 10 min at 20 °C (see also http://www.endocytosis.org).

### 3.3.6 Liposome tubulation by negative stain electron microscopy

Liposome deformation assays were done by mixing 10 µM of the Mic60 and/or 20 µM of the Mic19 constructs in 20 mM HEPES/NaOH, pH 7.5, 150 mM NaCl with Folch liposomes in a 20 µl reaction volume at final liposome concentrations of 0.8 mg/ml. Upon incubation for 30 min at room temperature, the sample was spotted onto carbon-coated grids and stained with 2% (w/v) uranyl acetate. Images were taken on a Zeiss EM910.

Liposome tubulation was quantified by counting the number of tubulated and non-tubulated liposomes (diameter ≥120 nm) from three different images (47 µm x 30 µm) Mic60 variant. If membrane tubules were observed, their outer diameter was measured at 3-5 positions, and at least 20 tubules per construct were quantified. The branching efficiency of each mutant was assessed by counting the number of branches per tubule for at least 20 tubules in each image field (47 µm x 30 µm).

### 3.3.7 Slicing yeast cells for negative stain electron microscopy

The following protocol was established and performed by Dr. Séverine Kunz and Dr. Bettina Purfürst form the electron core facility at the MDC-Berlin.

To prepare samples for cryo-ultramicrotomy, yeast cells were fixed for 3 h with 4% (w/v) paraformaldehyde, 0.5% (v/v) glutaraldehyde in 0.1 M citrate buffer (pH and temperature adjusted to growth conditions) (Vogel et al., 2006). Samples were treated with 1% (w/v) sodium metaperiodate for 1 hour at room temperature. Yeast cells were embedded in 10% (w/v) gelatin, infiltrated with 2.3 M sucrose and frozen in liquid nitrogen. Ultrathin sections were cut at - 90 °C (Reichert Ultracut S, Leica) and collected on 100 mesh copper grids (Plano) coated with formvar and carbon. Sections were stained with 3% (w/v) tungstosilicic acid hydrate in 2.5% (w/v) polyvinyl alcohol. Dried grids were imaged with a transmission electron microscope (EM910, Zeiss) and acquisition was done with the iTEM software on a CDD camera (Quemesa, Emsis)

### 3.3.8 CD measurements

Mic60 and Mic19 constructs were dialyzed against 20 mM sodium phosphate buffer pH 7.5 and 150 mM NaF and diluted to 0.2 mg/ml. CD measurements were performed in three replicates at 20 °C in a Chirascan CD spectrometer (Applied Photophysics).

### 3.3.9 Isothermal titration calorimetry

ITC experiments were performed at 10 °C in a VP-ITC (Microcal) in 20 mM HEPES/NaOH pH 7.5, 150 mM NaCl. The Mic60 concentration in the reaction chamber was around 40 µM and the Mic19 concentration in the syringe was approximately 450 µM. Microcal ORIGIN software was used to integrate the binding isotherms and calculate the binding parameters.

### 3.3.10 Liposome leakage assays

The following protocol was established and performed by Audrey H. Xavier from the MDC-Berlin using Mic60 and Mic19 variants from *Chaetomium thermophilum*, expressed and purified by me.

An existing protocol (Michaud et al., 2016) was modified as follows: 2.5 mg Folch lipids were dried under vacuum for at least 3 hours and resuspended in 20 mM HEPES/NaOH, pH 7.5, 100 mM NaCl, 180 mM sucrose supplemented with 12.5 mM of the fluorescent dye ANTS (8-aminonaphtalene-1,3,6-trisulfonic acid) and 25 mM of its contact quencher DPX (p-xylene-bis-pyridinium bromide) (Sigma-Aldrich). The lipid suspension was incubated for 1 h at room temperature while repeatedly vortexed and then sonicated in a water bath for 30 sec. Liposomes were extruded at least 11 times with 0.4 µm filters and centrifuged at 12,000 x g, for 10 min at room temperature. The liposome pellet was resuspended in 20 mM HEPES/NaOH pH 7.5, 100 mM NaCl at a concentration of 1 mg/ml. Dye release was measured in a 96 well plate with 1 mg/ml liposomes containing ANTS and DPX and 50 nM protein concentration in a 100 µl reaction per well, using a FLUOstar Optima plate reader (BMG Labtech) (excitation wavelength 355 nm, emission wavelength 520 nm). As a positive control, 1% Triton X-100 (final concentration) was added. Data were normalized relative to the first data point. Averages were calculated from three independent experiments, each containing 2-3 parallel reactions

### 3.3.11 Yeast strains and plasmids

The following protocol was established and performed by Dr. Ralf M. Zerbes (University of Freiburg) and Dr. Heike Rampelt (University of Freiburg).

*Saccharomyces cerevisiae* strains used in this study are derivates of YPH499 (ref. (Sikorski and Hieter, 1989)). $Mic60_{ProtA}$, *mic60*Δ and $Mic60_{ProtA}$*mic19*Δ strains as well as the pRS426 plasmid encoding *MIC19* have been described before (von der Malsburg et al., 2011). Strains expressing the lipid binding deficient Mic60 variants $Mic60\_LBS1\Delta_{ProtA}$ and $Mic60\_RW433\text{-}434DD_{ProtA}$ were generated by replacing the *MIC60* open reading frame by a cassette encoding the Mic60 variants followed by a tobacco etch virus (TEV) protease cleavage site, a protein A moiety, and a *HIS3* marker gene.

### 3.3.12 Growth of yeast cells and mitochondrial isolation

The following protocol was established and performed by Dr. Ralf M. Zerbes (University of Freiburg) and Dr. Heike Rampelt (University of Freiburg).

For isolation of mitochondria, cells were grown either in YPG medium (1% (w/v) yeast extract, 2% (w/v) peptone, 3% (v/v) glycerol) or synthetic minimal medium (0.67% (w/v) yeast nitrogen base, 0.07% (w/v) CSM -URA amino acid mix, 3% (v/v) glycerol, 0.1% (w/v) glucose) at 30 °C. Mitochondria were isolated by differential centrifugation. To assess respiratory growth, yeast cells were grown either in YPG medium or on synthetic minimal medium, respectively, washed in $dH_2O$, and subsequently serial dilutions were spotted on to either SC lactate plates (0.67% (w/v) yeast nitrogen base without amino acids, 0.2% (w/v) synthetic complete mix, 2.5% (w/v) bacto-agar, 0.05% (w/v) $CaCl_2$, 0.06% (w/v) $MgCl_2$, 0.1% (w/v) $KH_2PO_4$, 0.1% (w/v) $NH_4Cl$, 0.05% (w/v) NaCl, 0.8% (w/v) NaOH, 2% (v/v) lactic acid) or synthetic minimal lactate plates (0.67% (w/v) yeast nitrogen base without amino acids, 0.07% (w/v) CSM -URA amino acid mix, 2.5% (w/v) bacto-agar, 0.05% (w/v) $CaCl_2$, 0.06% (w/v) $MgCl_2$, 0.1% (w/v) $KH_2PO_4$, 0.1% (w/v) $NH_4Cl$, 0.05% (w/v) NaCl, 0.8% (w/v) NaOH, 2% (v/v) lactic acid). For electron microscopy, cells were grown for 24 h at 30 °C in synthetic complex medium(van Dijken et al., 1976) with 0.07% (w/v) CSM amino acid mix including all amino acids or lacking uracil, 2% (v/v) L-lactate pH 5.0 and 0.1% (w/v) glucose. Subsequently, cells were diluted into media lacking glucose and grown over night at 30 °C.

### 3.3.13 Affinity purifications

The following protocol was established and performed by Dr. Ralf M. Zerbes (University of Freiburg) and Dr. Heike Rampelt (University of Freiburg).

For affinity purification of Protein A-tagged proteins, mitochondria were solubilized in solubilization buffer (20 mM Tris-HCl pH 7.4, 50 mM NaCl, 0.1 mM EDTA, 10% (v/v) glycerol, 1% (w/v) digitonin, 2 mM PMSF, 1x EDTA-free Protease Inhibitor Cocktail [Roche]). Subsequently non-solubilized material was removed by centrifugation before mitochondrial extracts were incubated with pre-equilibrated human IgG-coupled Sepharose beads (1.5 h, 4 °C). After extensive washing of the beads with washing buffer (20 mM Tris-HCl pH 7.4, 60 mM NaCl, 0.5 mM EDTA, 10% (v/v) glycerol, 0.3% (w/v) digitonin, 2 mM PMSF), bound proteins were eluted either by TEV protease cleavage or SDS. Samples were analyzed by SDS-PAGE.

### 3.3.14 Respiratory chain complex activity measurements

The following protocol was established and performed by Dr. Ralf M. Zerbes (University of Freiburg) and Dr. Heike Rampelt (University of Freiburg).

Complex III and IV activities were measured spectrophotometrically. Complex III activity measurements were carried out in complex III assay buffer (120 mM KCl, 11 µM oxidized cytochrome *c* (from equine heart), 5 mM malate, 5 mM pyruvate, 5 mM succinate, 0.5 mM NADH, 10 mM Tris-HCl, pH 7.4) and started by the addition of intact mitochondria that were pretreated with 10 mM KCN to inhibit complex IV activity. Reduction of cytochrome *c* by complex III was measured as an increase in absorbance at 550 nm. Mitochondria pretreated with 8 µM Antimycin A served as negative control. Complex IV activity measurements were performed in complex IV assay buffer (120 mM KCl, 11 µM reduced cytochrome *c* (from equine heart), 10 mM Tris-HCl, pH 7.4) and initiated by the addition of Triton X-100 (0.5 % (v/v) in reaction buffer) solubilized mitochondrial membranes. Cytochrome *c* was fully reduced with 0.5 mM DTT prior to addition to the assay buffer. Oxidation of cytochrome *c* by complex IV was measured as decrease in absorbance at 550 nm. Triton X-100 solubilized mitochondrial membranes pretreated with 10 mM KCN served as negative control.

# 4 Results

The majority of the results reported in this thesis have already been published in (Hessenberger et al., 2017). http://dx.doi.org/10.1038/ncomms15258

## 4.1 Characterization of Mic60 and Mic19

### 4.1.1 Expression and purification

Mic60 and Mic19 are composed of specific domains (Figure 13). Mic60 has an approximate molecular weight of 60 kDa and is composed of an N-terminal transmembrane domain, a central coiled-coil domain and a highly conserved mitofilin domain. Mic19 is the only soluble member of MICOS and has a central coiled-coil domain, a C-terminal coiled-coil helix coiled-coil helix (CHCH) domain and an approximate molecular weight of 20 kDa.

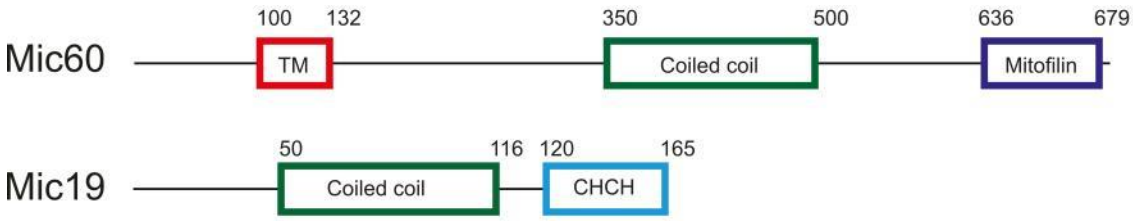


**Figure 13. Domain architecture of Mic60 (A) and Mic19 (B). TM - transmembrane domain; CHCH - coiled-coil-helix coiled-coil-helix domain**

For a biochemical characterization of the proteins, an expression protocol for Mic60 and Mic19 was established (see 3.3.3). Initial constructs employed the yeast and human Mic60 and Mic19 sequences, but it turned out that yeast Mic60 and human Mic19 were both insoluble when expressed in bacteria and could therefore not be used for this study (see 3.2.12). Instead, Mic60 and Mic19 of the thermostable fungus *Chaetomium thermophilum* were chosen for further experiments.

The cDNAs of both proteins were commercially synthesized (see 3.2.1 and appendix) and expressed in *E. coli* as His-tagged fusion proteins (see 3.3.3). Following affinity purifications, high yields were obtained using constructs $Mic60_{sol}$ (ΔN-terminus, residues: 208-691) and Mic19 (Residues: 1-164) (see 3.2.12). Upon cleavage of the

His-tag by Prescission protease, the proteins were further purified by size-exclusion chromatography (SEC). An example of the purifications is shown in Figure 14A-B. Circular dichroism (CD) measurements indicated that both proteins have a mostly α-helical content, pointing to their correct folding (Figure 14C, see 3.3.8).

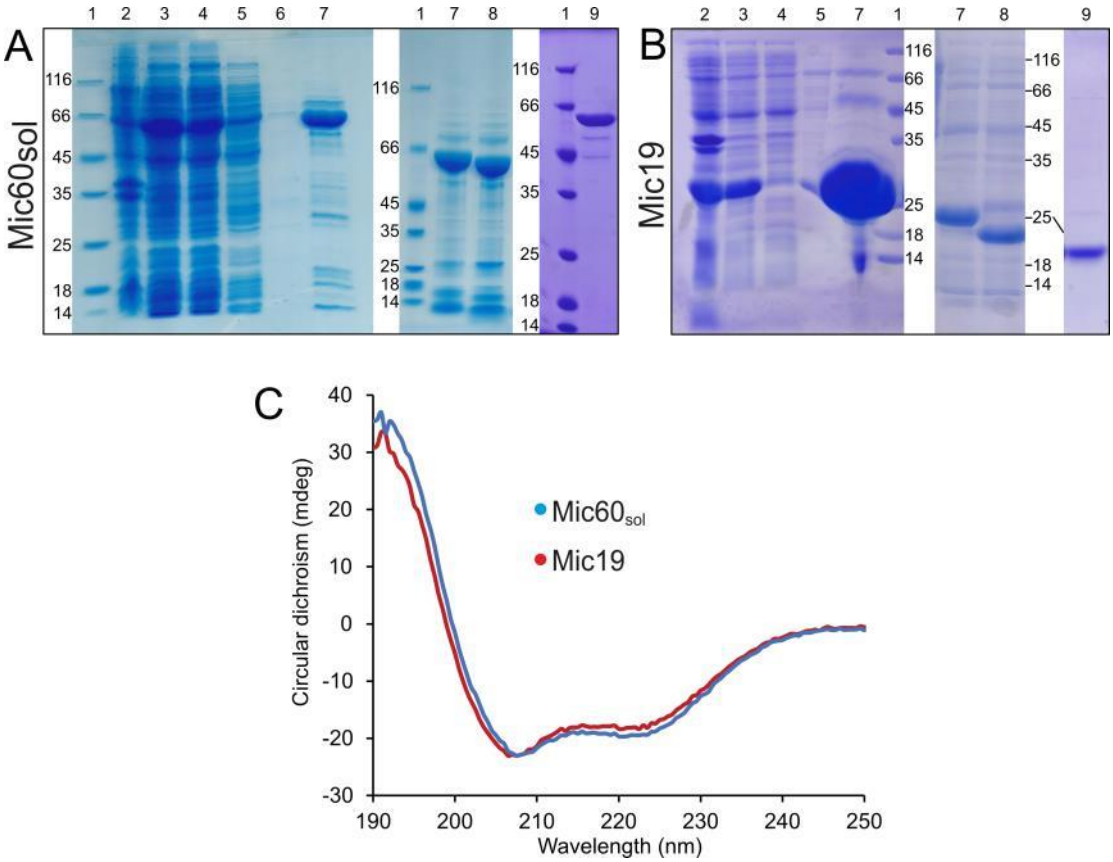


**Figure 14. Purification of His-tagged Mic60 (A) and Mic19 (B) using immobilized metal affinity chromatography (IMAC) and size exclusion chromatography (SEC). Fractions were analyzed by SDS-PAGE. (1) protein ladder (numbers indicate the molecular weight in kDa), (2) pellet, (3) supernatant, (4) flowthrough, (5) wash I (70ml), (6) wash II (30ml), (7) elution, (8) protein after His-tag removal by Prescission protease, (9) pooled SEC fractions. (C) CD measurements of $Mic60_{sol}$ and Mic19 analyzed in this study indicated a mostly α-helical fold, as seen by the negative bands at 208 and 222 nm.**

### 4.1.2 Biochemical characterization of Mic60 and Mic19

During the SEC runs, it became obvious that Mic60 and Mic19 form higher molecular weight species. Especially, Mic60 was not running at the expected retention volume of a monomer (Figure 15A) but eluted earlier indicating a higher oligomeric species. However, as the coiled-coil domain might be present in an elongated form, SEC is not an adequate method to analyze the precise oligomeric state. Therefore, native PAGE (see 3.3.2) and AUC (see 3.3.4) were used in addition.

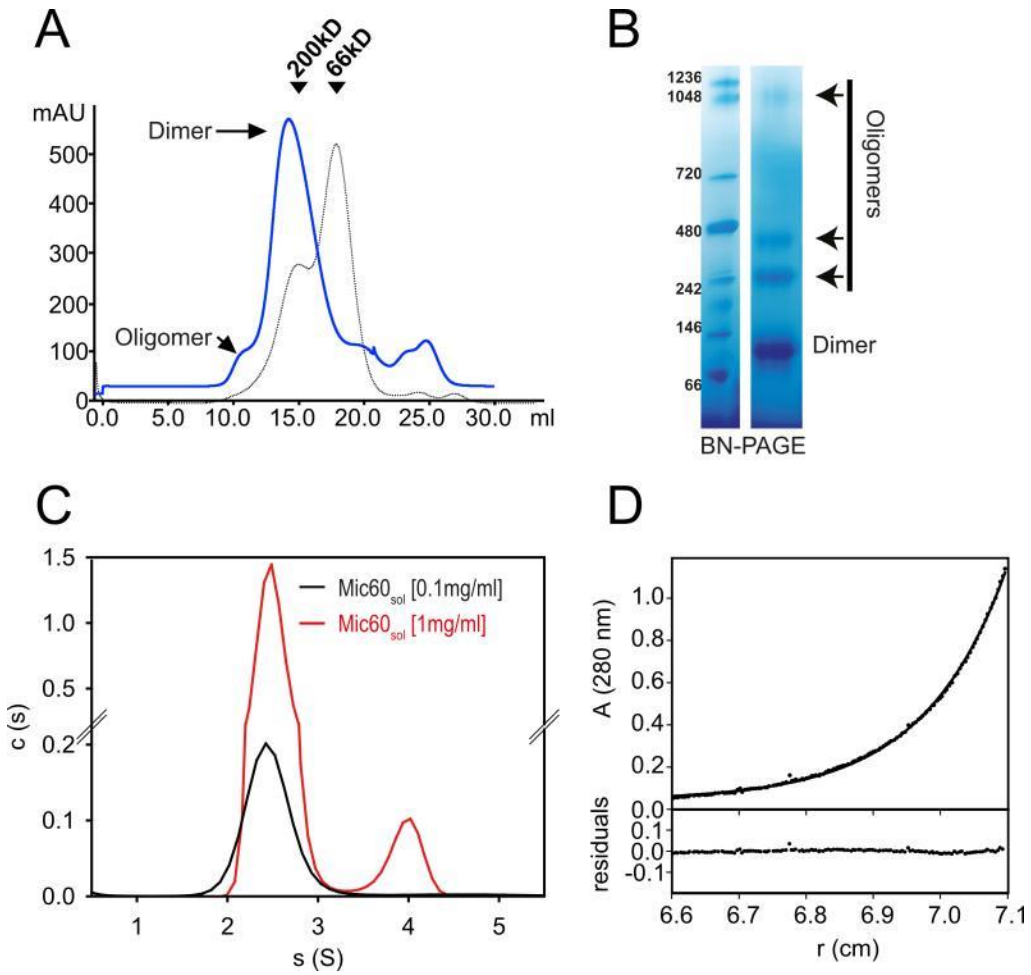


**Figure 15. Biochemical characterization of $Mic60_{sol}$. (A) SEC profile of $Mic60_{sol}$ (blue) revealed that Mic60 runs as a higher molecular weight species, which may indicate an extended coiled-coil structure. Arrowheads represent molecular weight standards (dashed line); Bovine albumin (66 kD); Rabbit muscle myosin (200 kD). (B) BN-PAGE analysis of $Mic60_{sol}$ indicates a mainly dimeric species. Arrows indicate higher-order oligomers. Numbers indicate the molecular weight in kDa (C) Sedimentation velocity analysis of $Mic60_{sol}$ at a protein concentration of 0.1 mg/ml using AUC results in a homogenous species with a sedimentation coefficient *s*(app)=2.43±0.08S (black). At a concentration of 1 mg/ml, an additional higher oligomeric species (8%) with *s*(app) of ~4 S appears. (D) Sedimentation equilibrium of $Mic60_{sol}$ at a protein concentration of 0.1 mg/ml yields a relative molecular mass of Mr=109±10 kDa, which corresponds to a dimer. The upper panel shows the experimental data (dots) and the fit (solid line), the lower panel displays the deviation of data and fit. Experiments in C and D were carried out by Haucke Lilie with proteins prepared by me.**

In agreement with earlier reports (John et al., 2005; Rabl et al., 2009), $Mic60_{sol}$ was predominantly dimeric in blue native (BN) PAGE, while a smaller fraction assembled into higher-order oligomers (Figure 15B). Sedimentation velocity and equilibrium analytical ultracentrifugation (AUC) experiments were performed by our collaboration partner Hauke Lilie (Universität Halle-Wittenberg) and confirmed that the predominant species of $Mic60_{sol}$ is a stable dimer (measured relative molecular weight (Mr) 109 +/- 10 kDa, theoretical Mr of the dimer: 109 kDa) in the

concentration range of 0.02-2 mg/ml (Figure 15C-D). The measured sedimentation velocity of 2.4 S is very small for a 109 kDa dimeric $Mic60_{sol}$ and indicative of a highly elongated protein structure, consistent with the predicted high coiled-coil content of $Mic60_{sol}$. At a concentration of 1 mg/ml and higher, an additional species with an apparent sedimentation velocity of approximately 4 S appeared (Figure 15C), probably reflecting the capability of $Mic60_{sol}$ to form higher oligomeric structures.

Mic19 shows a gelfiltration profile with two dominant peaks, reflecting dimers and monomers (Figure 16). Non-reducing SDS-PAGE (see 3.3.2) revealed that the dimers depend on the formation of an intermolecular disulfide bridge using conserved cysteines located in the CHCH domain (Figure 16B). Interestingly, even higher molecular weight species were observed on reducing and non-reducing SDS-PAGE.

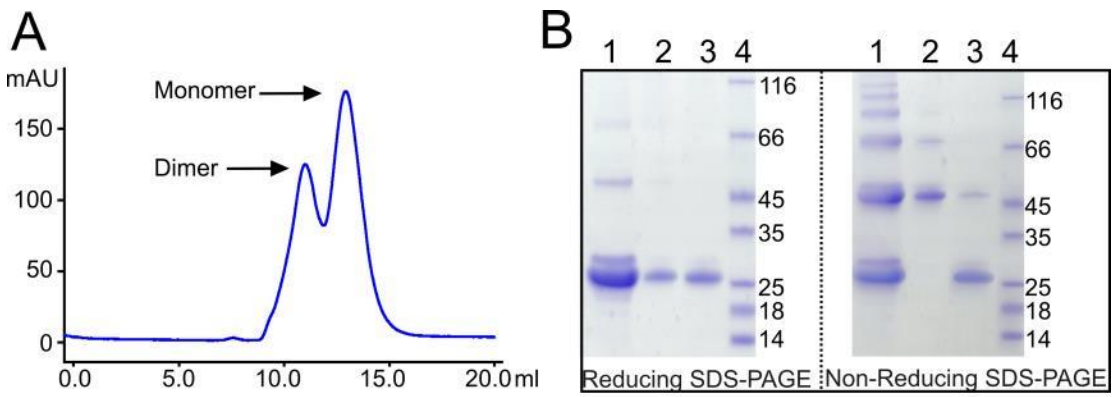


**Figure 16. (A) Gelfiltration profile of Mic19 shows two peaks representing dimers and monomers, according to the retention volume. (B) Reducing SDS-PAGE (left) and Non-Reducing SDS-PAGE (right) confirmed higher oligomeric species, sensitive to reducing agents. (1) Injected Mic19 on the SEC column, (2) fraction of the first peak (Dimer), (3) fraction of the second peak (Monomer), (4) protein ladder (numbers indicate the molecular weight in kDa).**

### 4.1.3 Oligomerization mode of Mic19

Sequence alignment of the Mic19_CHCH domain of different species revealed the presence of conserved cysteines, flanking the loop between two predicted alpha helices. Interestingly, fungi and yeast only contain two cysteines (Figure 17A), whereas in other species four are present. As shown in Figure 16 the CHCH domain can form intermolecular disulfide bridges *in vitro* which results in the formation of higher oligomers. To test the role of these cysteines, they were mutated to serines and the resulting constructs analyzed by SEC. In the absence of reducing agents (see

3.3.2) the single mutation C132S resulted in a pure peak representing a dimer (Figure 17B). This may indicate that in the absence of a cysteine at position 132, Cys143 becomes more reactive to mediate the formation of an intermolecular disulfide bridge. In the absence of any cysteine in the C132S/C143S mutant, Mic19 was a pure monomer. Accordingly, stable dimer formation depends on the presence of only one cysteine residue in the CHCH domain as replacement of both cysteines in the mutant resulted in a purely monomeric variant.

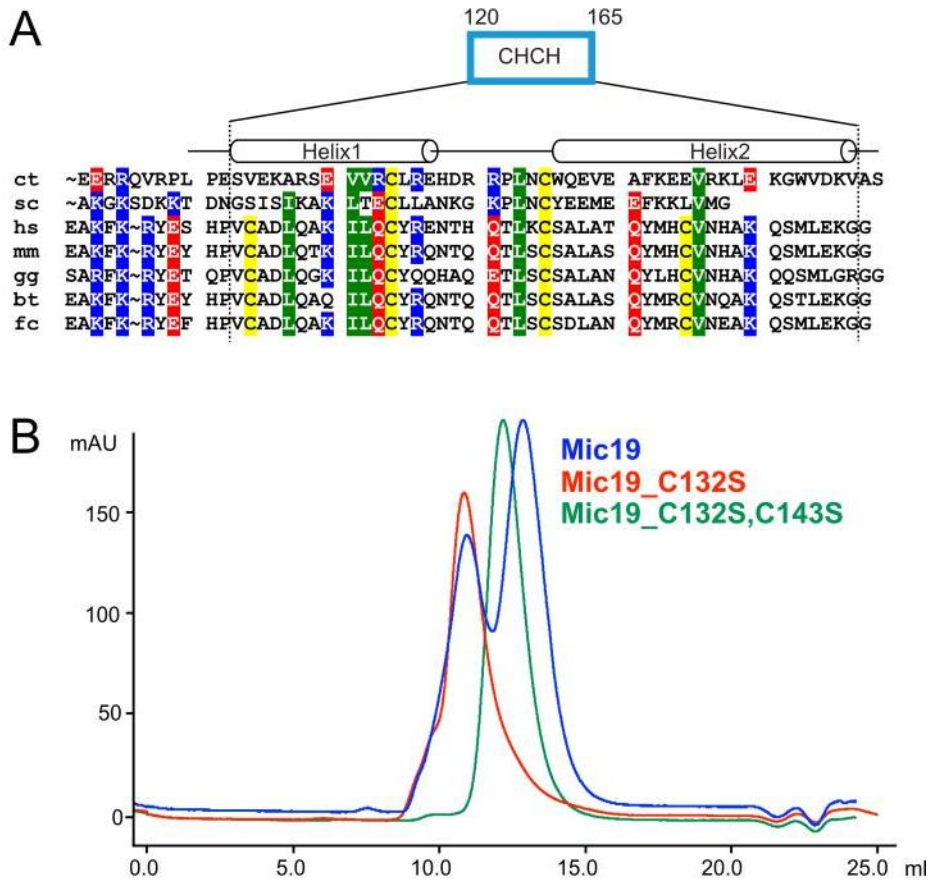


**Figure 17. Analysis of the conserved cysteines of Mic19. (A) Sequence alignment of Mic19 CHCH, coiled-coil-helix coiled-coil-helix domain. Sequences of Mic19 from *C. thermophilum* (ct), *S. cerevisiae* (sc), *H. sapiens* (hs), *M. musculus*(mm), *B. Ta urus* (bt), *G. gallus* (gg), and *F. catus* (fc) were aligned. Cysteines within the CHCH domain are marked in yellow, positively charged residues in blue; negatively charged residues in red, hydrophobic residues in green. (B) Gelfiltration profile of Mic19 (blue), Mic19_C132S (red) and Mic19_C132S,C143S (green) on a Superdex 200 column, revealed its oligomerization potential by forming disulfide bridges.**

### 4.1.4 Oligomerization mode of Mic60

To identify the domain or the region, which regulates the oligomerization of Mic60, several truncated constructs were tested in native PAGE analyses (see 3.3.2). A

publication from the Reichert lab (Korner et al., 2012) suggests that a decisive motif for oligomerization might be the highly conserved mitofilin domain. To test this assumption, two constructs were tested, one lacking the mitofilin domain ($Mic60_{sol}\Delta Mito$; 208-608) and the second additionally the linker between the mitofilin and coiled-coil domain ($Mic60_{sol}\Delta Mito\Delta LBS$; 208-562). The native PAGE clearly showed that both constructs were not affected in its oligomerization (Figure 18). These data indicate that the coiled-coil domain is actively involved in this process.

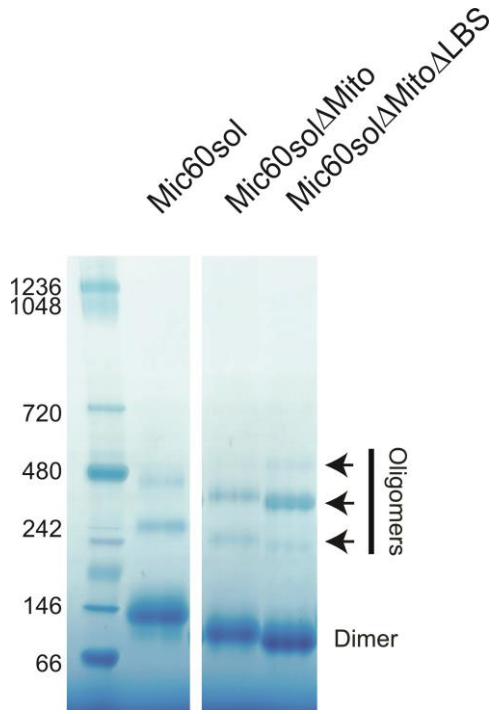


**Figure 18. BN-PAGE analysis of $Mic60_{sol}$ indicates a mainly dimeric species. $Mic60_{sol}$ variants with either a deletion of the mitofilin domain ($Mic60_{sol}\Delta Mito$) or the isolated coiled-coil ($Mic60_{sol}\Delta Mito\Delta LBS$) did not influence the oligomerization potential. Arrows indicate higher-order oligomers numbers the molecular weight in kDa.**

## 4.2 The function of Mic60

### 4.2.1 Mic60 liposome binding

To characterize a possible function of $Mic60_{sol}$ in membrane binding, liposome co-sedimentation assays were performed (see 3.3.5). In these assays, the protein was incubated for 30 min with liposomes of various compositions. Following sedimentation of the liposomes by centrifugation, the distribution of the protein in the pellet and supernatant was analyzed.

Surprisingly, $Mic60_{sol}$ bound to negatively charged Folch liposomes (Figure 19) derived from bovine brain total lipids, despite the absence of its N-terminal transmembrane anchor. Recently, it was shown that cardiolipin positively effects lipid binding of Mic60 of *Arabidopsis thaliana* by increasing the binding affinity (Michaud et al., 2016). Due to this reason, the effect of this lipid on Mic60 membrane interaction was tested, by including 15, 20, or 30% cardiolipin to the Folch liposomes. However, as can be seen in Figure 19, cardiolipin did not affect membrane binding.

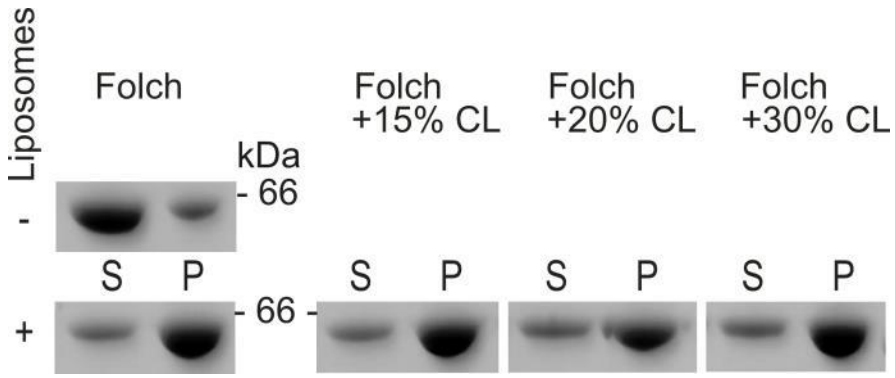


**Figure 19. Folch liposome co-sedimentation assays with $Mic60_{sol}$ (S) Supernatant; (P) Pellet: (CL) cardiolipin**

### 4.2.2 Identification of the Lipid binding site of Mic60

To identify the putative membrane-binding region in the hydrophilic IMS part of Mic60, $Mic60_{sol}\Delta$Mito and $Mic60_{sol}\Delta$Mito$\Delta$LBS were initially used for liposome sedimentation assays (Figure 20A). Deletion of the mitofilin domain did not affect membrane binding but the variant truncated after the predicted coiled-coil domain did not co-sediment with liposomes (Figure 20A), indicating that a lipid-binding site (LBS) may be located in the linker region between the coiled-coil and mitofilin domains (Figure 20B).

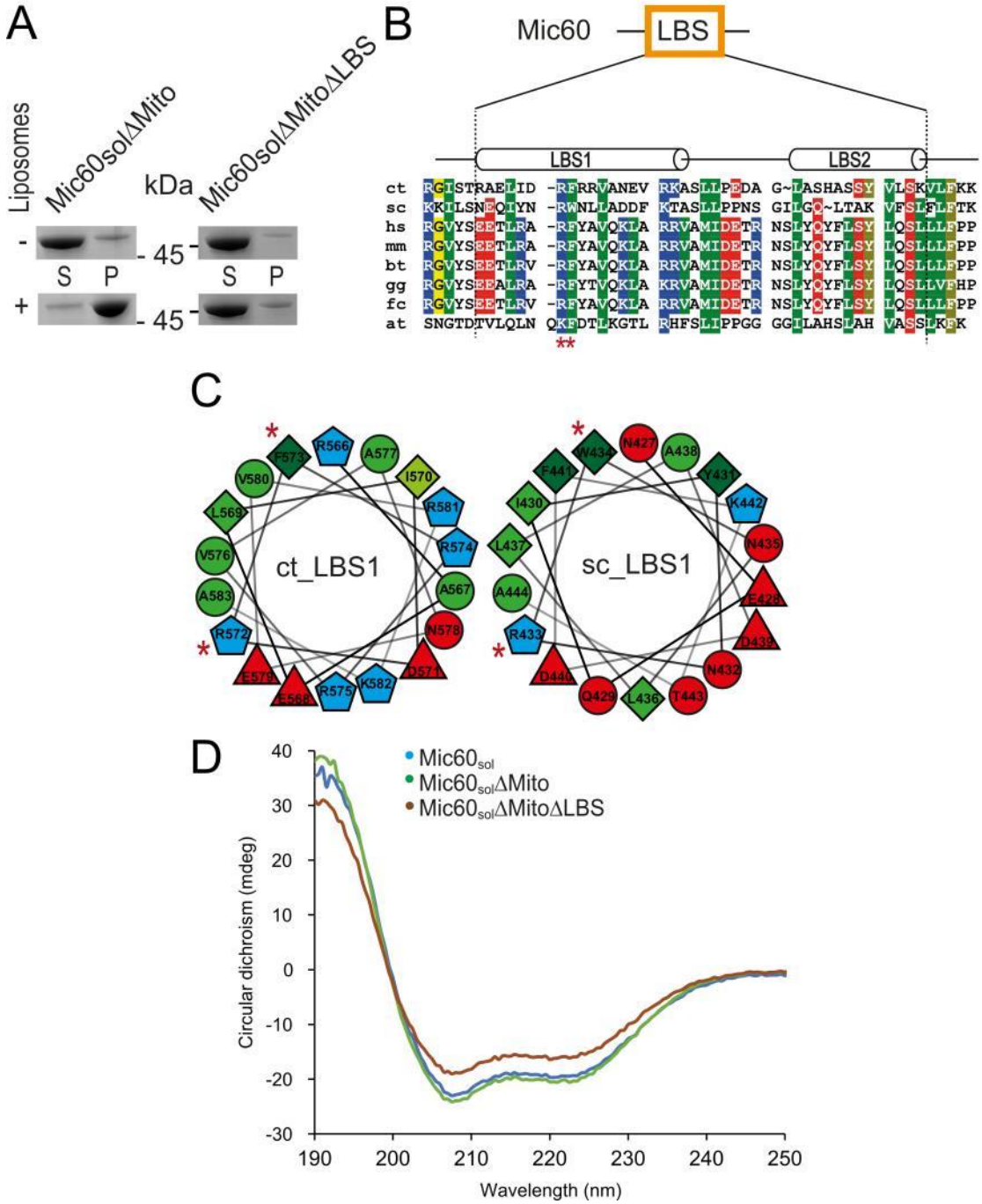


**Figure 20. (A) Folch liposome co-sedimentation assays with $Mic60_{sol}$ΔMito (left) and $Mic60_{sol}$ΔMitoΔLBS (right). (S) Supernatant; (P) Pellet. (B) Sequence alignment of the predicted LBS in Mic60, with secondary structure predictions on top. Sequences of Mic60 from *C. thermophilum* (ct), *S. cerevisiae* (sc), *H. sapiens* (hs), *M. musculus* (mm), *B. Taurus* (bt), *G. gallus* (gg), *F. catus* (fc) and *A. thaliana* (at) were aligned. Positively charged residues in blue; negatively-charged residues in red, hydrophobic residues in green and uncharged residues in yellow. (C) Helical wheel projections of the LBS1 from *Chaetomium thermophilum* (ct_LBS1) and S*accharomyces cerevisiae* (sc_LBS1) indicate the amphipathic nature of the predicted α-helix. The red asterisks mark residues mutated in this study. (D) CD measurements of $Mic60_{sol}$ truncations analyzed in this study indicated a mostly α-helical fold, as seen by the negative bands at 208 and 222 nm.**

Bioinformatic analysis predicted the presence of two α-helices in this linker region, to which in the following is referred to LBS1 and LBS2. A helical wheel projection of LBS1 revealed a conserved amphipathic character, a known feature for membrane inserting helices (Figure 20B-C, see 3.3.1). The used Mic60 constructs showed a similar CD profile compared to $Mic60_{sol}$ indicative for a proper folded protein (Figure 20D).

The deletion of LBS2 together with the mitofilin domain ($Mic60_{sol}$ΔMitoΔLBS2, residues 208-582) reduced membrane interaction of Mic60 up to approximately 50% (Figure 21A). To demonstrate a possible requirement of LBS1 in membrane binding, this region was specifically removed from the soluble Mic60 variant via an internal deletion ($Mic60_{sol}$ΔLBS1). Indeed, this variant did not bind to liposomes, indicating the importance of LBS1 for membrane binding (Figure 21A).

To exactly pinpoint membrane binding residues, attention was focused on the conserved residues Arg572 and Phe573. Arg572 represents a potential binding partner for the negatively charged phospholipid head groups, whereas Phe573 may insert into the hydrophobic core of the lipid bilayer. In line with this hypothesis, individual replacements of Arg572 or Phe573 by aspartate ($Mic60_{sol}$R572D or $Mic60_{sol}$F573D) considerably reduced liposome binding. Simultaneous replacement of Arg572 and Phe573 with aspartate residues (RF572-573DD variant) completely abolished liposome binding, suggesting that these two residues are directly involved in membrane interaction (Figure 21A). Additionally, CD experiments showed that all used Mic60 constructs and mutants contained secondary structure elements, which reflects a proper folded protein (Figure 21B).

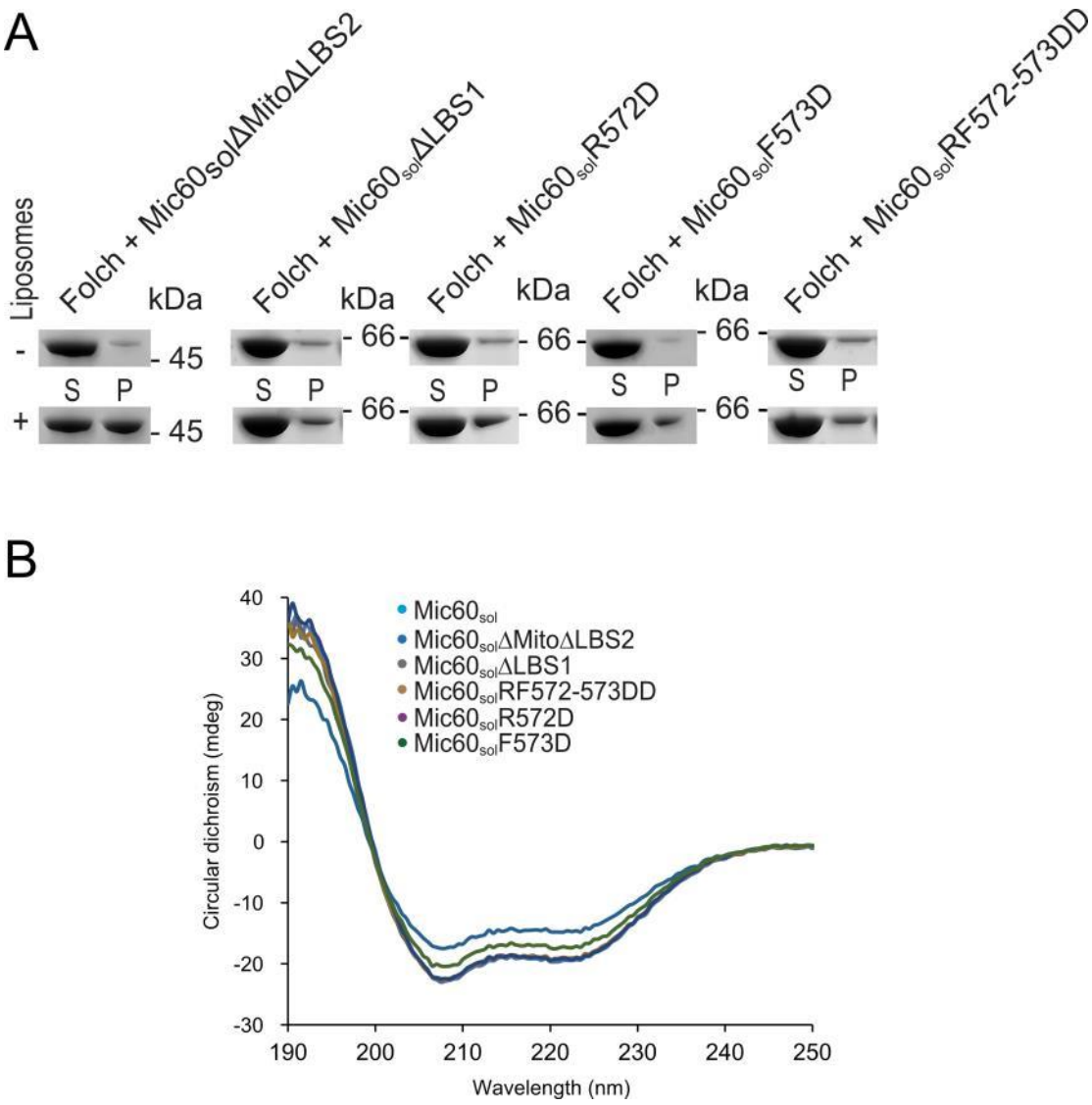


**Figure 21. Mic60's LBS is crucial for proper binding to Folch liposomes. (A) Folch liposome co-sedimentation assays using $Mic60_{sol}$ containing different mutations and deletions as indicated. (S) Supernatant; (P) Pellet. (B) CD measurements of $Mic60_{sol}$ truncations and mutants analyzed in this study indicated a mostly α-helical fold, as seen by the negative bands at 208 and 222 nm.**

### 4.2.3 Liposome tubulation by Mic60

To analyze the effect of $Mic60_{sol}$ binding to liposomes, negative stain electron microscopy was used. In this assay, the indicated Mic60 constructs were incubated with the liposomes for 30 min at room temperature and then spotted on a carbon grid. The samples were negatively stained using uranyl acetate and examined with EM (see. 3.3.6).

Strikingly, $Mic60_{sol}$ binding resulted in massive liposome deformation, as shown by the appearance of long (up to 30 µm), mostly unbranched membrane tubules. They

showed a more or less constant diameter of 90 ± 30 nm in EM (Figure 22A). These results indicate that Mic60 is actively involved in membrane remodeling. Interestingly, $Mic60_{sol}$ΔMito did not affect membrane tubulation but this variant showed an increased appearance of membrane branches (Figure 22B,K), which may be a hint for even increased membrane remodeling activity. In contrast, $Mic60_{sol}$ΔMitoΔLBS completely lost its ability to deform liposomes (Figure 22C). The $Mic60_{sol}$ΔMitoΔLBS2 variant showed reduced liposome binding but still tubulated membranes, similar to $Mic60_{sol}$ (Figure 22D). All point mutated constructs, which were previously tested for membrane binding, also failed to remodel liposomes except of the $Mic60_{sol}$R572D mutant (Figure 22E-H). This variant often induced deformed liposomes to a beads-on-a-string pattern in EM analyses.

The tubulation efficiency of all used constructs was quantified by counting the number of tubulated liposomes per image field, whereas the highest rate was recorded using the $Mic60_{sol}$ΔMito variant (Figure 22I, see 3.3.6). Observed tubules had a similar width except of $Mic60_{sol}$ΔMitoΔLBS2 showing a slightly reduced diameter of approximately 60 ± 30 nm and the $Mic60_{sol}$R572D mutant with a larger average diameter of 140 ± 20 nm, pointing to a reduced potential to deform membranes (Figure 22J).

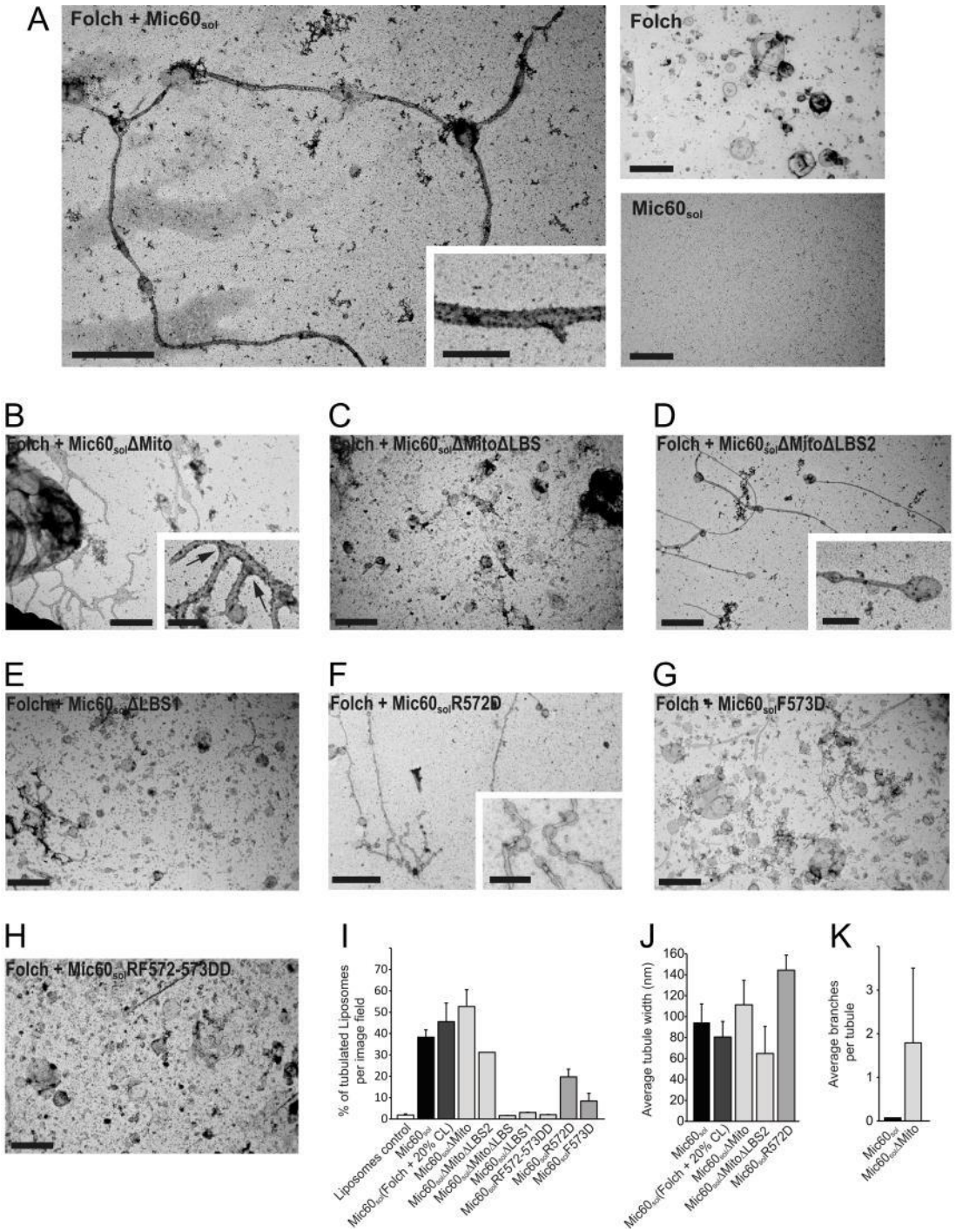


**Figure 22. Mic60 in liposome tubulation. (A) Electron micrograph of negatively stained deformed liposomes after incubation with $Mic60_{sol}$. Electron micrographs of liposomes (top, right) and $Mic60_{sol}$ protein (bottom, right) are shown as controls. (B-H) Electron micrographs of Folch liposomes incubated with the indicated Mic60 constructs. Arrows indicate tubule branches. Scale bars represent 2 µm and 500 nm within the close-up, respectively. (I) Quantification of the percentage of membrane tubules per image field for the indicated Mic60 variants, are shown. Only liposomes with a diameter ≥120 nm were considered in this analysis (tubulating Mic60 variants n~200, non-tubulating Mic60 variants n~1000, error bars denote the standard deviation). (J) Quantification of membrane tubule width for the indicated Mic60 variants (n=4 per tubule, with a total of 20 tubules per image field, error bars denote the standard deviation of the mean). For the R572D variant, only straight membrane tubules were quantified. (K) Quantification of branching points per tubule for the indicated Mic60 variants. n≥20, error bars denote the standard deviation.**

## 4.3 The function of the Mic60-Mic19 complex

### 4.3.1 Mic60-Mic19 binding studies

It is known, that Mic60 together with Mic19 form a subcomplex within MICOS (van der Laan et al., 2016). So far, this subcomplex has not been thoroughly characterized at a biochemical level. To analyze the interaction between Mic60 and Mic19 and to further quantify the stoichiometry of this complex, a number of Mic19 variants were expressed and purified (see 3.3.3): full length Mic19, the coiled-coil domain of Mic19, the CHCH domain of Mic19 and a full length variant, in which the two cysteines in the CHCH domain were mutated to serines (Figure 17, see 3.2.10).

First, CD experiments ensured that all Mic19 constructs contained secondary structure elements, which reflects a proper folded protein (Figure 23). As expected, the CD measurements showed profiles, typical for α-helical containing proteins, except of the Mic19_C132S,C143S mutant, which may be partially unfolded.

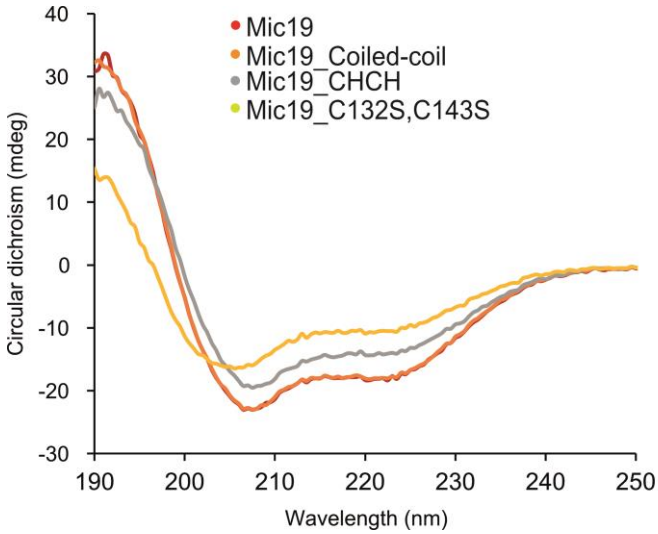


**Figure 23. CD measurements of the Mic19 constructs. A mostly α-helical fold was observed, as seen by the negative bands at 208 and 222 nm. Mutation of two cysteines in the CHCH domain of Mic19 led to a reduction in secondary structure, in agreement with a structural role of these two residues.**

To analyze the interaction of Mic60 and Mic19, isothermal titration calorimetry (ITC) was used, as described in 3.3.9. Around 450 µM of Mic19 was stepwise titrated to approximately 40 µM of $Mic60_{sol}$ and the resulting heat change monitored. The binding isotherm was used to derive binding constants. Both proteins clearly interacted with each other with high affinity ($K_D$ of 170 nM ± 20 nM) (Figure 24A). Interestingly, a binding number of 0.7 was observed, i.e. only 70% of the Mic19 molecules bound to $Mic60_{sol}$. Gel filtration analysis of purified Mic19 revealed a mixture of approximately 70% monomers and 30% dimers (Figure 16A and 17B). It was therefore suspected that only the monomeric form of Mic19 could bind to $Mic60_{sol}$.

Next, the experiment was performed with the monomeric Mic19_C132S,C143S, as analyzed by SEC. This variant showed a reduced binding affinity to $Mic60_{sol}$ ($K_D$ = 3.5 µM ± 0.8 µM), but displayed a binding number of 1 (Figure 24B). These results suggest that formation of an intramolecular disulfide bond in the CHCH domain of Mic19 is critical for the correct folding of the CHCH domain and high affinity binding to Mic60. In contrast, formation of an intermolecular disulfide bond results in a dimeric species that cannot bind to Mic60.

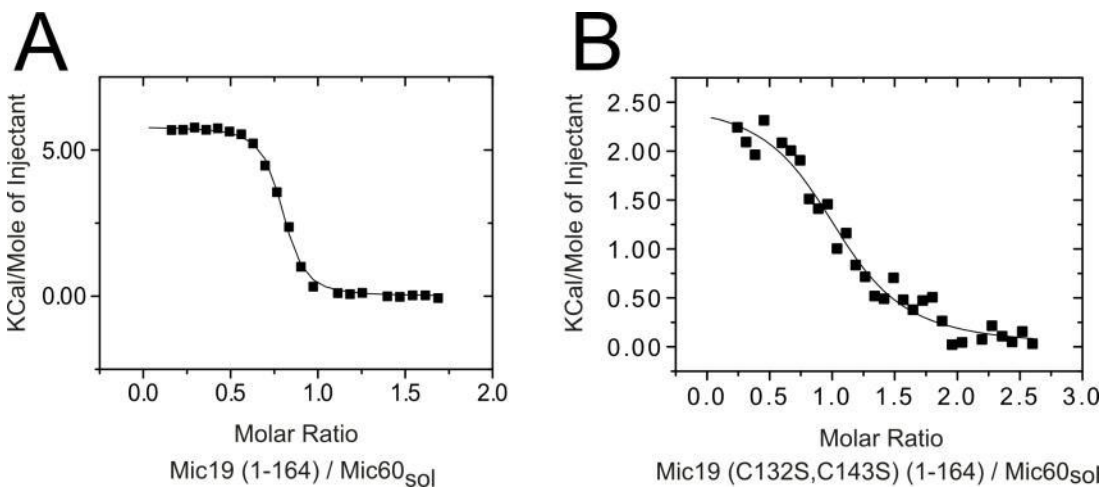


**Figure 24. ITC experiments using $Mic60_{sol}$ and indicated Mic19 constructs. Here, a 450 µM solution of the indicated Mic19 constructs was titrated into 40 µM of $Mic60_{sol}$ at 10 °C, and the resulting heat changes were monitored. Fitted values for (A): $K_D$ = 170 nM ± 20 nM, binding number n = 0.73 ± 0.01 and for (B): $K_D$ = 3.5 µM ± 0.8 µM, binding number n = 1**

Deletion of the mitofilin domain in $Mic60_{sol}$ led to a complete loss of Mic19 binding (Figure 25A), suggesting a critical role of the mitofilin domain for the interaction with Mic19. The isolated mitofilin domain of Mic60 aggregated at concentrations > 1 mg/ml, precluding its use in ITC studies. In contrast, the isolated coiled-coil

domain of Mic19 (Mic19_Coiled-coil, 39-113) was soluble, but did not bind to $Mic60_{sol}$ (Figure 25B). However, the isolated CHCH domain of Mic19 (Mic19_CHCH, 116-164) bound to $Mic60_{sol}$ with a $K_D$ of 390 nM ± 60 nM, i.e. with a comparably high affinity as full-length Mic19 (Figure 25C). Thus, these binding studies using untagged proteins indicate that the Mic60-Mic19 subcomplex of MICOS forms via interaction of the CHCH domain of Mic19 and the mitofilin domain of Mic60.

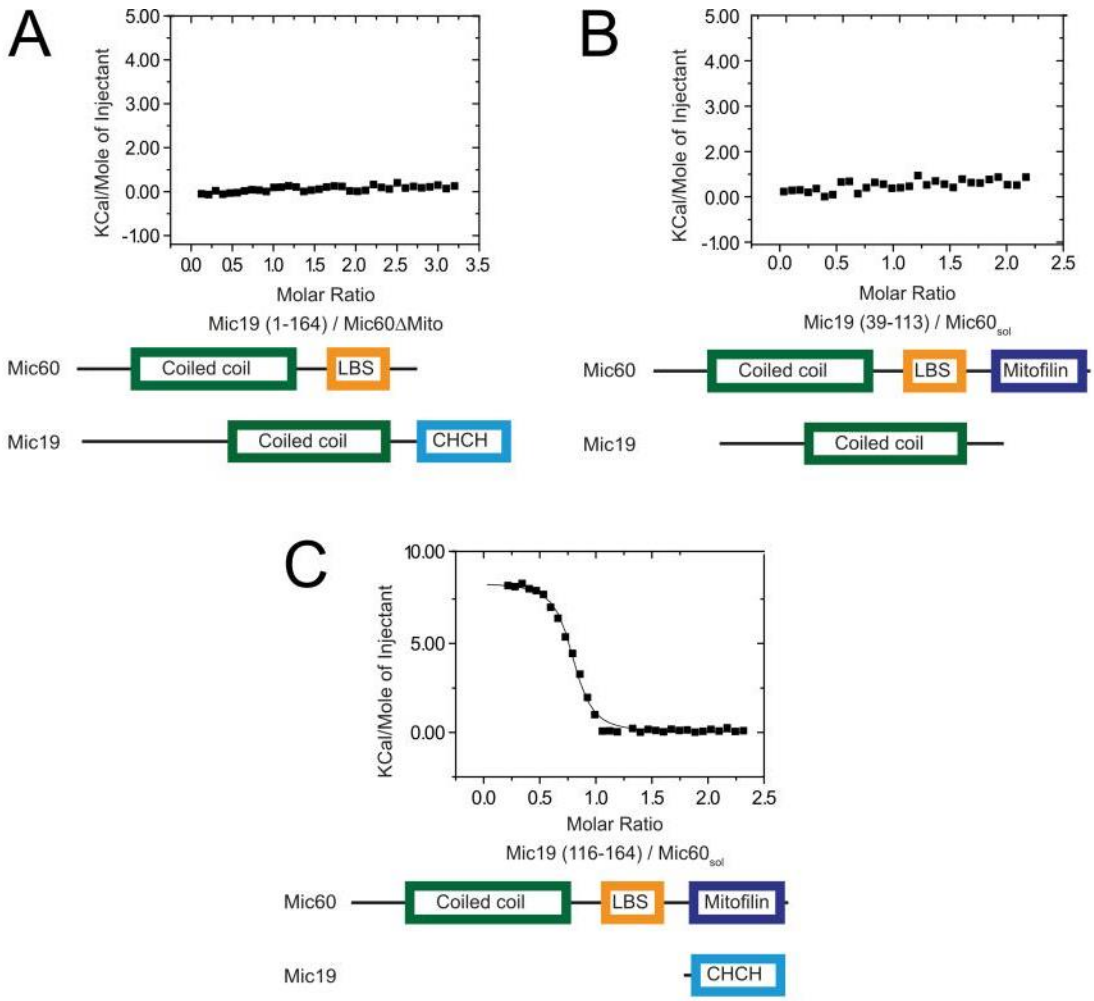


**Figure 25. Performed ITC experiments using indicated Mic60 and Mic19 variants under the same conditions reported in Figure 24. (A) No binding. (B) No binding. (C) $K_D$ = 390 nM ± 60 nM, binding number n = 0.77 ± 0.01.**

### 4.3.2 Mic60-Mic19 subcomplex in liposome binding and tubulation

It was shown that $Mic60_{sol}$ can actively remodel liposomes but the role of Mic19 within the subcomplex remained unclear. To investigate a possible function of the Mic60-Mic19 complex, liposome co-sedimentation assays and electron microscopy was used on negative stained liposomes incubated with the Mic60-Mic19 complex

(see 3.3.5 and 3.3.6). First, membrane binding of Mic19 alone was analyzed but no interaction with Folch liposomes in co-sedimentation assays, nor membrane tubulation was found (Figure 26A left and 26B). However, when $Mic60_{sol}$ was co-incubated with Mic19, co-sedimentation of the Mic60-Mic19 complex with liposomes was observed, suggesting that the two proteins interact when bound to membranes (Figure 26A right). Remarkably, the Mic60-Mic19 complex induced liposome tubulation and branching, as $Mic60_{sol}\Delta$Mito (Figure 26C). A similar phenotype was also observed for the Mic19_C132S,C143S mutant indicating that under the conditions of this assay, the Mic19 mutant can still interact with Mic60 at the membrane (Figure 26D). Addition of the isolated CHCH domain to $Mic60_{sol}$ enhanced membrane tubulation compared to $Mic60_{sol}$ alone, but fewer branches were observed indicating that other parts of Mic19 also contribute to the functional cooperation with Mic60 (Figure 26E). The tubulation efficiency of all used constructs were quantified similarly as described in chapter 4.2.3 (Figure 26F-H). Interestingly, less tubulated liposomes were counted after incubation with the $Mic60_{sol}$-Mic19 and $Mic60_{sol}$-Mic19_C132S,C143S complex (Figure 26F), whereas the tubule width was unaltered (Figure 26G). It is speculated that the Mic60-Mic19 complex accelerates the tubulation rate, observed as tubule branches (Figure 26C-D,H).

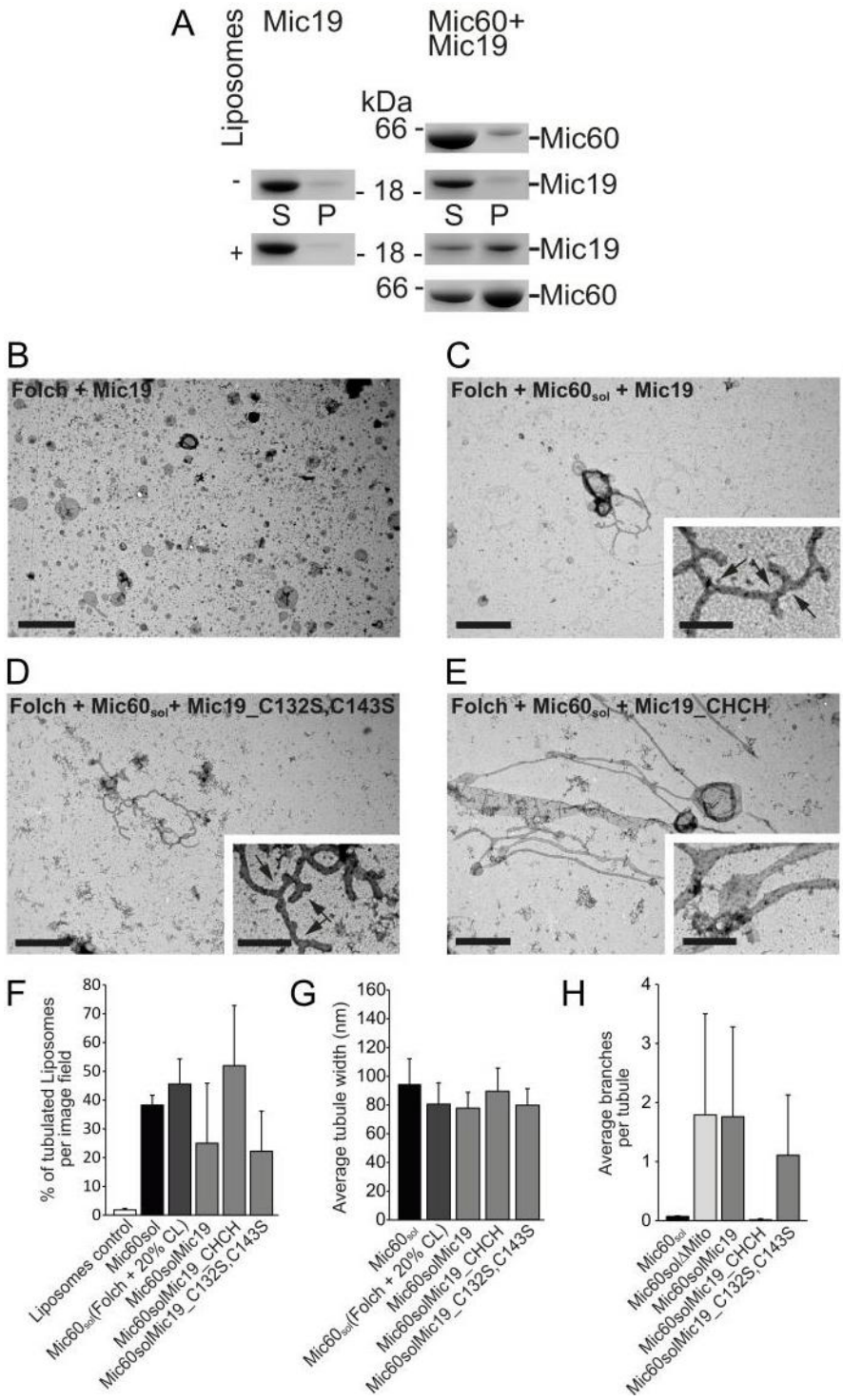


**Figure 26. Liposome binding and tubulation of the Mic60-Mic19 subcomplex. (A) Liposome co-sedimentation assays of Mic19 alone (left) and Mic19 co-incubated with $Mic60_{sol}$ (right). (B-E) Negatively stained electron micrographs of liposomes incubated with (B) Mic19 (C) $Mic60_{sol}$-Mic19 complex (D) $Mic60_{sol}$-Mic19_CHCH and (E) $Mic60_{sol}$-Mic19_C132S,C143S. Arrows in the magnification indicate tubule branches. Scale bars represent 2 µm and 500 nm within the close-ups, respectively. (F) Quantification of the percentage of membrane tubules per image field for the indicated Mic60 and Mic19 variants. (G) Quantification of membrane tubule width for the indicated Mic60 and Mic19 variants (error bars denote the standard deviation of the mean). (H) Quantification of branching points per tubule for the indicated Mic60 and Mic19 variants. n≥20, error bars denote the standard deviation. Quantification was performed according to the method in 3.3.6**

### 4.3.3 Analyses of the Mic60-Mic19 liposome tubulation efficiency

When closely inspecting EM micrographs of liposomes incubated with the Mic60-Mic19 complex, small particles reminiscent of membrane remnants were seen. An explanation might be that such particles may be generated by fragmentation of membrane tubules caused by enhanced membrane remodeling. To properly quantify the membrane remodeling activity of the Mic60-Mic19 complex, an established membrane leakage assay was used (see 3.3.10). In brief, following the addition of protein to liposomes, the release of the fluorescent dye 8-aminonapthalene-1,3,6 trisulfonic acid (ANTS) and its quencher p-xylene-bis-pyridinium bromide (DPX) from the interior of liposomes into solution was observed as a time-dependent fluorescence increase (Figure 27A).

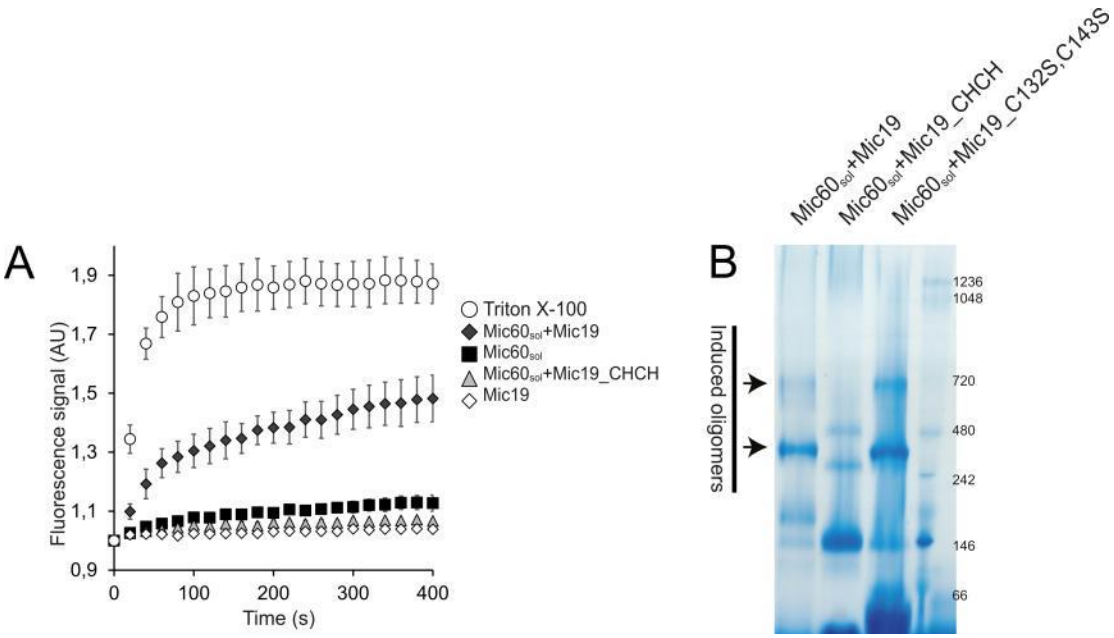


**Figure 27. Membrane tubulation and oligomerization efficiency of the Mic60-Mic19 complex. (A) Membrane leakage of Folch liposomes pre-loaded with the fluorescent dye ANTS and its quencher DPX was induced by the addition of the indicated constructs (or 1% Triton X-100 as a control) and monitored by following the time-dependent increase of the fluorescence signal (n≥7, error bars denote the standard deviation (s.d.) of each data point). Experiments were performed by A. Xavier with proteins supplied by me. (B) Native PAGE analyses of the indicated Mic60-Mic19 complexes induced higher oligomers only in the presence of the Mic19's coiled-coil domain. Higher oligomers are marked as arrows. Numbers indicate the molecular weight in kDa.**

As expected, $Mic60_{sol}$ alone induced liposome leakage indicative of a membrane remodeling activity (Figure 27A). Incubation with Triton X-100 and Mic19 alone served as positive and negative control, respectively. Strikingly, Mic19 greatly enhanced membrane leakage when co-incubated with $Mic60_{sol}$. In contrast, addition of the isolated CHCH domain reduced the membrane leakage activity of $Mic60_{sol}$.

These results are consistent with a model in which, Mic60 membrane-remodeling activity is enhanced by Mic19. The mitofilin-CHCH domain interaction promotes tubulation but is not sufficient to enhance membrane leakage.

It is concluded that the Mic60-Mic19 complex cooperatively remodels membranes, which in addition to the CHCH domain requires Mic19's coiled-coil domain. Indeed, native PAGE analyses revealed that Mic19 and also Mic19_C132S,C143S induced Mic60 oligomerization but not when incubated with the isolated CHCH domain (Figure 27B). These results further underline the importance of Mic19's coiled-coil domain to accelerate membrane remodeling.

## 4.4 The cellular function of the Mic60-Mic19 subcomplex

According to the previous results, it was shown that the Mic60-Mic19 subcomplex is essential for proper membrane remodeling and may therefore be important for cristae formation. The newly identified LBS mediates the membrane contact but it remained unclear if the LBS is similarly important during cristae formation. To examine the physiological role of Mic60-mediated membrane binding for mitochondrial membrane architecture, the yeast *Saccharomyces cerevisiae* was used as a model organism. Most of the following experiments were performed in the laboratories of our collaboration partners Martin van der Laan (University of Saarland) and Nikolaus Pfanner (University of Freiburg).

### 4.4.1 MICOS protein levels after manipulation of the LBS1 in yeast cells

To investigate the necessity of the LBS1 *in vivo*, yeast strains were engineered carrying chromosomally integrated *MIC60* mutants encoding protein variants with either a deletion of the homologous LBS1 region or an RW433-434DD amino acid replacement in LBS1 (Figure 28A-B), which is equivalent to the RF572-573DD substitution in *Chaetomium thermophilum* Mic60 (Figure 20B). To enable the purification of the MICOS complex from mutant mitochondria and the co-isolation of MICOS interacting proteins, a Protein A (ProtA) moiety was fused to the C-terminus of the Mic60 variants (see 3.3.11). It has been reported and was confirmed by this study that the lack of Mic60 leads to strongly reduced Mic19 levels. Mic19 levels induced by the loss of Mic60 could be restored by Mic19 re-expression from a plasmid (pMIC19 +) (Figure 28B). Mic19 levels were also decreased in mitochondria harboring Mic60 variants with a defective lipid binding site indicating that these variants may not be functional. In contrast, the protein levels of Mic10, Mic26, Mic12, and control proteins, like Tom40, the $F_1F_o$-ATP synthase subunit Atp21 and the respiratory chain complex III subunit Cor1 were not affected.

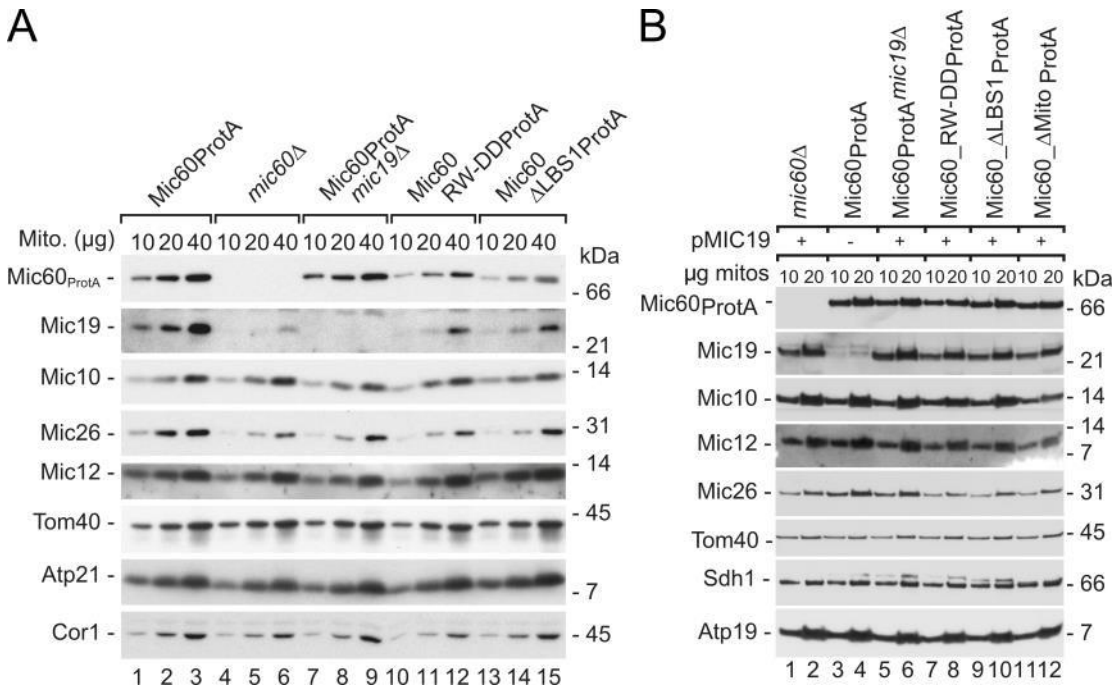


**Figure 28. The LBS is important for MICOS assembly. (A-B) Mitochondrial steady state levels of the indicated individual proteins were assessed by SDS-PAGE. (B) Mic19 levels were restored in mutants with reduced endogenous Mic19 by Mic19 re-expression from a plasmid (pMIC19 +). Cells with normal endogenous Mic19 levels were supplemented with the empty vector (pMIC19 –). These experiments were performed by R. Zerbes and H. Rampelt.**

### 4.4.2 MICOS integrity and the LBS1

To test if inactivation of the Mic60 LBS disturbs MICOS integrity, the complex was purified from isolated mitochondria by affinity chromatography with Protein A-tagged wild-type Mic60 and the variants ΔLBS1 and RW433-434DD as bait proteins (Figure 29, see 3.3.11, 3.3.12 and 3.3.13). To make sure that the observed effects were not due to a (partial) loss of Mic19 in mitochondria containing LBS1-defective Mic60 variants, Mic60$_{ProtA}$*mic19*Δ mitochondria for comparison was included. Co-isolation efficiency of other MICOS components together with lipid-binding-deficient Mic60 variants was strongly reduced compared to the co-isolation efficiency with wild-type Mic60$_{ProtA}$, whereas the loss of Mic19 had only moderate effects on the overall integrity of MICOS (Figure 29A left). Of note, the co-isolation of the outer membrane binding partner Tom40, the central subunit of the TOM complex, was not reduced with the mutant mitochondria, indicating that LBS1-defective Mic60 variants can still form IM-OM contact sites. In agreement with the observed MICOS deficiency, yeast strains expressing the lipid-binding-deficient variants of Mic60 showed impaired growth similar to *mic60*Δ cells on media that require maximal

mitochondrial activity (Figure 29A right). Next, Mic19 in the analyzed mutant yeast strains was expressed from a plasmid leading to the restoration of Mic19 protein levels in mitochondria (Figure 29B left). Re-expression of Mic19 in the Mic60_ΔLBS1- and Mic60_RW433-434DD-expressing strains or in a strain lacking the mitofilin domain of Mic60, neither rescued the assembly of the MICOS complex nor the growth phenotype of the *mic60* mutant yeast strains on a non-fermentable carbon source (Figure 29B right). From these data, it is concluded that efficient binding of Mic60 to membranes is crucial for MICOS integrity.

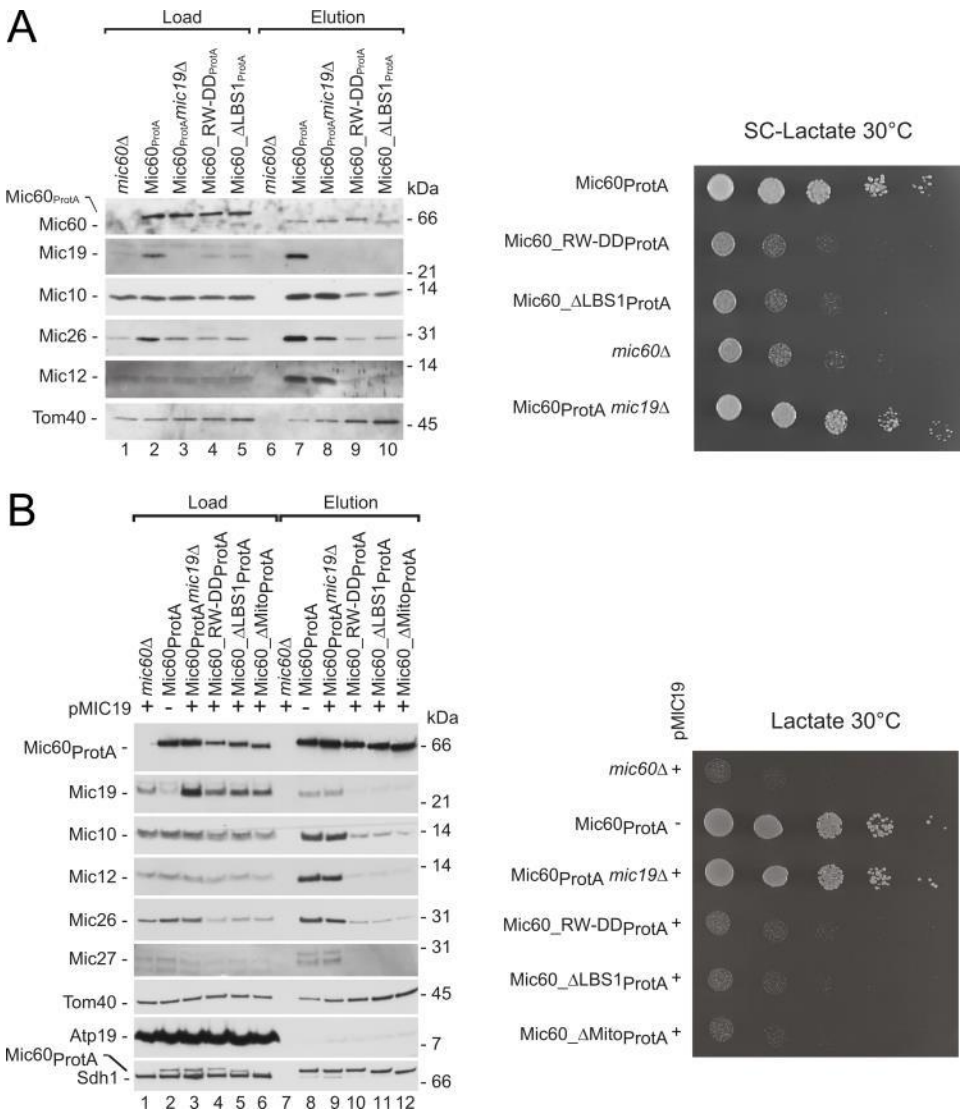


**Figure 29. The LBS1 regulates MICOS integrity and cell growth. (A, left) MICOS integrity in the indicated yeast strains was assessed by affinity chromatography experiments from isolated, digitonin-solubilized mitochondria. Load 5%, eluate 100%. (A, right) Yeast growth was assessed under respiratory conditions by spotting the indicated strains on agar plates containing lactate as sole carbon (SC) source. (B, left) MICOS integrity in the indicated yeast strains was assessed as described in (A) after re-expression of Mic19 (pMIC19+). Load 10%, eluate 100%. (B, right) Growth of the indicated yeast strains re-expressing Mic19 was assessed, as described in (A). These experiments were performed by R. Zerbes and H. Rampelt.**

### 4.4.3 Mitochondrial ultrastructure of LBS mutants

To directly test MICOS functionality in the *mic60* mutant strains, mitochondrial ultrastructure was examined by electron microscopy (Figure 30A-G, see 3.3.7 and 3.3.12). In $Mic60_{ProtA}$-expressing cells, mitochondria showed typical membrane architecture with clearly defined cristae that had extensive contacts to the boundary IM via CJs (Figure 30C-D). Deletion of the entire *MIC60* gene or removal of only the Mic60 mitofilin (Zerbes et al., 2012a) domain led to a grossly aberrant mitochondrial ultrastructure with increased IM surface and detached lamellar cristae membranes as expected, independently of Mic19 re-expression (Figure 30B,G). Moreover, deletion of *MIC19* in the $Mic60_{ProtA}$-expressing strain had a similar effect on mitochondrial architecture (Figure 30A). Re-expression of Mic19 from a plasmid in *mic19*Δ cells fully rescued this phenotype confirming that plasmid-encoded Mic19 is functional (Figure 30D). Deletion of LBS1 in $Mic60_{ProtA}$ in Mic19 re-expressing cells ($Mic60\_\Delta LBS1_{ProtA}$) induced a similar phenotype as the complete absence of Mic60, the IM showing an increased membrane surface and virtually no CJs (Figure 30E). Analysis of cells expressing the $Mic60_{ProtA}$ variant RW433-434DD with an inactivated lipid binding site and re-expressing Mic19 revealed a similar mitochondrial phenotype (Figure 30F). Quantifications of the number of cristae junctions per mitochondrial sections were consistent with the observed mitochondrial ultrastructure (Figure 30H). Only $Mic60_{ProtA}$ pRS426 (plasmid encoding *MIC19*) and $Mic60_{ProtA}$*mic19Δ*Mic19 variants showed normal CJs. Taken together, these findings indicate a requirement of Mic60 membrane binding via the LBS1 domain for maintenance of the native mitochondrial ultrastructure.

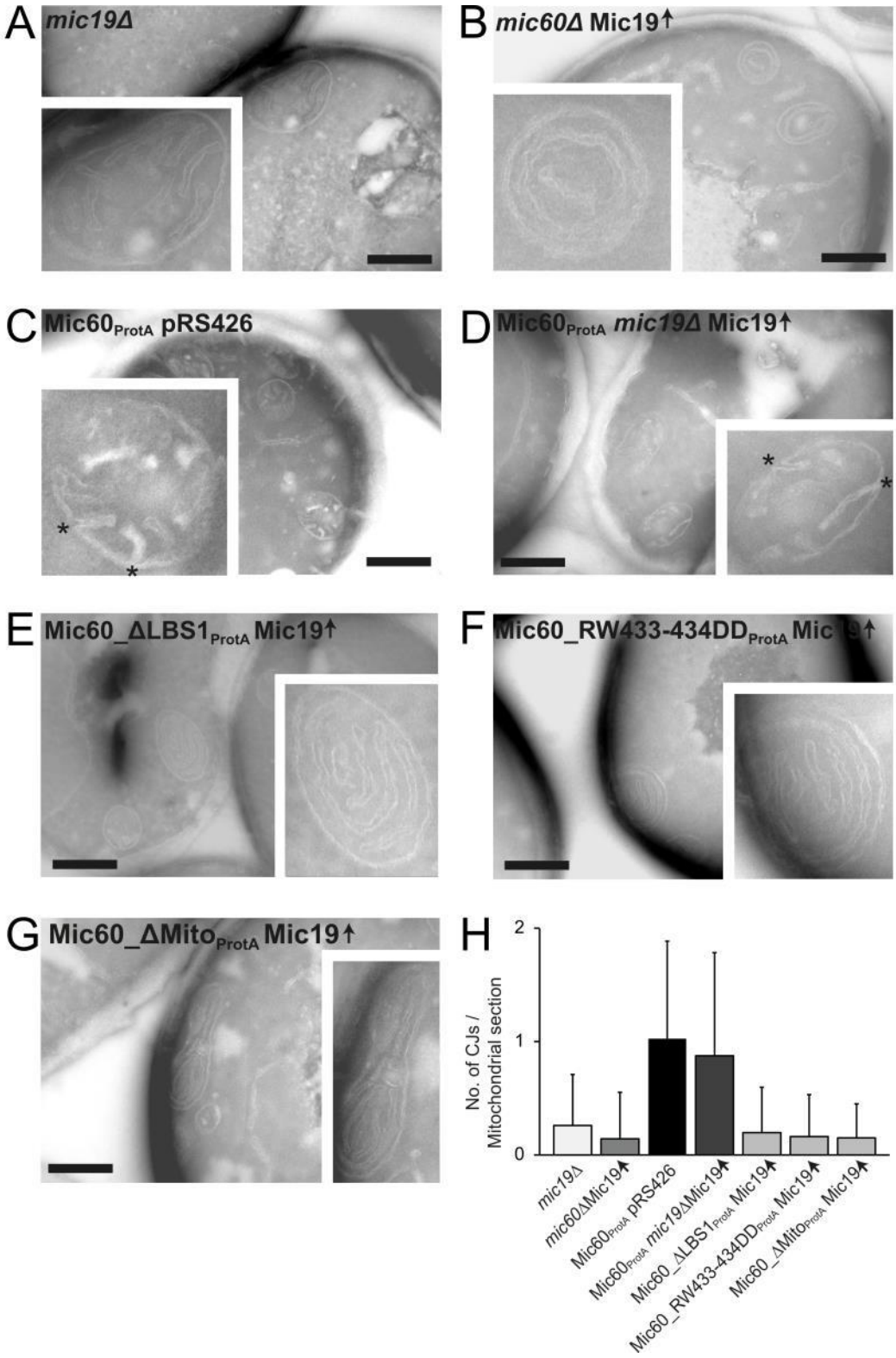


**Figure 30. An intact LBS is crucial for cristae junction formation. (A-G) Representative electron micrographs of mitochondria in ultrathin cryo-sections from yeast strains re-expressing Mic19. Asterisks mark crista junctions. Scale bars represent 500 nm. (H) Number of CJs in electron micrographs of mitochondrial sections from the various yeast strains. n>=40, error bars indicate the standard deviation. Experiments were done by S. Kunz and B. Purfürst with yeast strains from R. Zerbes and H. Rampelt.**

### 4.4.4 Membrane binding of Mic60 is required for full mitochondrial activity

With the previous results, it was shown that an intact LBS is important for mitochondrial ultrastructure and the correct assembly of MICOS components. To test, if LBS mutants have an influence on other mitochondrial proteins like the electron transport chain complexes, a respiratory activity assay was performed (see 3.3.14). Indeed, loss of Mic60 lipid binding in mitochondria negatively affected respiratory metabolism (Figure 31). Even though the steady state levels of respiratory chain (super-) complexes were similar in wild-type, *mic60*Δ, and Mic60 LBS1-defective mitochondria as judged by blue native-PAGE analysis (Figure 31C), a considerable reduction in the enzymatic activities of complex III (cytochrome $bc_1$) (Figure 31A) and complex IV (cytochrome *c* oxidase) (Figure 31B), was observed. The reduction of the respiratory activity was thus comparable to that of mitochondria lacking the MICOS core component Mic10 (Bohnert et al., 2015). It is concluded that lipid binding of Mic60 is crucial for MICOS integrity, mitochondrial membrane architecture and mitochondrial fitness.

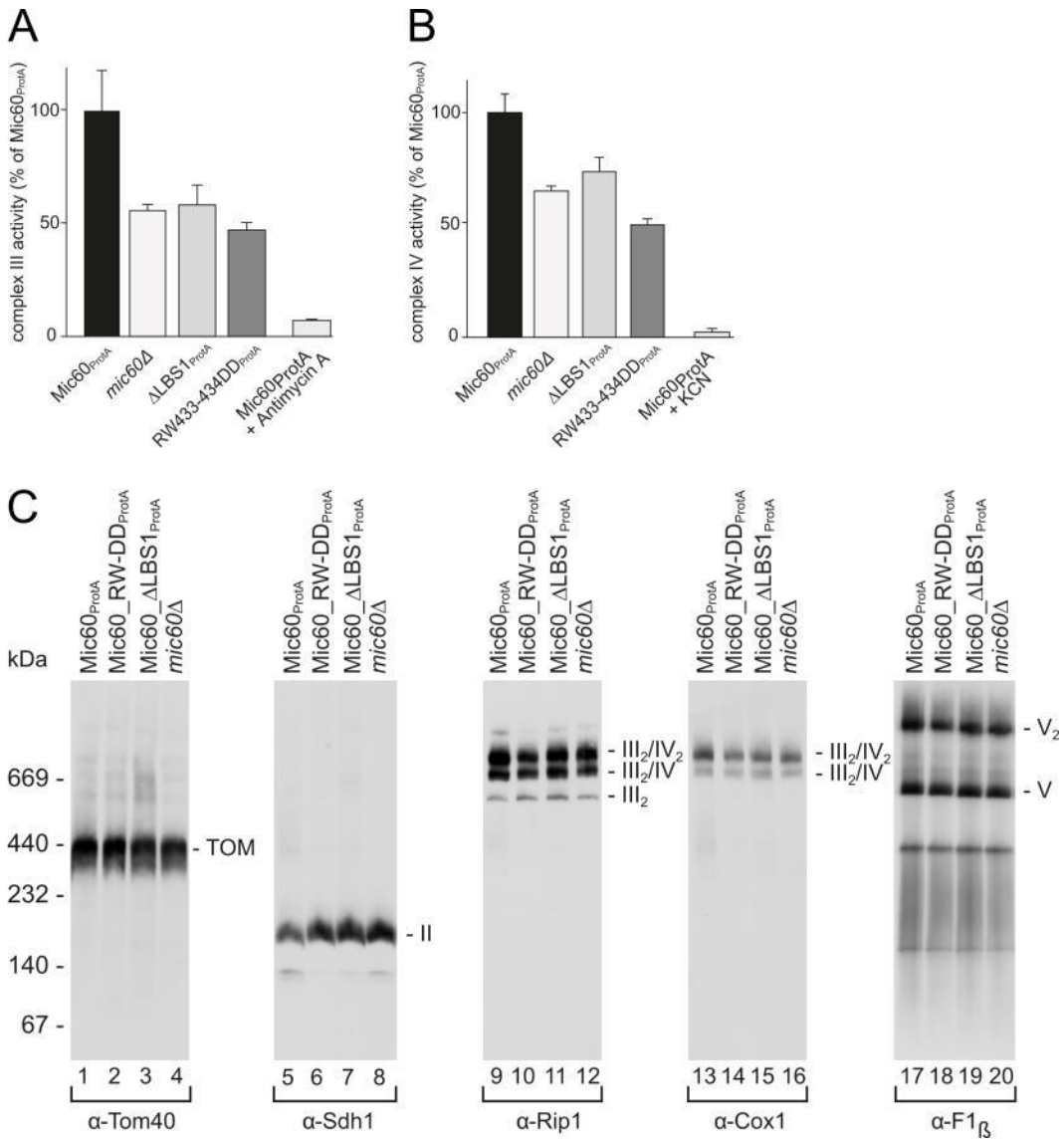


**Figure 31. (A) Complex III and (B) complex IV activity of the indicated yeast strains were measured spectrophotometrically (n=3), error bars represent standard errors of the mean. $Mic60_{ProtA}$ mitochondria pretreated with Antimycin A or KCN served as negative controls for complex III or complex IV activity, respectively. (C) Mitochondrial steady state levels of the indicated native protein complexes were assessed by blue native-PAGE. TOM – translocase of the outer membrane; II – complex II (succinate dehydrogenase); $III_2$ – complex III dimer (cytochrome $bc_1$ complex); $III_2/IV$ – supercomplex consisting of a complex III dimer and one copy of complex IV (cytochrome *c* oxidase); $III_2/IV_2$ – supercomplex consisting of a complex III dimer and a complex IV dimer; V - $F_1\beta$ – β subunit of $F_1F_o$-ATP synthase. Experiments were performed by R. Zerbes and H. Rampelt.**

# 5 Discussion

This work reports an unexpected function of the contact site-forming MICOS core subunit Mic60. By directly binding and remodeling membranes, Mic60 plays a crucial role in CJ formation and shaping inner membrane cristae. An amphipathic helix that is located between the coiled-coil and mitofilin domains of Mic60 is critical for this membrane-shaping activity. Furthermore, it is shown that Mic60's membrane remodeling activity is regulated by Mic19.

## 5.1 Membrane curvature induction processes

Inducing curvatures on membranes is an important process for defining the morphology of cells and organelles (Shibata et al., 2009). Furthermore, uptake and release of membranous vesicles from the cells (endo- and exocytosis, respectively) (Haucke et al., 2011), membrane fusion (Martens and McMahon, 2008) and fission (Ferguson and De Camilli, 2012) critically involve the generation and stabilization of membrane curvature. In the following paragraphs, the role of membrane curvature in mitochondrial homeostasis is discussed.

Earlier cryo EM tomography analyses indicated that the $F_1F_o$-ATP synthase in mitochondria of yeast and mammals forms V-shaped dimers, which assemble along the highly curved ridges of lamellar cristae, thereby stabilizing cristae curvature (Davies et al., 2011; Muhleip et al., 2016). Also the mitochondrial dynamin-like GTPase OPA1 has been shown to play a crucial role in cristae remodeling and mitochondrial fusion (Barrera et al., 2016; Frezza et al., 2006; Glytsou et al., 2016; Meeusen et al., 2006; Olichon et al., 2003). Furthermore, a direct involvement of the MICOS component Mic10 in creating membrane curvature was recently demonstrated (Barbot et al., 2015; Bohnert et al., 2015) indicating that Mic10 directly participates in mitochondrial membrane remodeling by oligomerization. It has been proposed that the two transmembrane domains of Mic10 adopt a helical hairpin conformation in the IM with an asymmetric wedge shape. Moreover, several lines of evidence exist that specific phospholipids are also involved in cristae membrane organization and the generation of membrane curvature at crista junctions in

cooperation with MICOS (Aaltonen et al., 2016; Acehan et al., 2007; Friedman et al., 2015; Guarani et al., 2015; Harner et al., 2014; Martensson et al., 2017; Mileykovskaya and Dowhan, 2009; Weber et al., 2013). The analysis of this work now indicates that Mic60 directly contributes to membrane remodeling and mitochondrial IM architecture at crista junctions, but uses a mechanism different from Mic10. These results are in agreement with recently published data, using full length Mic60 from *Saccharomyces cerevisiae*, which bent the membrane from large unilamellar vesicles (LUV) (Tarasenko et al., 2017).

Changes in the lipid composition and asymmetry of a membrane bilayer can also induce membrane curvatures (Figure 32) (McMahon and Boucrot, 2015). The inner mitochondrial membrane is composed of a specific lipid composition with approximately 18% cardiolipin (CL) (Horvath and Daum, 2013). This phospholipid contains four fatty acid chains, two per phosphate head groups connected via a glycerol backbone. In comparison, other phospholipids like phosphatidylserine, phosphatidylethanolamine and others only have two acyl chains, which allow CL to occupy a higher volume in the hydrophobic core of the bilayer. In this way, cardiolipin incorporates into mitochondrial membranes and competes for space with the remaining lipids. It was shown that CJs are highly enriched in CL, which may induce membrane curvature at this side (Ikon and Ryan, 2017). As described in the introduction part, MICOS is also located at CJs and sensitive to CL. A recent study showed, that also N-terminal truncated Mic60 of *Arabidopsis thaliana* is associated with CL (Michaud et al., 2016). In this thesis, I could not find an effect of including additional cardiolipin in the Folch liposomes for Mic60 binding (Figure 19). This could be explained due to the use of different organisms (*Arabidopsis thaliana* versus *Chaetomium thermophilum*), which vary in their domain length and also by the use of different construct lengths. Additionally, Michaud et al used a defined lipid composition for their experiments. Thus, Folch liposomes may already contain sufficient concentrations of negatively charged phospholipids including cardiolipin to mediate maximal binding of Mic60.

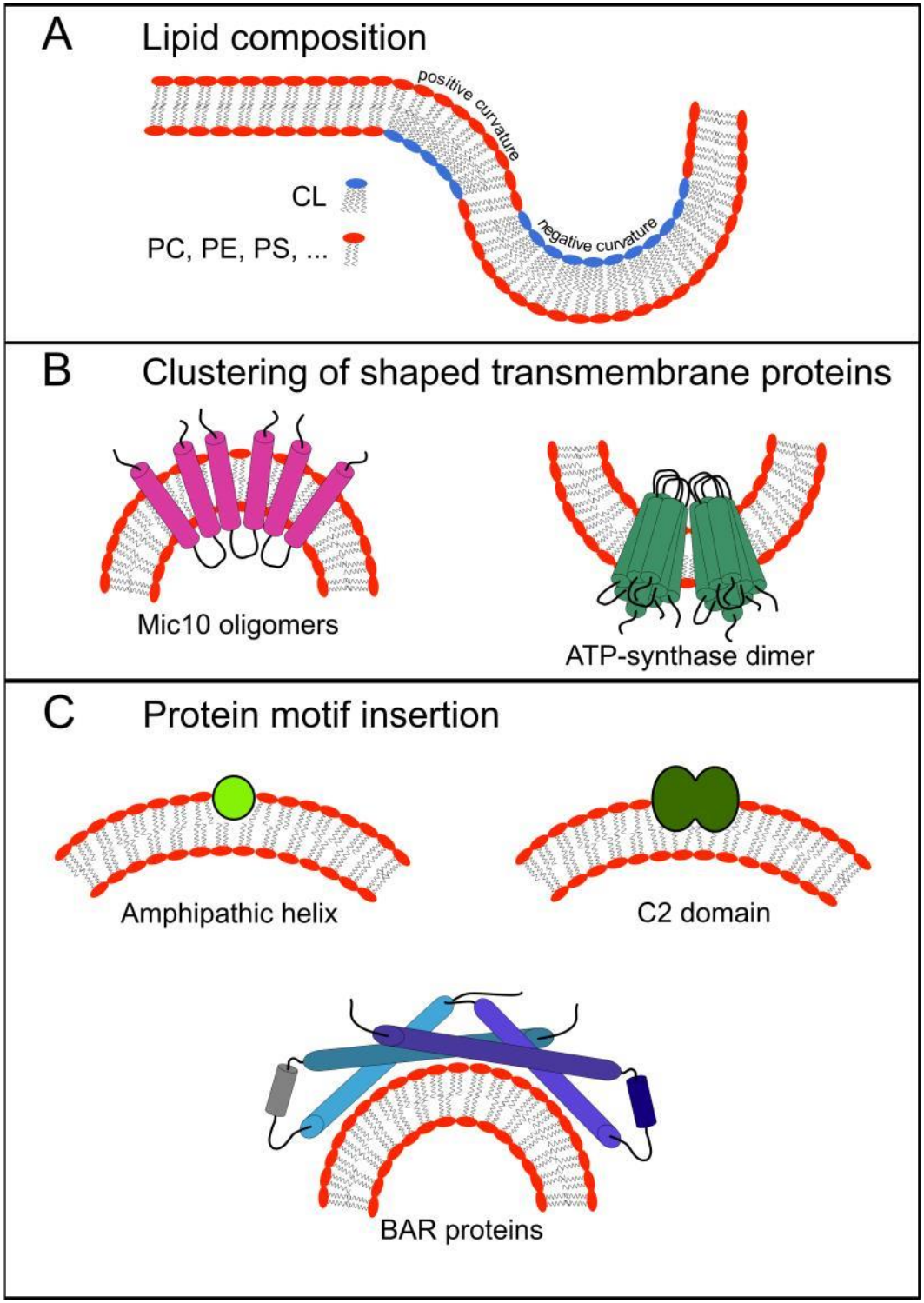


**Figure 32. Overview of membrane curvature inducing lipids and proteins. (A) Insertion of specific lipids like cardiolipin (CL) in one of the bilayers can induce curvature to membranes mainly composed of – Phosphotidylcholine (PC), Phosphotidylethanolamine (PE), and Phosphotidylserine (PS). (B) Shaped transmembrane proteins are clustering inside the membrane to induce membrane curvatures. (C) Specific protein domains like amphipathic helices, C2 domains from synaptotagmin and BAR-domains are well characterized elements, which can induce membrane curvatures. Modified from (McMahon and Boucrot, 2015).**

The insertion of protein motifs like amphipathic helices (Drin and Antonny, 2010), C2 domains and loops (Daumke et al., 2007; Martens et al., 2007), N-Bin/Amphiphysin/Rvs (BAR) domains (Peter et al., 2004) and clustering of shaped transmembrane proteins (McMahon and Boucrot, 2015) can induce membrane curvature (Figure 32). Amphipathic helices (AHs) are well-characterized mediators for creating and/or sensing positive membrane curvature, known for instance from Amphipathic Lipid Packing Sensor (ALPS) domain-containing proteins or small GTPases of the Arf and Sar1 family (Drin et al., 2007). While they display low conservation at the sequence level, their amphipathic character is well conserved throughout evolution. It is reported that AHs are mostly unfolded in ionic buffers but fold upon recognizing the negatively charged membrane surface. The hydrophobic effect forces the helix to be transferred into the membrane, while hydrophobic side-chains are positioned between the fatty-acid chains and water molecules are released (Seelig, 2004). This process enforces membrane curvature by asymmetrically inserting the helix into the lipid bilayer and competing for space with the lipid head groups (Kozlov et al., 2014). Often, membrane curvature, which is formed by amphipathic helices is supported by rigid membrane scaffolds that impose their bent shape on the underlying membrane. Interestingly, as the main part of Mic60 is pointing to the IMS, the AH is incorporated into the IM at this site to introduce positive curvature. As cristae formation involves also negative curvature, it is speculated that Mic60 is not involved in the initialization of these invaginations but rather in stabilizing the resulting positive curvature of CJs.

## 5.2 Comparison of Mic60 to BAR domain proteins

Some proteins of the BAR-domain family have an amphipathic helix at the N-terminus, also known as N-BAR proteins. As described above, this AH is inserted into the membrane, thereby inducing membrane curvature, while the BAR-domain homo- or heterodimers adopt a crescent shape to bind membranes (Peter et al., 2004). Over the years, three main types of BAR-domain containing proteins were classified. N-BAR and F-BAR (FCH-BAR) proteins are inducing positive curvature whereas I-BAR proteins (I for invert) force the membrane to form a negative curvature (Figure 33).

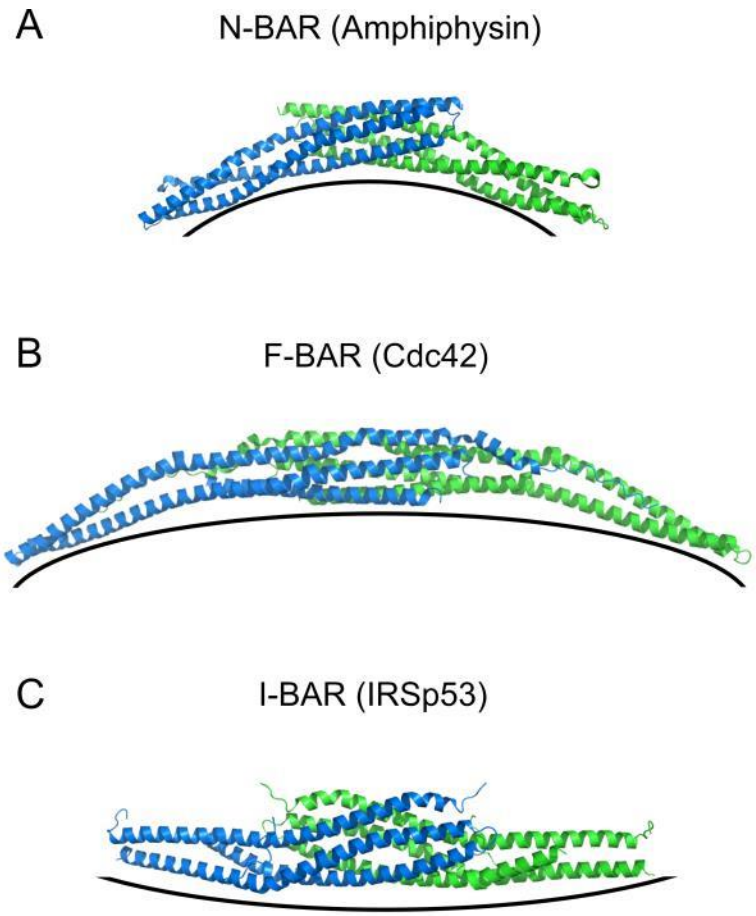


**Figure 33. Overview of different types of BAR domains. All shown examples are forming homodimers (green and blue) (A) N-BAR domains like Amphiphysin and (B) F-BAR like Cdc42 are sensing positive membrane curvature with high or low angles, respectively. (C) I-BAR proteins like IRSp53 are the only variants, inducing negative curvatures. For more details see endocytosis.org.**

Additional domains were found like the Scr Homology 3 domain (SH3), which allows binding to poly-proline motifs of target proteins (Rao et al., 2010). Members of the BAR protein family have a conserved structure by forming a three helix coiled-coil core to adopt its typical 'banana shape' but lack characteristic signature sequence motifs, which makes a sequence based prediction difficult (Mim and Unger, 2012). Membrane curvature generated by BAR proteins involves the AH but such proteins also act as curved scaffolds to impose their shape on the membrane. This mechanism is supported by molecular dynamic simulations and is known as the 'scaffolding' mechanism (McMahon and Gallop, 2005). One highly investigated and well described BAR domain containing protein is endophilin, which regulates clathrin-coated endocytosis (Gallop et al., 2006; Masuda et al., 2006). Its N-terminal amphipathic helix cooperates with a dimeric or oligomeric curved BAR-domain scaffold to create membrane curvature.

Similar to endophilin, the dimeric coiled-coil domain of Mic60 may assist the amphipathic LBS1 in shaping the mitochondrial membrane. Furthermore, similar to BAR proteins, Mic60 is predicted to form a coiled-coil structure from three alpha helices. The isolated coiled-coil of Mic60 was tested in liposome co-sedimentation assays but failed to bind to membranes. This resulted in the identification of the AH and, further, indicated a very weak binding affinity of Mic60's coiled-coil to membranes. Overall, the observation that Mic60 can generate positive membrane curvature is in agreement with a role of MICOS at the rim of CJs, where positive membrane curvature needs to be stabilized. The coordination of the membrane remodeling activities of Mic60 and Mic10 likely involves Mic12 since this subunit is crucial for the coupling of both MICOS subcomplexes (Zerbes et al., 2016). As the identification of BAR domain motifs is very difficult, a crystal structure of the isolated coiled-coil domain of Mic60 may shed light on its fold and function.

## 5.3 Mic60-Mic19 subcomplex activation

In several BAR domain proteins such as PACSINs, membrane binding and remodeling is regulated by intramolecular auto-inhibitory actions of the SH3 domain which is released upon binding to interaction partners such as dynamin (Rao et al., 2010). This work envisages a similar scenario for the C-terminal mitofilin domain in Mic60, which controls membrane tubulation by intramolecular interactions or binding to the CHCH domain of Mic19. It has been demonstrated that the mitofilin domain is of crucial importance for the integrity of the MICOS machinery (Korner et al., 2012; Zerbes et al., 2012a). Deletion of this domain strongly impaired the co-isolation of all other subunits with Mic60 including Mic19. A possible interpretation is that a precise regulation of Mic60 membrane interaction is critical for MICOS stability. However, the mitofilin domain of Mic60 may well have distinct roles for MICOS assembly, functionality and coupling to partner protein complexes (Korner et al., 2012; Zerbes et al., 2012a), in agreement with the strong conservation of this domain. In addition, the presence of some residual crista junctions in Mic60 deletion strains (Alkhaja et al., 2012; Friedman et al., 2015; Harner et al., 2011; Hoppins et al., 2011; von der Malsburg et al., 2011) argues for a second, Mic60-independent pathway for the formation of crista junctions.

These findings suggest that Mic19 augments the membrane-shaping activity of Mic60. This may explain the defective cristae morphology in *mic19*Δ cells (Harner et al., 2011; Hoppins et al., 2011; von der Malsburg et al., 2011) and the observation that Mic19 knockdown in mammalian cells results in a reduced crista junction diameter (Darshi et al., 2011). The CHCH domain of Mic19 mediates the contact to the mitofilin domain of Mic60, but also the coiled-coil domain of Mic19 is required for enhancing the membrane remodeling activity of Mic60. The CHCH domain of Mic19 contains conserved cysteine residues (Figure 17) (Darshi et al., 2012) but only oxidized Mic19 carrying an intramolecular disulfide bond was found in the MICOS complex (Sakowska et al., 2015). ITC data reveal a strong influence of the Mic19 cysteine residues on the interaction between Mic19 and Mic60. Removal of the two cysteines in Mic19 reduced the affinity for Mic60, suggesting that the intramolecular disulfide bond in the CHCH domain stabilizes the Mic60-bound conformation of Mic19, thereby modulating Mic60 membrane binding.

Taken together, this work has elucidated a so far unknown conserved function of the Mic19-Mic60 subcomplex of MICOS in generating membrane curvature at CJs, which is crucial for proper mitochondrial architecture and function.

## 5.4 Model of the Mic60-Mic19 complex in crista junction and contact site formation

Mic60 is nuclear-encoded and adopts a specific fold of the coiled-coil domain after its expression. The isolated mitofilin domain tends to aggregate similar to other N-terminal truncated Mic60 constructs. Secondary structure prediction revealed two alpha helices between the TM and the coiled-coil domain. If theses helices are present, constructs become soluble again. These helices might therefore work as an intramolecular interaction platform for mitofilin stabilization (Figure 34A).

Next, the signaling sequence is used to guide Mic60 to the TOM complex (Figure 34B) to be transferred into the mitochondrion. The signaling sequence is cleaved and remains outside of the organelle (Figure 34C). Mic60s transmembrane is incorporated into the inner membrane, while the mitofilin binds to Tom40 (Figure 34D). This process is necessary to keep the LBS distant from the IM and therefore be in an inactive state. Folding of the coiled-coil adopts a crescent shape to sense membrane curvatures by the AH and the coiled-coil but also lead to membrane tension and pulls the IM close to the OM to induce contact sites (Figure 34E). Dimerization of Mic60 stabilizes this curvature but also serves as a stabilizer for cristae junctions (Figure 34F). Recent studies observed stable contact sites and also some cristae junctions even in the absence of Mic19 (Darshi et al., 2011). This work elucidated the importance of Mic19 to effectively induce membrane curvatures but it may also have a role in stabilizing cristae junctions of defined angles. Mic19 is nuclear-encoded and is further N-terminal myristoylated, a posttranslational modification, which is a sensor for membranes. The reducing condition of the cytoplasm prevents the CHCH domain to form disulfide bonds (Figure 34G). After the import of Mic19, the CHCH domain binds to the membrane bound oxidoreductase Mia40, which introduces a disulfide bond (Figure 34H). The folded CHCH domain can now interact with the mitofilin domain to be released from the TOM complex (Figure 34I).

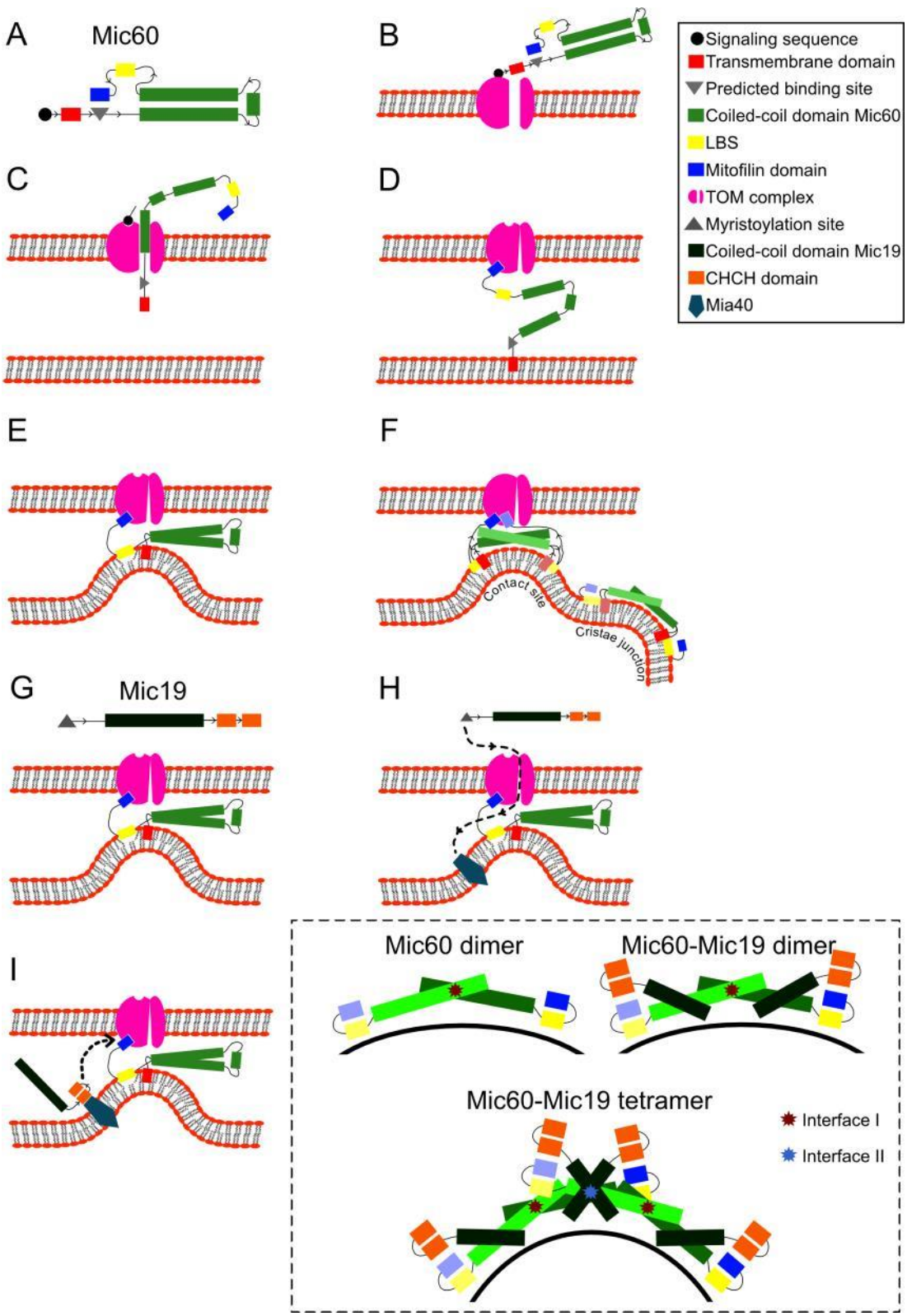


**Figure 34. A cartoon model, which illustrates a possible mode of action in contact site and cristae junction formation by the Mic60-Mic19 complex. The top box contains the used abbreviations with the color code and form. The bottom dashed line box illustrates a possible interface (red and blue stars) to form Mic60 dimers (top, left) but also Mic60-Mic19 complex dimers (top, right). A second interface (blue star) is formed between two Mic60-Mic19 complex dimers including two Mic19 molecules. The mode of action is explained within the text. Light colors represent the adjacent chain within the Mic60 dimer.**

Native PAGE analyzes revealed that Mic19 has the potential to form Mic60 tetramers from dimers. This oligomer formation includes Mic19's coiled-coil, as the isolated CHCH cannot induce a tetramer (Figure 27B). Mic60 dimers are formed via their coiled-coil domain and induce membrane curvature with a defined diameter by incorporating the AH into the membrane. Binding of Mic19 to Mic60 occurs via mitofilin and Mic19's CHCH domain. This work clearly showed that Mic19's coiled-coil cannot bind or is only weakly interacting with Mic60. However, Mic19's CHCH domain strongly binds to the mitofilin domain and may allow the coiled-coil of Mic60 and Mic19 to create a second interface to form stable tetramers (Figure 34 right lower box). Such tetramers could form oligomers with a highly reduced diameter compared to the Mic60 dimer. This model could explain, why the Mic60-Mic19 complex shows increased liposome leakage but also why small particles reminiscent of membrane remnants were seen within the electron micrographs (Figure 35). Furthermore, the complex may also introduce scission to the membrane by oligomerizing around lipid necks *in vitro*. An open question is, how the remaining parts of the MICOS complex contribute to membrane remodeling. Future studies using the entire purified or reconstitute MICOS complex can be used to address this issue.

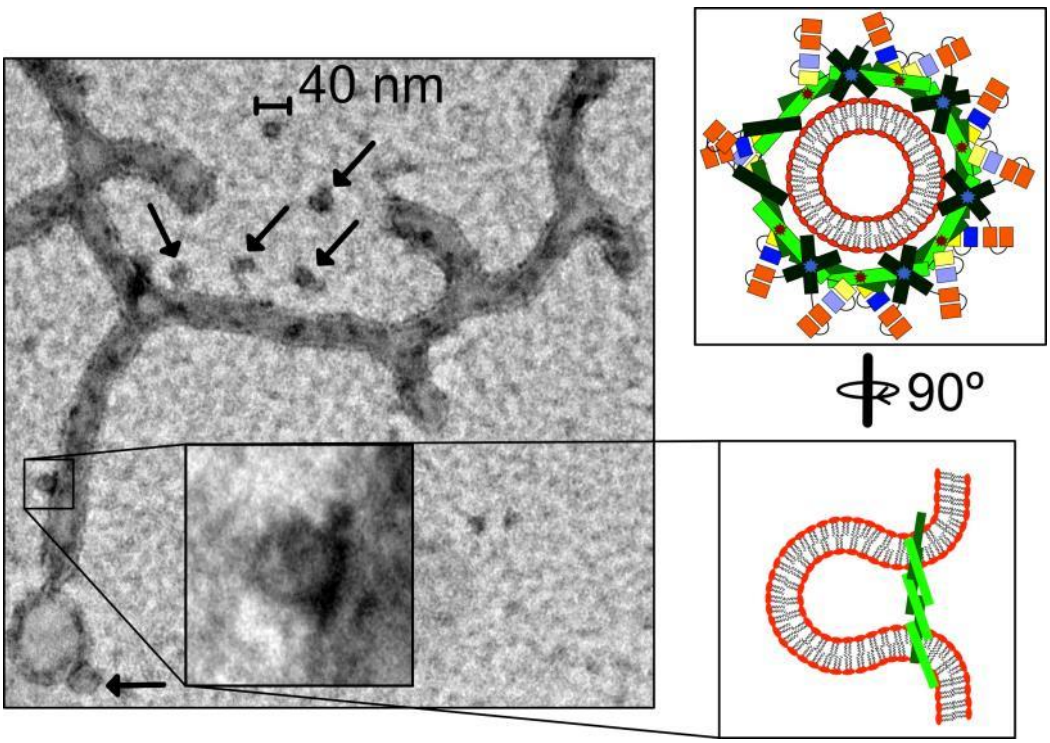


**Figure 35. Electron micrograph of liposomes incubated with Mic60 and Mic19 (left). Arrows indicate several small particles reminiscent of membrane remnants. The close up shows a tubule, which is constricted off the membrane. The black density represents a high protein density around the tubule neck. The right cartoon models show the Mic60-Mic19 oligomers at the tubule neck.**

# 6 References


Aaltonen, M.J., Friedman, J.R., Osman, C., Salin, B., di Rago, J.P., Nunnari, J., Langer, T., and Tatsuta, T. (2016). MICOS and phospholipid transfer by Ups2-Mdm35 organize membrane lipid synthesis in mitochondria. J Cell Biol *213*, 525-534.

Acehan, D., Xu, Y., Stokes, D.L., and Schlame, M. (2007). Comparison of lymphoblast mitochondria from normal subjects and patients with Barth syndrome using electron microscopic tomography. Lab Invest *87*, 40-48.

Alberts, B., Johnson, A., J, L., and al, e. (2002). Molecular Biology of the Cell. (New York: Garland Science).

Alexander, C., Votruba, M., Pesch, U.E., Thiselton, D.L., Mayer, S., Moore, A., Rodriguez, M., Kellner, U., Leo-Kottler, B., Auburger, G., et al. (2000). OPA1, encoding a dynamin-related GTPase, is mutated in autosomal dominant optic atrophy linked to chromosome 3q28. Nature genetics *26*, 211-215.

Alkhaja, A.K., Jans, D.C., Nikolov, M., Vukotic, M., Lytovchenko, O., Ludewig, F., Schliebs, W., Riedel, D., Urlaub, H., Jakobs, S., et al. (2012). MINOS1 is a conserved component of mitofilin complexes and required for mitochondrial function and cristae organization. Mol Biol Cell *23*, 247-257.

An, J., Shi, J., He, Q., Lui, K., Liu, Y., Huang, Y., and Sheikh, M.S. (2012). CHCM1/CHCHD6, novel mitochondrial protein linked to regulation of mitofilin and mitochondrial cristae morphology. J Biol Chem *287*, 7411-7426.

Ban, T., Heymann, J.A., Song, Z., Hinshaw, J.E., and Chan, D.C. (2010). OPA1 disease alleles causing dominant optic atrophy have defects in cardiolipin-stimulated GTP hydrolysis and membrane tubulation. Human molecular genetics *19*, 2113-2122.

Barbot, M., Jans, D.C., Schulz, C., Denkert, N., Kroppen, B., Hoppert, M., Jakobs, S., and Meinecke, M. (2015). Mic10 oligomerizes to bend mitochondrial inner membranes at cristae junctions. Cell Metab *21*, 756-763.

Barrera, M., Koob, S., Dikov, D., Vogel, F., and Reichert, A.S. (2016). OPA1 functionally interacts with MIC60 but is dispensable for crista junction formation. FEBS Lett *590*, 3309-3322.

Becker, T., Pfannschmidt, S., Guiard, B., Stojanovski, D., Milenkovic, D., Kutik, S., Pfanner, N., Meisinger, C., and Wiedemann, N. (2008). Biogenesis of the mitochondrial TOM complex: Mim1 promotes insertion and assembly of signal-anchored receptors. J Biol Chem *283*, 120-127.

Bhatia, V.K., Madsen, K.L., Bolinger, P.Y., Kunding, A., Hedegard, P., Gether, U., and Stamou, D. (2009). Amphipathic motifs in BAR domains are essential for membrane curvature sensing. EMBO J *28*, 3303-3314.

Bohnert, M., Zerbes, R.M., Davies, K.M., Muhleip, A.W., Rampelt, H., Horvath, S.E., Boenke, T., Kram, A., Perschil, I., Veenhuis, M., et al. (2015). Central role of Mic10 in the mitochondrial contact site and cristae organizing system. Cell Metab *21*, 747-755.

Cao, Y.L., Meng, S., Chen, Y., Feng, J.X., Gu, D.D., Yu, B., Li, Y.J., Yang, J.Y., Liao, S., Chan, D.C., et al. (2017). MFN1 structures reveal nucleotide-triggered dimerization critical for mitochondrial fusion. Nature *542*, 372-376.

Chacinska, A., Pfannschmidt, S., Wiedemann, N., Kozjak, V., Sanjuan Szklarz, L.K., Schulze-Specking, A., Truscott, K.N., Guiard, B., Meisinger, C., and Pfanner, N. (2004). Essential role of Mia40 in import and assembly of mitochondrial intermembrane space proteins. EMBO J *23*, 3735-3746.

Chan, D.C. (2006). Mitochondria: dynamic organelles in disease, aging, and development. Cell *125*, 1241-1252.

Chatzi, A., Manganas, P., and Tokatlidis, K. (2016). Oxidative folding in the mitochondrial intermembrane space: A regulated process important for cell physiology and disease. Biochim Biophys Acta *1863*, 1298-1306.

Cipolat, S., Martins de Brito, O., Dal Zilio, B., and Scorrano, L. (2004). OPA1 requires mitofusin 1 to promote mitochondrial fusion. Proc Natl Acad Sci U S A *101*, 15927-15932.

Cogliati, S., Frezza, C., Soriano, M.E., Varanita, T., Quintana-Cabrera, R., Corrado, M., Cipolat, S., Costa, V., Casarin, A., Gomes, L.C., et al. (2013). Mitochondrial cristae shape determines respiratory chain supercomplexes assembly and respiratory efficiency. Cell *155*, 160-171.

Cui, H., Mim, C., Vazquez, F.X., Lyman, E., Unger, V.M., and Voth, G.A. (2013). Understanding the role of amphipathic helices in N-BAR domain driven membrane remodeling. Biophys J *104*, 404-411.

Darshi, M., Mendiola, V.L., Mackey, M.R., Murphy, A.N., Koller, A., Perkins, G.A., Ellisman, M.H., and Taylor, S.S. (2011). ChChd3, an inner mitochondrial membrane protein, is essential for maintaining crista integrity and mitochondrial function. J Biol Chem *286*, 2918-2932.

Darshi, M., Trinh, K.N., Murphy, A.N., and Taylor, S.S. (2012). Targeting and import mechanism of coiled-coil helix coiled-coil helix domain-containing protein 3 (ChChd3) into the mitochondrial intermembrane space. J Biol Chem *287*, 39480-39491.

Daumke, O., Lundmark, R., Vallis, Y., Martens, S., Butler, P.J., and McMahon, H.T. (2007). Architectural and mechanistic insights into an EHD ATPase involved in membrane remodelling. Nature *449*, 923-927.

Davies, K.M., Strauss, M., Daum, B., Kief, J.H., Osiewacz, H.D., Rycovska, A., Zickermann, V., and Kuhlbrandt, W. (2011). Macromolecular organization of ATP synthase and complex I in whole mitochondria. Proc Natl Acad Sci U S A *108*, 14121-14126.

de Marcos-Lousa, C., Sideris, D.P., and Tokatlidis, K. (2006). Translocation of mitochondrial inner-membrane proteins: conformation matters. Trends Biochem Sci *31*, 259-267.

Ding, C., Wu, Z., Huang, L., Wang, Y., Xue, J., Chen, S., Deng, Z., Wang, L., Song, Z., and Chen, S. (2015). Mitofilin and CHCHD6 physically interact with Sam50 to sustain cristae structure. Sci Rep *5*, 16064.

Drin, G., and Antonny, B. (2010). Amphipathic helices and membrane curvature. FEBS Lett *584*, 1840-1847.

Drin, G., Casella, J.F., Gautier, R., Boehmer, T., Schwartz, T.U., and Antonny, B. (2007). A general amphipathic alpha-helical motif for sensing membrane curvature. Nature structural & molecular biology *14*, 138-146.

Endo, T., and Yamano, K. (2009). Multiple pathways for mitochondrial protein traffic. Biol Chem *390*, 723-730.

Enriquez, J.A. (2016). Supramolecular Organization of Respiratory Complexes. Annu Rev Physiol *78*, 533-561.

Ernster, L., and Schatz, G. (1981). Mitochondria: a historical review. J Cell Biol *91*, 227s-255s.

Ferguson, S.M., and De Camilli, P. (2012). Dynamin, a membrane-remodelling GTPase. Nature reviews. Molecular cell biology *13*, 75-88.

Frezza, C., Cipolat, S., Martins de Brito, O., Micaroni, M., Beznoussenko, G.V., Rudka, T., Bartoli, D., Polishuck, R.S., Danial, N.N., De Strooper, B., et al. (2006). OPA1 controls apoptotic cristae remodeling independently from mitochondrial fusion. Cell *126*, 177-189.

Friedman, J.R., Mourier, A., Yamada, J., McCaffery, J.M., and Nunnari, J. (2015). MICOS coordinates with respiratory complexes and lipids to establish mitochondrial inner membrane architecture. Elife *4*.

Frohlich, C., Grabiger, S., Schwefel, D., Faelber, K., Rosenbaum, E., Mears, J., Rocks, O., and Daumke, O. (2013). Structural insights into oligomerization and mitochondrial remodelling of dynamin 1-like protein. EMBO J *32*, 1280-1292.

Furukawa, A., Kawamoto, Y., Chiba, Y., Takei, S., Hasegawa-Ishii, S., Kawamura, N., Yoshikawa, K., Hosokawa, M., Oikawa, S., Kato, M., et al. (2011). Proteomic identification of hippocampal proteins vulnerable to oxidative stress in excitotoxin-induced acute neuronal injury. Neurobiology of disease *43*, 706-714.

Gallop, J.L., Jao, C.C., Kent, H.M., Butler, P.J., Evans, P.R., Langen, R., and McMahon, H.T. (2006). Mechanism of endophilin N-BAR domain-mediated membrane curvature. EMBO J *25*, 2898-2910.

Gieffers, C., Korioth, F., Heimann, P., Ungermann, C., and Frey, J. (1997). Mitofilin is a transmembrane protein of the inner mitochondrial membrane expressed as two isoforms. Experimental cell research *232*, 395-399.

Gilkerson, R.W., Selker, J.M., and Capaldi, R.A. (2003). The cristal membrane of mitochondria is the principal site of oxidative phosphorylation. FEBS Lett *546*, 355-358.

Glytsou, C., Calvo, E., Cogliati, S., Mehrotra, A., Anastasia, I., Rigoni, G., Raimondi, A., Shintani, N., Loureiro, M., Vazquez, J., et al. (2016). Optic Atrophy 1 Is Epistatic to the Core MICOS Component MIC60 in Mitochondrial Cristae Shape Control. Cell reports *17*, 3024-3034.

Griparic, L., Kanazawa, T., and van der Bliek, A.M. (2007). Regulation of the mitochondrial dynamin-like protein Opa1 by proteolytic cleavage. J Cell Biol *178*, 757-764.

Guarani, V., McNeill, E.M., Paulo, J.A., Huttlin, E.L., Frohlich, F., Gygi, S.P., Van Vactor, D., and Harper, J.W. (2015). QIL1 is a novel mitochondrial protein required for MICOS complex stability and cristae morphology. Elife *4*.

Habib, S.J., Neupert, W., and Rapaport, D. (2007). Analysis and prediction of mitochondrial targeting signals. Methods in cell biology *80*, 761-781.

Harner, M., Korner, C., Walther, D., Mokranjac, D., Kaesmacher, J., Welsch, U., Griffith, J., Mann, M., Reggiori, F., and Neupert, W. (2011). The mitochondrial contact site complex, a determinant of mitochondrial architecture. EMBO J *30*, 4356-4370.

Harner, M.E., Unger, A.K., Geerts, W.J., Mari, M., Izawa, T., Stenger, M., Geimer, S., Reggiori, F., Westermann, B., and Neupert, W. (2016). An evidence based hypothesis on the existence of two pathways of mitochondrial crista formation. Elife *5*.

Harner, M.E., Unger, A.K., Izawa, T., Walther, D.M., Ozbalci, C., Geimer, S., Reggiori, F., Brugger, B., Mann, M., Westermann, B., et al. (2014). Aim24 and MICOS modulate respiratory function, tafazzin-related cardiolipin modification and mitochondrial architecture. Elife *3*, e01684.

Haucke, V., Neher, E., and Sigrist, S.J. (2011). Protein scaffolds in the coupling of synaptic exocytosis and endocytosis. Nature reviews. Neuroscience *12*, 127-138.

Head, B.P., Zulaika, M., Ryazantsev, S., and van der Bliek, A.M. (2011). A novel mitochondrial outer membrane protein, MOMA-1, that affects cristae morphology in Caenorhabditis elegans. Mol Biol Cell *22*, 831-841.

Hell, K. (2008). The Erv1-Mia40 disulfide relay system in the intermembrane space of mitochondria. Biochim Biophys Acta *1783*, 601-609.

Henle, J. (1841). Allgemeine Anatomie. Leipzig.

Hessenberger, M., Zerbes, R.M., Rampelt, H., Kunz, S., Xavier, A.H., Purfurst, B., Lilie, H., Pfanner, N., van der Laan, M., and Daumke, O. (2017). Regulated membrane remodeling by Mic60 controls formation of mitochondrial crista junctions. Nature communications *8*, 15258.

Hohr, A.I., Straub, S.P., Warscheid, B., Becker, T., and Wiedemann, N. (2015). Assembly of beta-barrel proteins in the mitochondrial outer membrane. Biochim Biophys Acta *1853*, 74-88.

Hoppins, S., Collins, S.R., Cassidy-Stone, A., Hummel, E., Devay, R.M., Lackner, L.L., Westermann, B., Schuldiner, M., Weissman, J.S., and Nunnari, J. (2011). A mitochondrial-focused genetic interaction map reveals a scaffold-like complex required for inner membrane organization in mitochondria. J Cell Biol *195*, 323-340.

Horvath, S.E., and Daum, G. (2013). Lipids of mitochondria. Progress in lipid research *52*, 590-614.

Horvath, S.E., Rampelt, H., Oeljeklaus, S., Warscheid, B., van der Laan, M., and Pfanner, N. (2015). Role of membrane contact sites in protein import into mitochondria. Protein science : a publication of the Protein Society *24*, 277-297.

Houtkooper, R.H., and Vaz, F.M. (2008). Cardiolipin, the heart of mitochondrial metabolism. Cellular and molecular life sciences : CMLS *65*, 2493-2506.

Ikon, N., and Ryan, R.O. (2017). Cardiolipin and mitochondrial cristae organization. Biochim Biophys Acta *1859*, 1156-1163.

Itoh, K., Tamura, Y., Iijima, M., and Sesaki, H. (2013). Effects of Fcj1-Mos1 and mitochondrial division on aggregation of mitochondrial DNA nucleoids and organelle morphology. Mol Biol Cell *24*, 1842-1851.

John, G.B., Shang, Y., Li, L., Renken, C., Mannella, C.A., Selker, J.M., Rangell, L., Bennett, M.J., and Zha, J. (2005). The mitochondrial inner membrane protein mitofilin controls cristae morphology. Mol Biol Cell *16*, 1543-1554.

Kharbanda, S., Pandey, P., Schofield, L., Israels, S., Roncinske, R., Yoshida, K., Bharti, A., Yuan, Z.M., Saxena, S., Weichselbaum, R., et al. (1997). Role for Bcl-xL as an inhibitor of cytosolic cytochrome C accumulation in DNA damage-induced apoptosis. Proc Natl Acad Sci U S A *94*, 6939-6942.

Koehler, C.M. (2004). The small Tim proteins and the twin Cx3C motif. Trends Biochem Sci *29*, 1-4.

Koehler, C.M., Leuenberger, D., Merchant, S., Renold, A., Junne, T., and Schatz, G. (1999). Human deafness dystonia syndrome is a mitochondrial disease. Proc Natl Acad Sci U S A *96*, 2141-2146.

Koob, S., Barrera, M., Anand, R., and Reichert, A.S. (2015a). Data supporting the role of the non-glycosylated isoform of MIC26 in determining cristae morphology. Data in brief *4*, 135-139.

Koob, S., Barrera, M., Anand, R., and Reichert, A.S. (2015b). The non-glycosylated isoform of MIC26 is a constituent of the mammalian MICOS complex and promotes formation of crista junctions. Biochim Biophys Acta *1853*, 1551-1563.

Kornberg, H. (2000). Krebs and his trinity of cycles. Nature reviews. Molecular cell biology *1*, 225-228.

Korner, C., Barrera, M., Dukanovic, J., Eydt, K., Harner, M., Rabl, R., Vogel, F., Rapaport, D., Neupert, W., and Reichert, A.S. (2012). The C-terminal domain of Fcj1 is required for formation of crista junctions and interacts with the TOB/SAM complex in mitochondria. Mol Biol Cell *23*, 2143-2155.

Kozlov, M.M., Campelo, F., Liska, N., Chernomordik, L.V., Marrink, S.J., and McMahon, H.T. (2014). Mechanisms shaping cell membranes. Curr Opin Cell Biol *29*, 53-60.

Kutik, S., Guiard, B., Meyer, H.E., Wiedemann, N., and Pfanner, N. (2007). Cooperation of translocase complexes in mitochondrial protein import. J Cell Biol *179*, 585-591.

Li, H., Ruan, Y., Zhang, K., Jian, F., Hu, C., Miao, L., Gong, L., Sun, L., Zhang, X., Chen, S., et al. (2016). Mic60/Mitofilin determines MICOS assembly essential for mitochondrial dynamics and mtDNA nucleoid organization. Cell Death Differ *23*, 380-392.

Liu, H., and Naismith, J.H. (2008). An efficient one-step site-directed deletion, insertion, single and multiple-site plasmid mutagenesis protocol. BMC biotechnology *8*, 91.

MacVicar, T., and Langer, T. (2016). OPA1 processing in cell death and disease - the long and short of it. Journal of cell science *129*, 2297-2306.

Mannella, C.A. (2006). Structure and dynamics of the mitochondrial inner membrane cristae. Biochim Biophys Acta *1763*, 542-548.

Martens, S., Kozlov, M.M., and McMahon, H.T. (2007). How synaptotagmin promotes membrane fusion. Science *316*, 1205-1208.

Martens, S., and McMahon, H.T. (2008). Mechanisms of membrane fusion: disparate players and common principles. Nature reviews. Molecular cell biology *9*, 543-556.

Martensson, C.U., Doan, K.N., and Becker, T. (2017). Effects of lipids on mitochondrial functions. Biochim Biophys Acta *1862*, 102-113.

Masuda, M., Takeda, S., Sone, M., Ohki, T., Mori, H., Kamioka, Y., and Mochizuki, N. (2006). Endophilin BAR domain drives membrane curvature by two newly identified structure-based mechanisms. EMBO J *25*, 2889-2897.

McMahon, H.T., and Boucrot, E. (2015). Membrane curvature at a glance. Journal of cell science *128*, 1065-1070.

McMahon, H.T., and Gallop, J.L. (2005). Membrane curvature and mechanisms of dynamic cell membrane remodelling. Nature *438*, 590-596.

Meeusen, S., DeVay, R., Block, J., Cassidy-Stone, A., Wayson, S., McCaffery, J.M., and Nunnari, J. (2006). Mitochondrial inner-membrane fusion and crista maintenance requires the dynamin-related GTPase Mgm1. Cell *127*, 383-395.

Michaud, M., Gros, V., Tardif, M., Brugiere, S., Ferro, M., Prinz, W.A., Toulmay, A., Mathur, J., Wozny, M., Falconet, D., et al. (2016). AtMic60 Is Involved in Plant Mitochondria Lipid Trafficking and Is Part of a Large Complex. Curr Biol *26*, 627-639.

Mileykovskaya, E., and Dowhan, W. (2009). Cardiolipin membrane domains in prokaryotes and eukaryotes. Biochim Biophys Acta *1788*, 2084-2091.

Milone, M., and Benarroch, E.E. (2012). Mitochondrial dynamics: general concepts and clinical implications. Neurology *78*, 1612-1619.

Mim, C., and Unger, V.M. (2012). Membrane curvature and its generation by BAR proteins. Trends Biochem Sci *37*, 526-533.

Mokranjac, D., and Neupert, W. (2010). The many faces of the mitochondrial TIM23 complex. Biochim Biophys Acta *1797*, 1045-1054.

Mozdy, A.D., and Shaw, J.M. (2003). A fuzzy mitochondrial fusion apparatus comes into focus. Nature reviews. Molecular cell biology *4*, 468-478.

Muhleip, A.W., Joos, F., Wigge, C., Frangakis, A.S., Kuhlbrandt, W., and Davies, K.M. (2016). Helical arrays of U-shaped ATP synthase dimers form tubular cristae in ciliate mitochondria. Proc Natl Acad Sci U S A *113*, 8442-8447.

Mun, J.Y., Lee, T.H., Kim, J.H., Yoo, B.H., Bahk, Y.Y., Koo, H.S., and Han, S.S. (2010). Caenorhabditis elegans mitofilin homologs control the morphology of mitochondrial cristae and influence reproduction and physiology. J Cell Physiol *224*, 748-756.

Munoz-Gomez, S.A., Slamovits, C.H., Dacks, J.B., Baier, K.A., Spencer, K.D., and Wideman, J.G. (2015a). Ancient homology of the mitochondrial contact site and cristae organizing system points to an endosymbiotic origin of mitochondrial cristae. Curr Biol *25*, 1489-1495.

Munoz-Gomez, S.A., Slamovits, C.H., Dacks, J.B., and Wideman, J.G. (2015b). The evolution of MICOS: Ancestral and derived functions and interactions. Communicative & integrative biology *8*, e1094593.

Myung, J., Gulesserian, T., Fountoulakis, M., and Lubec, G. (2003). Deranged hypothetical proteins Rik protein, Nit protein 2 and mitochondrial inner membrane protein, Mitofilin, in fetal Down syndrome brain. Cellular and molecular biology *49*, 739-746.

Neupert, W., and Herrmann, J.M. (2007). Translocation of proteins into mitochondria. Annu Rev Biochem *76*, 723-749.

Nicholas, K.B., Nicholas H.B. Jr., and Deerfield, D.W.II. (1997). GeneDoc: Analysis and Visualization of Genetic Variation. In EMBNEW.

Nunnari, J., and Suomalainen, A. (2012). Mitochondria: in sickness and in health. Cell *148*, 1145-1159.

Odgren, P.R., Toukatly, G., Bangs, P.L., Gilmore, R., and Fey, E.G. (1996). Molecular characterization of mitofilin (HMP), a mitochondria-associated protein with predicted coiled coil and intermembrane space targeting domains. Journal of cell science *109 ( Pt 9)*, 2253-2264.

Olichon, A., Baricault, L., Gas, N., Guillou, E., Valette, A., Belenguer, P., and Lenaers, G. (2003). Loss of OPA1 perturbates the mitochondrial inner membrane structure and integrity, leading to cytochrome c release and apoptosis. J Biol Chem *278*, 7743-7746.

Olichon, A., Guillou, E., Delettre, C., Landes, T., Arnaune-Pelloquin, L., Emorine, L.J., Mils, V., Daloyau, M., Hamel, C., Amati-Bonneau, P., et al. (2006). Mitochondrial dynamics and disease, OPA1. Biochim Biophys Acta *1763*, 500-509.

Otera, H., Wang, C., Cleland, M.M., Setoguchi, K., Yokota, S., Youle, R.J., and Mihara, K. (2010). Mff is an essential factor for mitochondrial recruitment of Drp1 during mitochondrial fission in mammalian cells. J Cell Biol *191*, 1141-1158.

Ott, C., Dorsch, E., Fraunholz, M., Straub, S., and Kozjak-Pavlovic, V. (2015). Detailed analysis of the human mitochondrial contact site complex indicate a hierarchy of subunits. PLoS One *10*, e0120213.

Park, Y.U., Jeong, J., Lee, H., Mun, J.Y., Kim, J.H., Lee, J.S., Nguyen, M.D., Han, S.S., Suh, P.G., and Park, S.K. (2010). Disrupted-in-schizophrenia 1 (DISC1) plays essential roles in mitochondria in collaboration with Mitofilin. Proc Natl Acad Sci U S A *107*, 17785-17790.

Pernas, L., and Scorrano, L. (2016). Mito-Morphosis: Mitochondrial Fusion, Fission, and Cristae Remodeling as Key Mediators of Cellular Function. Annu Rev Physiol *78*, 505-531.

Peter, B.J., Kent, H.M., Mills, I.G., Vallis, Y., Butler, P.J., Evans, P.R., and McMahon, H.T. (2004). BAR domains as sensors of membrane curvature: the amphiphysin BAR structure. Science *303*, 495-499.

Pfanner, N., van der Laan, M., Amati, P., Capaldi, R.A., Caudy, A.A., Chacinska, A., Darshi, M., Deckers, M., Hoppins, S., Icho, T., et al. (2014). Uniform nomenclature for the mitochondrial contact site and cristae organizing system. J Cell Biol *204*, 1083-1086.

Pratt, D.V.J.G.V.C.W. (2006). Fundamentals of Biochemistry. (John Wiley and Sons, Inc).

Qiu, J., Wenz, L.S., Zerbes, R.M., Oeljeklaus, S., Bohnert, M., Stroud, D.A., Wirth, C., Ellenrieder, L., Thornton, N., Kutik, S., et al. (2013). Coupling of mitochondrial import and export translocases by receptor-mediated supercomplex formation. Cell *154*, 596-608.

Rabl, R., Soubannier, V., Scholz, R., Vogel, F., Mendl, N., Vasiljev-Neumeyer, A., Korner, C., Jagasia, R., Keil, T., Baumeister, W., et al. (2009). Formation of cristae and crista junctions in mitochondria depends on antagonism between Fcj1 and Su e/g. J Cell Biol *185*, 1047-1063.

Rampelt, H., Bohnert, M., Zerbes, R.M., Horvath, S.E., Warscheid, B., Pfanner, N., and van der Laan, M. (2017a). Mic10, a Core Subunit of the Mitochondrial Contact Site and Cristae Organizing System, Interacts with the Dimeric F1Fo-ATP Synthase. J Mol Biol *429*, 1162-1170.

Rampelt, H., Zerbes, R.M., van der Laan, M., and Pfanner, N. (2017b). Role of the mitochondrial contact site and cristae organizing system in membrane architecture and dynamics. Biochim Biophys Acta *1864*, 737-746.

Rao, Y., Ma, Q., Vahedi-Faridi, A., Sundborger, A., Pechstein, A., Puchkov, D., Luo, L., Shupliakov, O., Saenger, W., and Haucke, V. (2010). Molecular basis for SH3 domain regulation of F-BAR-mediated membrane deformation. Proc Natl Acad Sci U S A *107*, 8213-8218.

Resh, M.D. (1999). Fatty acylation of proteins: new insights into membrane targeting of myristoylated and palmitoylated proteins. Biochim Biophys Acta *1451*, 1-16.

Rizzuto, R., Marchi, S., Bonora, M., Aguiari, P., Bononi, A., De Stefani, D., Giorgi, C., Leo, S., Rimessi, A., Siviero, R., et al. (2009). Ca(2+) transfer from the ER to mitochondria: when, how and why. Biochim Biophys Acta *1787*, 1342-1351.

Sakowska, P., Jans, D.C., Mohanraj, K., Riedel, D., Jakobs, S., and Chacinska, A. (2015). The Oxidation Status of Mic19 Regulates MICOS Assembly. Mol Cell Biol *35*, 4222-4237.

Sambrook, J., Fritsch, E., and Maniatis, T. (1989). Molecular cloning - A Laboratory Manual. Cold Spring Harbor Laboratory, Cold Spring Harbor, NY.

Schmidt, O., Pfanner, N., and Meisinger, C. (2010). Mitochondrial protein import: from proteomics to functional mechanisms. Nature reviews. Molecular cell biology *11*, 655-667.

Schuck, P. (2000). Size-distribution analysis of macromolecules by sedimentation velocity ultracentrifugation and lamm equation modeling. Biophys J *78*, 1606-1619.

Seelig, J. (2004). Thermodynamics of lipid-peptide interactions. Biochim Biophys Acta *1666*, 40-50.

Shibata, Y., Hu, J., Kozlov, M.M., and Rapoport, T.A. (2009). Mechanisms shaping the membranes of cellular organelles. Annual review of cell and developmental biology *25*, 329-354.

Sickmann, A., Reinders, J., Wagner, Y., Joppich, C., Zahedi, R., Meyer, H.E., Schonfisch, B., Perschil, I., Chacinska, A., Guiard, B., et al. (2003). The proteome of

Saccharomyces cerevisiae mitochondria. Proc Natl Acad Sci U S A *100*, 13207-13212.

Sievers, F., Wilm, A., Dineen, D., Gibson, T.J., Karplus, K., Li, W., Lopez, R., McWilliam, H., Remmert, M., Soding, J., et al. (2011). Fast, scalable generation of high-quality protein multiple sequence alignments using Clustal Omega. Mol Syst Biol *7*, 539.

Sikorski, R.S., and Hieter, P. (1989). A system of shuttle vectors and yeast host strains designed for efficient manipulation of DNA in Saccharomyces cerevisiae. Genetics *122*, 19-27.

Smith, R.A., Hartley, R.C., Cocheme, H.M., and Murphy, M.P. (2012). Mitochondrial pharmacology. Trends in pharmacological sciences *33*, 341-352.

Steffen, J., Vashisht, A.A., Wan, J., Jen, J.C., Claypool, S.M., Wohlschlegel, J.A., and Koehler, C.M. (2017). Rapid degradation of mutant SLC25A46 by the ubiquitin-proteasome system results in MFN1/2-mediated hyperfusion of mitochondria. Mol Biol Cell *28*, 600-612.

Tarasenko, D., Barbot, M., Jans, D.C., Kroppen, B., Sadowski, B., Heim, G., Mobius, W., Jakobs, S., and Meinecke, M. (2017). The MICOS component Mic60 displays a conserved membrane-bending activity that is necessary for normal cristae morphology. J Cell Biol *216*, 889-899.

van der Laan, M., Bohnert, M., Wiedemann, N., and Pfanner, N. (2012). Role of MINOS in mitochondrial membrane architecture and biogenesis. Trends in cell biology *22*, 185-192.

van der Laan, M., Horvath, S.E., and Pfanner, N. (2016). Mitochondrial contact site and cristae organizing system. Curr Opin Cell Biol *41*, 33-42.

van Dijken, J.P., Otto, R., and Harder, W. (1976). Growth of Hansenula polymorpha in a methanol-limited chemostat. Physiological responses due to the involvement of methanol oxidase as a key enzyme in methanol metabolism. Arch Microbiol *111*, 137-144.

Van Laar, V.S., Mishizen, A.J., Cascio, M., and Hastings, T.G. (2009). Proteomic identification of dopamine-conjugated proteins from isolated rat brain mitochondria and SH-SY5Y cells. Neurobiology of disease *34*, 487-500.

Vance, J.E., and Shiao, Y.J. (1996). Intracellular trafficking of phospholipids: import of phosphatidylserine into mitochondria. Anticancer research *16*, 1333-1339.

Varabyova, A., Topf, U., Kwiatkowska, P., Wrobel, L., Kaus-Drobek, M., and Chacinska, A. (2013). Mia40 and MINOS act in parallel with Ccs1 in the biogenesis of mitochondrial Sod1. The FEBS journal *280*, 4943-4959.

Vogel, F., Bornhovd, C., Neupert, W., and Reichert, A.S. (2006). Dynamic subcompartmentalization of the mitochondrial inner membrane. J Cell Biol *175*, 237-247.

Vogtle, F.N., Wortelkamp, S., Zahedi, R.P., Becker, D., Leidhold, C., Gevaert, K., Kellermann, J., Voos, W., Sickmann, A., Pfanner, N., et al. (2009). Global analysis of the mitochondrial N-proteome identifies a processing peptidase critical for protein stability. Cell *139*, 428-439.

von der Malsburg, K., Muller, J.M., Bohnert, M., Oeljeklaus, S., Kwiatkowska, P., Becker, T., Loniewska-Lwowska, A., Wiese, S., Rao, S., Milenkovic, D., et al. (2011). Dual role of mitofilin in mitochondrial membrane organization and protein biogenesis. Developmental cell *21*, 694-707.

Wai, T., and Langer, T. (2016). Mitochondrial Dynamics and Metabolic Regulation. Trends Endocrinol Metab *27*, 105-117.

Wajant, H. (2002). The Fas signaling pathway: more than a paradigm. Science *296*, 1635-1636.

Wang, C., and Youle, R.J. (2009). The role of mitochondria in apoptosis*. Annual review of genetics *43*, 95-118.

Weber, T.A., Koob, S., Heide, H., Wittig, I., Head, B., van der Bliek, A., Brandt, U., Mittelbronn, M., and Reichert, A.S. (2013). APOOL is a cardiolipin-binding constituent of the Mitofilin/MINOS protein complex determining cristae morphology in mammalian mitochondria. PLoS One *8*, e63683.

Weibel, E.R., and Palade, G.E. (1964). New Cytoplasmic Components in Arterial Endothelia. J Cell Biol *23*, 101-112.

Weihofen, A., Thomas, K.J., Ostaszewski, B.L., Cookson, M.R., and Selkoe, D.J. (2009). Pink1 forms a multiprotein complex with Miro and Milton, linking Pink1 function to mitochondrial trafficking. Biochemistry *48*, 2045-2052.

Wenz, L.S., Opalinski, L., Schuler, M.H., Ellenrieder, L., Ieva, R., Bottinger, L., Qiu, J., van der Laan, M., Wiedemann, N., Guiard, B., et al. (2014). The presequence pathway is involved in protein sorting to the mitochondrial outer membrane. EMBO reports *15*, 678-685.

Wiedemann, N., and Pfanner, N. (2017). Mitochondrial Machineries for Protein Import and Assembly. Annu Rev Biochem.

Wong, E.D., Wagner, J.A., Gorsich, S.W., McCaffery, J.M., Shaw, J.M., and Nunnari, J. (2000). The dynamin-related GTPase, Mgm1p, is an intermembrane space protein required for maintenance of fusion competent mitochondria. J Cell Biol *151*, 341-352.

Wurm, C.A., and Jakobs, S. (2006). Differential protein distributions define two sub-compartments of the mitochondrial inner membrane in yeast. FEBS Lett *580*, 5628-5634.

Xie, J., Marusich, M.F., Souda, P., Whitelegge, J., and Capaldi, R.A. (2007). The mitochondrial inner membrane protein mitofilin exists as a complex with SAM50, metaxins 1 and 2, coiled-coil-helix coiled-coil-helix domain-containing protein 3 and 6 and DnaJC11. FEBS Lett *581*, 3545-3549.

Yen, W.L., and Klionsky, D.J. (2008). How to live long and prosper: autophagy, mitochondria, and aging. Physiology *23*, 248-262.

Zerbes, R.M., Bohnert, M., Stroud, D.A., von der Malsburg, K., Kram, A., Oeljeklaus, S., Warscheid, B., Becker, T., Wiedemann, N., Veenhuis, M., et al. (2012a). Role of MINOS in mitochondrial membrane architecture: cristae morphology and outer membrane interactions differentially depend on mitofilin domains. J Mol Biol *422*, 183-191.

Zerbes, R.M., Hoss, P., Pfanner, N., van der Laan, M., and Bohnert, M. (2016). Distinct Roles of Mic12 and Mic27 in the Mitochondrial Contact Site and Cristae Organizing System. J Mol Biol *428*, 1485-1492.

Zerbes, R.M., van der Klei, I.J., Veenhuis, M., Pfanner, N., van der Laan, M., and Bohnert, M. (2012b). Mitofilin complexes: conserved organizers of mitochondrial membrane architecture. Biol Chem *393*, 1247-1261.

Zick, M., Rabl, R., and Reichert, A.S. (2009). Cristae formation-linking ultrastructure and function of mitochondria. Biochim Biophys Acta *1793*, 5-19.

# 7 Appendix

| | |
|---|---|
| C-terminal | Carboxy-terminal |
| $Ca^+$ | Calcium ion |
| $CaCl_2$ | Calcium chloride |
| cDNA | coding DNA |
| Da | Dalton |
| $dH_2O$ | distilled water |
| DNA | Deoxyribonucleic acid |
| DTT | Dithiothreitol |
| E. coli | Escherichia coli |
| EDTA | Ethylenediaminetetraacetic acid |
| $FADH_2$ | Flavin adenine dinucleotide (hydroquinone form) |
| GTP | Guanosine-5'-triphosphate |
| h | Hour |
| $H^+$ | Hydrogen ion |
| Kan | Kanamycin |
| KCN | Potassium cyanide |
| $K_D$ | Dissociation constant |
| kDa | kilo Dalton |
| $KH_2PO_4$ | Potassium di-hydrogen phosphate |
| M | Molar |
| mAU | milli Absorption unit |
| MES | 2-(N-morpholino)ethanesulfonic acid |
| $MgCl_2$ | Magnesium chloride |
| MOPS | 3-(N-morpholino)propanesulfonic acid |
| MW | Molecular weight |
| N-terminal | Amino-terminal |
| NaCl | Sodium chloride |
| NADH | Nicotinamide adenine dinucleotide (hydroquinone form) |
| NaF | Sodium fluoride |
| NaOH | Sodium hydroxide |
| $NH_4Cl$ | Ammonium chloride |

| | |
|---|---|
| $OD_{600}$ | Optical density at 600 nm |
| pH | potential of hydrogen |
| PMSF | Phenylmethane sulfonyl fluoride |
| RNA | Ribonucleic acid |
| rpm | rotation per minute |
| rRNA | ribosomal RNA |
| S | Sedimentation coefficient |
| SDS | Sodium dodecyl sulfate |
| TAE | Tris-Acetate-EDTA-Buffer |
| TRIS | Tris(hydroxymethyl)-aminomethan |
| tRNA | transfer RNA |
| V | Volt |
| w/v | weight per volume |
| x g | Gravity force |
| YPG | Yeast extract-peptone-glycerol |

List of amino acids in one and three letter code

| | | | | | | | | |
|---|---|---|---|---|---|---|---|---|
| A | Ala | alanine | I | Ile | isoleucine | R | Arg | arginine |
| C | Cys | cysteine | K | Lys | lysine | S | Ser | serine |
| D | Asp | aspartate | L | Leu | leucine | T | Thr | threonine |
| E | Glu | glutamate | M | Met | methionine | V | Val | valine |
| F | Phe | phenylalanine | N | Asn | asparagine | W | Trp | tryptophane |
| G | Gly | glycine | P | Pro | proline | Y | Tyr | tyrosine |
| H | His | histidine | Q | Gln | glutamine | | | |

Codon-optimized cDNA of Mic60 (R108–E691) of *Chaetomium thermophilum* synthesized by MWG (Eurofins)

ATG CGT CGT CTG CGC AAC TAC ATT CTC ACC CTG ACC TTC CTG AGT GCT CTG GCG TTT GGA GGC GGC GTG TGG TAT AGC CGC GTT AAC GAT AAC TTT CAC GAC TTC TTT ACG ACG TAT GTG CCC TAT GGA GAA CAG GCA GTT CTG TAC TTA GAG GAA CTG GAT CTC AAG AAA CGC TTT CCT AAC ATT GCA GAC CGC GTA GGC TCT AGC CGT CGC TCA GAC CTC GGG GAT TCC GTC AAA GTT GCG CCC CAC TCA GGT GCC AGC TGG CGT GTG GCC GAT GGT AGC GAA ATC AGC GCT CGT CAG TCA TCT AGC ATC CAA GCT GTA GAA AGT GCC AAG AAG GAA GCT AAA GTA ACA CGT GCG AAA CCA GCA GTC ATC GAA GAG GCG AAA AAA AAG GAA GAA GAG AAA GAA GAG CAA ACT CCA AAA GAA GCG GCT GCC AGC GTG GTT CAG GAA AAG AAA ACG GTC CCG AAG CCA GAA CCG CCG AAA TCC GAG CCG TCC TCT CCT GCT GCG GCA ATC GTA CCG GCG GCT GCA CTT GTG GAA GAG AAG AAA GAA GAA GAG GAA GTG AAG AAG AAG AAA TGG AAA GCC CCG GAA GTA GAT GAA CCG AGC CGT TGG CCG CCC GCC TCA CCG ATT GAT CCG ATC ACA GTA CCG GAC GCG GCT GAA CCA GTC GTG CAA GAG TTG GTT CGG ATG TTA AAC GAC ATT ATC ACC GTA ATT AAT CAC GAC GGT GCG AAC GAG AAA TAT GGC GCC ACC ATC GGC AAA GCC AAA GAG AAA ATC GCG AAA GTT GGC CAG AAA ATC CGT GAT ATG AAA GCC GCG GCA GAA CAA GAA GCG GCA CAG CAA GTC AAA CAG AAA ATT GAT GAA TTT GAT AAG ACC GCC AAC GAA CTG GTG TCG CGT CTG GAA TCC GTG ATT GTA GCG CAG GAA CAG GCT TTT CGC CGT GAG TTC GAA GAG GAG ATG GCC CGC GTC AAG GCG TCG TAC GAT GCC AAA GTG CAA CTG ATT CAG CAA CGC GAA CGC CAG TTA GCC GAA CAA CGC CTG CAA AAT CAG TTG CTG GAA CAG GCG GTA GAG TTG CAG CGC CAT TTC GCC CGT GAA GTT CAG GAG CAA GTG GAG CGT GAA CGT GAT GGC CGC CTG GGT CGC TTG CAG GAG CTT TCG GCA GCG GTG GCG GAT CTC GAA CGC CTG ACT GCG GAC TGG AAC AGT GTC ATT GAC ACC AAT CTC CGC ACG CAG CAA CTT CAC GTT GCA GTG GAA GCT GTG CGC GCA TCC TTG GAC GAT GCG CGT CAT CCC CGT CCG TTC ATC CGT GAA CTG GTC GCC CTG AAA GAA ATT GCA GCC GGT GAT CCG GTT GTA GAT GCA GCC ATT GCC TCA ATT CCT CCG TCT GCC TAT CAG CGC GGT ATC AGT ACC CGC GCG GAG TTA ATT GAT CGT TTT CGT CGT GTG GCC AAT GAA GTT CGC AAA GCG AGT CTC CTG CCT GAA GAT GCT GGG CTG GCG AGC CAT GCT AGC TCA TAC GTC CTG TCG AAA GTT CTT TTC AAG AAG CCG GTG CCT GCC ACT ACC ACG ACT ACG GCG GGC GCA GTG GGC GAC GAC GTT GAA AGT ATC CTG GCA CGC ACA CAG GCG TTT CTG GAG GAA GGC GAT CTG GAT AAT GCA GCA CGC GAA ATG AAT GCA CTG ACC GGG TGG TCG AAA ACC TTA TCA CGT GAT TGG CTG GCC GAA GTT CGG AAA GTG CTG GAG GTC CGT CAA GCA TTG GAG GTG ATC CAG GCG GAA GCC CGT TTA CAG TCG TTG CGG CTT GAG

Codon-optimized cDNA of Mic19 (M1–E167) of *Chaetomium thermophilum* synthesized by MWG (Eurofins)

cat ATG GGC TCA AGC TCC AGT AAA CCC TCG AAT CCA GCT CCG CAT GTG TGG AAA GGC ACA CCA CAA CCT GGT GTG TCG CAG AAT CTG GTG GAA CAA CTG GAA ACC TCC AAC GAA ACC GAC ATT AGT CGC CAA CAA GCA GCC GAA CTG CTG GTT CAG CAG CGT GTC GCA GCG GAA CTG AAA CGC TTG CGC GAA CAG GAA ATC GAG GCG TTA CGC GAA GTC CAA CAG CGC CTG TCA GCT GAA CCG GAT TTG GCA GAG GAT CAG CAG CAG CAT CAG ACG AGC ATT ACT CGC CAA CAG GTT GCC AAA CAG ATC GAC GAT CTG CGG TCT AAG CTC GAA GAA CGC CGT CAA GTA CGC CCG TTA CCG GAG TCT GTC GAG AAA GCG CGT AGC GAA GTT GTG CGT TGT CTC CGG GAA CAC GAT CGT CGT CCG CTT AAC TGC TGG CAG GAA GTG GAG GCC TTT AAG GAG GAA GTG CGC AAA CTG GAG AAA GGG TGG GTT GAC AAA GTA GCG AGC TAA ctc gag

# 8 Zusammenfassung

Die Existenz von Mitochondrien wurde bereits vor mehr als 100 Jahren bestätigt. Diesem Organell wird eine Vielzahl von wichtigen Aufgaben zugeschrieben, unter Anderem die Regulierung des programmierten Zelltodes (Apoptose), die Energieproduktion, die Verteilung von Phospholipiden und vielen mehr. Die Untersuchung der mitochondrialen Struktur und Funktion hat sich zu einem aktiven Forschungsgebiet entwickelt. Auch wenn in den letzten Jahren große Fortschritte zum Verständnis der mitochondrialen Funktion wie Apoptose und Energieproduktion gemacht wurden, so ist bis heute unklar, wie Mitochondrien ihre spezifische Form zur Erhaltung ihrer Funktion bilden. Insbesondere die typischen Einstülpungen der inneren Membran (cristae) beinhaltet eine Vielzahl von unterschiedlichen Proteinen, jedoch wie diese zur Bildung von Cristae-Membranen beitragen, ist bisher unklar. Ein erst kürzlich entdeckter Proteinkomplex (MICOS) scheint eine entscheidende Komponente bei der Ausbildung von cristae und deren Übergang zur inneren Membran (cristae junctions) zu sein. MICOS enthält zwei Kernkomponenten. Während Mic10 Membran-Deformierungs-Aktivität zeigt, bildet Mic60 (mitofilin) die Kontaktstellen zwischen innerer und äußerer Membran.

In dieser Arbeit wird zum ersten Mal gezeigt, dass Mic60, aus dem thermostabilen Pilz *Chaetomium thermophilum,* über die Coiled-coil Domäne dimerisiert und die ursprünglich runden Liposomen in lange dünne Schläuche verwandelt. Zusätzlich wird gezeigt, dass neben Mic10, auch Mic60 eine aktive Rolle im Umbau von Membranen spielt. Zugleich wurde eine Membranbindestelle zwischen der Coiled-coil und der Mitofilin-Domäne identifiziert, welche durch eine vorhergesagte amphipathische Helix gebildet wird. Die Mitofilin-Domäne scheint die Membran-Deformierungs-Aktivität negativ zu beeinflussen. Es konnte auch gezeigt werden, dass die Mitofilin-Domäne von Mic60 stark an die CHCH-Domäne von Mic19 bindet. Isothermale Titrationskalorimetrie-Experimente zeigen, dass diese hochaffine Wechselwirkung zwei konservierte Cysteine innerhalb der CHCH-Domäne erfordert, die eine vorhergesagte intramolekulare Disulfidbrücke bilden. Die Bindung von Mic19 an die Mitofilin-Domäne fördert die Membrane-Deformierungs-Aktivität. Weitere biochemische Analysen zeigen auch, dass der Mic60-Mic19-Subkomplex

Tetramere bildet, die sowohl die CHCH-Mitofilin-Domänen als auch die Coiled-coil beider Proteine einschließt. Die Membranbindung aber auch deren Deformierung durch den konservierten Mic60-Mic19-Komplex ist für die Bildung der Cristae junctions und der mitochondrialen Membranarchitektur entscheidend, und reguliert auch die Aktivität der Atmungskette. Mic60 spielt also eine doppelte Rolle, indem es Cristae junctions aber auch Kontaktstellen zwischen der inneren und äußeren mitochondrialen Membran formt.

# Teilpublikation dieser Arbeit

**Hessenberger, M**., Zerbes, R.M., Rampelt, H., Kunz, S., Xavier, A.H., Purfurst, B., Lilie, H., Pfanner, N., van der Laan, M., and Daumke, O. (2017). Regulated membrane remodeling by Mic60 controls formation of mitochondrial crista junctions. Nature communications *8*, 15258.

http://dx.doi.org/10.1038/ncomms15258

# Erklärung

Ich versichere, dass ich die von mir vorgelegte Dissertation selbständig angefertigt, die benutzten Quellen und Hilfsmittel vollständig angegeben und die Stellen der Arbeit - einschließlich Tabellen und Abbildungen -, die anderen Werken im Wortlaut oder dem Sinn nach entnommen sind, in jedem Einzelfall als Entlehnung kenntlich gemacht habe; dass diese Dissertation noch keiner anderen Fakultät oder Universität zur Prüfung vorgelegen hat; dass sie - abgesehen von oben angegebener Teilpublikation - noch nicht veröffentlicht worden ist sowie, dass ich eine solche Veröffentlichung vor Abschluss des Promotionsverfahrens nicht vornehmen werde. Die Bestimmungen dieser Promotionsordnung sind mir bekannt. Die von mir vorgelegte Dissertation ist von Prof. Dr. O. Daumke und Prof. Dr. U. Heinemann betreut worden.

Berlin, Juli 2017

Manuel Hessenberger